Suitability of Biodegradable Polymersomes as Radionuclide Carriers

Thijs Johan Sanders

A Master thesis submitted to the
Section of Radiation and Isotopes for Health
Department of Radiation Science and Technology
Faculty of Applied Sciences

in partial fulfilment of the requirements for the Degree of
Master of Applied Science in Physics of the Delft University of Technology.
June 2014

Under the supervision of
Dr.ir. A.G. Denkova
Ir. R.M. de Kruijff

Graduation committee:
Dr. ir. A.G. Denkova
Prof. dr. H.T. Wolterbeek
Dr. ir. E. Mendes

Acknowledgments

With this I would like to take the opportunity to express my gratitude to those who have made both my thesis and time at the Reactor Institute of Delft such a wonderful experience.

Firstly, I would like to thank my supervisor Antonia Denkova, who, regardless of her busy schedule, always found the time to provide constructive comments and insightful recommendations. The useful experimental suggestions and remarks during meetings were invaluable in the learning process of my master thesis.

A special thanks goes out to my daily supervisor Robin de Kruijff, a wonderful person to work with as well as a great friend. Thank you so much for your support, insightfulness and enthusiasm. Conducting this research under your supervision was a true pleasure!

Furthermore my gratitude goes to out Astrid and Adrie. Thank you both for helping me get around in the lab. Thanks also to Erik of the Erasmus Medical Center for preparing the Indium-111 and accordingly Rene for being so friendly as to pick it up every two weeks. Furthermore, thanks Jan-Willem, your scientific words of wisdom and of course introducing me to the wonderful Rotavapor machine!

My grateful thanks also to extended Josette for frequently providing me with useful suggestions and good conversation. Guanglin also to you a sincere thanks for all your advice and for our (improvised) Mandarin conversations in the lab. 谢谢你!

To Folkert Geurink also thanks for all your technical support, both in the lab and in the sport of cycling. Cheers also to Koos and Henk for their endless enthusiasm and of course their amazing bar tendering skills at ‘t Koepeltje!

Vallín, gracias tanto delanteras todos los tiempos de la diversión! Yo no podría haber tenido un mejor amigo en la final de mi tesis que tú. Espero verlos pronto, tal vez en Cuba :)

Furthermore a big thanks a RIH and Education section, as well as the SBD for providing a great working environment and enjoyable coffee breaks.

To Alessia, Giacomo, Ivo, Klazien, Laurence, Laura, Michal, Nick, Niels and Roeland thank you for your friendship. I am grateful to have met you all and have greatly appreciated the time we spent together over the past nine months.

Abstract

In the fight against cancer, a promising solution has been found in the encapsulation of radionuclides into nano-carriers. Particularly polymersomes, nano-sized spherical vesicles have been shown to possess significant potential for their application in the field of radionuclide therapy. In this thesis, the suitability of biodegradable polymersomes functioning as radionuclide carriers is assessed.

Biodegradable polymersomes employed in this research were composed of either diblock copolymers, poly(caprolactone)-poly(ethylene oxide)(PCL-PEO) or poly(lactic acid)-poly(ethyleneoxide)(PLA-PEO). The initial aim was to investigate and optimize various methods for the formation and size reduction of these polymer vesicles. Significantly improved formation of PCL-PEO based polymersomes was observed at elevated temperatures. For assessing their fictionalization as radionuclide carriers, the polymersomes were actively loaded with the radionuclide Indium-111. For PCL-PEO and PLA-PEO based polymersomes radionuclide loading efficiencies of up to 82% and 71% respectively were established.

Alongside their ability to entrap radionuclides, the biodegradable character of the two polymersomes was of equal importance. Studies were conducted to assess their biostability. Various tests were conducted in conditions similar to those encountered in the human body and cancerous tissue. More specifically, polymer vesicle stability with respect to acidity and temperature were investigated. Reduced biostability with increased acidity was determined; however tests regarding temperature remained inconclusive.

Table of Contents

Abstract 5
1 Introduction 8
2 Theory 10
2.1 Radioactive Decay 10
2.2 Nuclear Medicine 12
2.2.1 Indium-111 13
2.2.2 Passive targeting: Enhanced Permeability and Retention (EPR) 14
2.3 Polymersomes 15
2.4 Biodegradability 18
2.4.1 Biodegradable Polymersomes 19
2.5 Active Loading 21
3 Analytical Techniques 23
3.1 Dynamic Light Scattering 23
3.2 Confocal Laser Scanning Microscopy 24
4 Materials and Apparatus 25
4.1 Materials 25
4.2 Apparatus 26
4.2.1 Dynamic Light Scattering 26
4.2.2 Wallac Detector 26
4.2.3 Ge-detector 26
4.2.4 Rotavapor 26
4.2.5 Confocal Laser Scanning Microscope 27
4.2.6 Sonicators 27
4.2.7 Freeze-thawing 27
4.2.8 Extruder 27
5 Methods 28
5.1 Preparation of Polymersomes 28
5.1.1 Confocal Laser Scanning Microscope Sample Preparation 30
5.1.2 Cyro-TEM Sample Preparation 31
5.2 Size Exclusion 31
5.2.1 Extrusion 31
5.2.2 Sonication 32
5.2.3 Freeze-thawing 32
5.3 Radiolabelling 32

5.4 Measuring the Loading Efficiency 33
5.4.1 Leakage 33
5.5 Biodegradability 33
6 Results and Discussion 35
6.1 Polymersome Formation 35
6.1.1 DLS 35
6.1.2 Cryo-TEM 37
6.1.3 Confocal Laser Scanning Microscopy 38
6.2 Polymersome Size Reduction 39
6.2.1 Extrusion 39
6.2.2 Freeze-thawing 43
6.3 Loading of Indium-111 45
6.3.1 Loading Efficiencies 45
6.3.2 Leakage 48
6.4 PCL-PEO Preparation and Formation 49
6.5 Biodegradability 53
6.5.1 Mean Intensity 53
6.5.2 Dependency on pH 55
6.5.3 Dependency on Loading Efficiency 56
6.5.4 Temperature 57
6.5.5 Size Distribution Over Time 59
6.6 Closing Remark 61
7 Conclusions 62
8 Recommendations 63
9 Appendices 65
9.1 Supplementary Tables 65
9.2 Supplementary Figures 67
9.3 Mechanisms 70
9.4 Calculations 71
9.5 List of Figures 72
9.6 Poster 74
10 References 75

1 Introduction

The WHO estimates that a total of 14.1 million new cancer cases were diagnosed in 2012[1]. Compared to the 12.7 million cases recorded in 2008, this figure continually reminds us of the mounting presence and severity of this disease. One of the main treatment methods, external irradiation of the tumour site, has been used in cancer treatment for decades. This has proven to be very useful for local tumour control, but it is not very effective against the major cause of high mortality rates: metastases. The difficulty in detecting as well and treating metastases has highlighted the need for developing novel techniques for improved therapy.

In 1999, Discher along with his co-workers opened a new door within the drug delivery field. They were successful in creating what they called “polymersomes”, a new class of artificial vesicles constructed from polymers[2]. Two years after their discovery, Discher and co-workers increasingly realized the tremendous potential polymersomes could have and ideas of applications in chemical reactors, biological systems and particularly as nano-carriers came to mind[3,4].

One can envision a polymersome as being a hollow sphere, having an inside capable of carrying a broad range of drugs and molecules. This transporting ability makes it what we call a “nano-carrier” and polymersomes have proven to have great prospects within this genre. Unlike liposomes composed of low molecular weight lipids, polymersomes are made of heavier macromolecular amphiphilic copolymers and therefore exhibit a much higher stability and have membrane properties which can be tuned much more easily[5].

In the treatment of metastases, polymersomes could therefore lead to a new type radiation therapy[6]. Radionuclides could be loaded into polymersomes and then transported to tumour sites. Once near or absorbed by tumour tissue, ionizing radiation emitted by the polymersome-trapped radionuclides could kill tumour-specific cells and limit the damage done to healthy tissue.

With the ever expanding research into drug delivery agents, polymersomes’ biodegradable properties have become of great interest. This biodegradability ideally allows them to be manufactured so that they can break down when subject to conditions similar to those found in the human body. In the vicinity of cancerous tissues for example, the increased acidity[7] could be utilized to degrade the polymersomes after having delivered the encapsulated radionuclides.

In recent research, polymersomes composed of polyester blocks, such as poly(lactic acid)(PLA) or poly(caprolactone)(PCL) together with poly(ethylene oxide)(PEO) have demonstrated such promising characteristics. PLA and PCL are block copolymers that slowly degrade by hydrolysis of their ester linkages in physiological conditions[8]. In drug delivery, therefore, polymersomes of this sort could biologically degrade over time, minimizing amounts of foreign substances remaining in the body.

In view of these two polymersome types, this thesis can largely be divided into two parts. The first half focuses on the formation, size exclusion and loading prospects of PCL-PEO based polymersomes. Different preparation methods which allowed for the self-assembly of the polymer vesicles were investigated. After formation of the polymersomes, size reduction techniques such as freeze-thaw extraction, filter extrusion and sonication were applied and accordingly assessed. Furthermore, for various preparation methods, the relative amounts of radionuclide that could be loaded in the polymersome were also determined.

For the second half of this research, PLA-PEO based polymersomes were taken into consideration. Polymersomes composed of heavy molecular weight, PLA_{10500}-PEO_{5000} copolymer blocks were assessed in their biodegradability. This was done by investigating the polymersomes under various environmental conditions. Radionuclide loading efficiency was assessed in acidities similar to those found in the blood stream and tumour cells, for example. Furthermore polymer vesicle stability with respect to changes in acidity and temperature were also taken into consideration.

All research for this thesis was conducted at the Reactor Institute Delft in the Radiation and Isotopes for Health (RIH) section of the department of Radiation Science and Technology. Experiments were carried out under the supervision of dr. ir. Antonia Denkova and ir. Robin de Kruijff in fulfilment of the Masters degree in Applied Physics within the faculty of Applied Sciences of the Delft University of Technology (TU Delft).

2 Theory

This chapter encompasses the essential principles required for comprehending experiments conducted throughout this research. Firstly a brief review of radiation and its applications in the field of medicine will be given. This will be followed by a section on (biodegradable) polymersomes, discussing their formation, size control, loading ability as well as their biodegradability. Following this section, the chapter will be concluded by providing a brief explanation of the concepts behind the instruments used the experiments.

2.1 Radioactive Decay

Radioactive decay describes a spontaneous process in which the nucleus of an unstable atom emits particles of ionizing radiation. In doing so, the atom's nucleus loses energy, transforming into a different isotope or element. At the level of single atoms radioactivity is a stochastic process, meaning that it is impossible to determine exactly when the atom will decay. When viewing the nuclear decay in terms of a larger number of atoms however we can model the decaying nature more easily. Working with a population one can define a specific "half-life time" associated to that atom; the time required for exactly half of the atoms in a population to decay. Atoms with a shorter half-life would thus half in population much faster and therefore exhibit a higher amount of activity. Radioactivity can thus be described as a function of this half-life behaviour:

$$A(t) = A_0 \cdot \left(\frac{1}{2}\right)^{\frac{t}{t_{½}}} \tag{2.1}$$

where:
$A(t)$ is the activity of the substance that decays at a time t,
A_0 is the initial activity of the substance that decays,
and λ is the decay constant defined as:

$$\lambda = \frac{ln2}{t_{½}} \tag{2.2}$$

Since this relationship involves a logarithmic constant, the activity described in equation (2.1) can conveniently be rewritten to:

$$A(t) = A_0 e^{-\lambda \cdot t} \tag{2.3}$$

which is a more conventional definition used when dealing with the radioactivity of a decaying substance.

As mentioned earlier, radioactivity is characteristic for all unstable atoms. By stability in this context we consider the ratio of protons to neutrons (Z:N) in the atom's nucleus. For a nucleus to be stable it should have a ratio roughly between 1:1 and 1:1.5 depending on the isotope's molar mass. Lighter stable elements usually have as many protons as they have neutrons. For heavier elements, repulsive forces between the protons begin to play a larger role, and addition of neutrons can actually contribute to stability. When the ratio becomes too disproportional however the atom becomes energetically instable. With atoms naturally favouring towards an energetically more stable state, the number of protons and neutrons will therefore be adjusted accordingly to more proportional ratio. In doing so, a loss of internal energy occurs, which is converted to either an emitted sub-atomic particle or an ionizing form of electromagnetic radiation[9]. This is in essence the process of a radioactive decay.

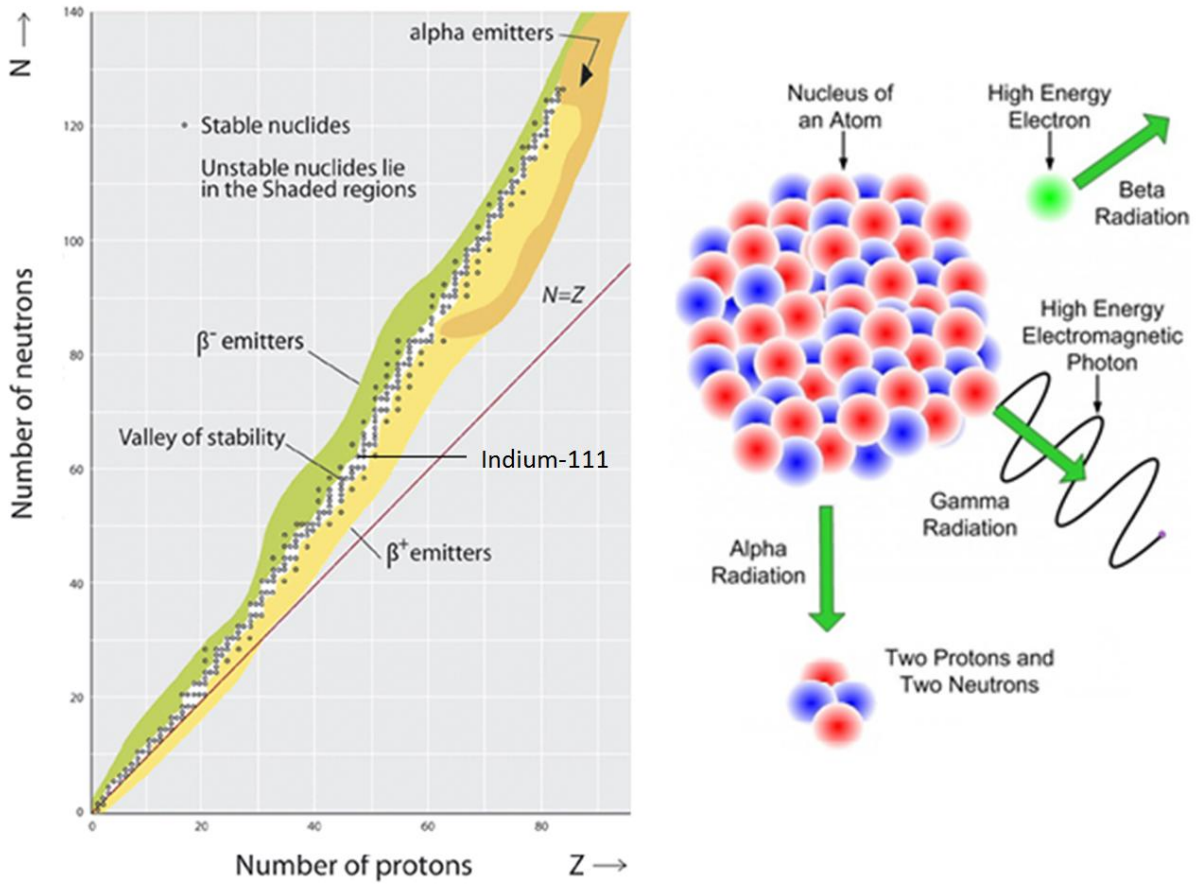

Figure 2.1 (Left) A radionuclide chart with the shaded regions roughly indicating unstable nuclei along with their respective modes of decay. (Right) A schematic representation of α, β and γ decay[10].

As an example of a radioactive decay we may take a look at an unstable isotope of the element Indium. The radionuclide Indium-111, employed throughout this research has for example 49 protons and 62 neutrons and thus a proton neutron ratio of 1 to 1.27. This ratio for Indium is slightly disproportional for atom stability and thus the isotope is radioactive and will eventually decay.

As a visual interpretation, Indium-111 can be seen in Figure 2.1 (Left) to lie just outside the belt or valley of stability. Conversion of a proton into a neutron by Indium-111 causes its decay to the isobar Cadmium-111 which is in turn stable. More detailed information on Indium-111 and its characteristics will be discussed later on in the chapter. At this stage it is important to note however that there are a number of notations are possible for isotopes. In this report isotopes are specified with the mass number noted after the element symbol.

Depending on their decay characteristics, unstable atoms (or radionuclides) can emit different types of particles. In the majority of decays, the sub-atomic particle emitted is either an α or β particle[11]. If the energy is lost in the form of electromagnetic radiation, photons of high energy known as γ radiation are emitted. Figure 2.1 (Right) shows a schematic of the common α, β and γ decays.

2.2 Nuclear Medicine

Not long after the discovery of artificial radiation the ideas of its applications in the field of medicine became apparent. Physicist Ernest Lawrence, famous for inventing the cyclotron, was investigating the production of artificial isotopes when his brother John, former haematologist at Yale Medical School, joined his efforts. With knowledge in both fields, pioneering research into use of radioactive iron for haematology was conducted, establishing one of the first diagnostic and therapeutic uses of a radioactive isotope[12]. Although many other instances merit mention, the Lawrence brothers' efforts could widely be considered as the birth of nuclear medicine as we now know it.

From there on the field quickly developed, in 1940 Saul Hertz found initial applications for patients, assessing the use of Iodine-131 as a possible therapy for thyroid cancer[13]. Furthermore John Lawrence also continued research into radionuclides, investigating Phosphorus-32 as a possible treatment for leukaemia[14]. Throughout the 50s and 60s, knowledge of radionuclides and their use in tracing biochemical processes greatly progressed. Discovery and development of radiotracers such as Technetium-99m allowed for improved techniques for measuring blood flow and identifying so-called cancer "hot spots"[15]. In the following decade, development of PET and SPECT imaging techniques, amongst others, enabled for the majority of organs to be visualized[16]. From the 70s onwards, clinical applications of nuclear medicine became widespread, brain tumour localization, liver and spleen scanning as well as imaging of the gastrointestinal tract all found their way into daily hospital practice. Furthermore the start of the digital era in the 80s allowed for additional computing power, further refining the already established techniques and also contributing to novel techniques such as cardiac imaging. As of today, nearly 100 different nuclear medicine imaging procedures are in existence. Nuclear medicine now provides means for early diagnosis, treatment and prevention of countless medical conditions. With imaging techniques capable of providing information about virtually every organ system, nuclear medicine has become an essential branch of the medical world.

2.2.1 Indium-111

Indium-111 disintegrates by means of (>99.99%) electron capture via the excited level of 416.6 keV into Cadmium-111 emitting gamma radiation with respective energies of 171.3 and 245.4 keV[17]. Rarely, Indium-111 also decays by an (≤0.01%) electron capture via the isomer level to Cadmium-111 at 396.15 keV, having a half-life of 48.5 min. The parent isotope of Indium-111 is Tin-111 also decaying by mode of electron capture. Indium-111 is also able to undergo isomeric transition, emitting a 0.537 MeV gamma ray with a half-life of 7.7 minutes.

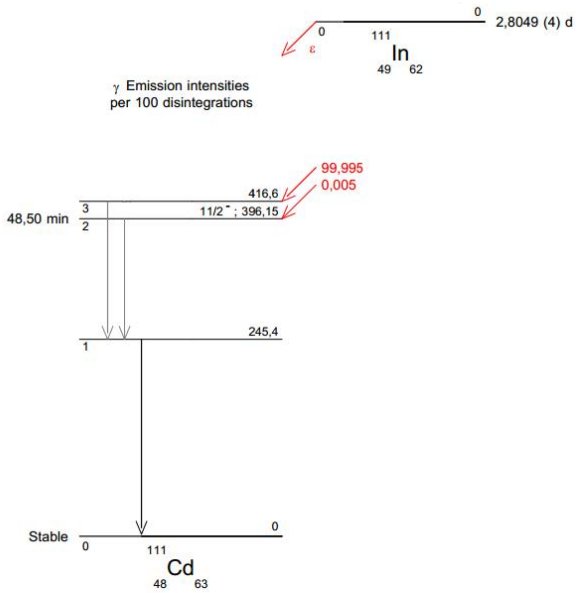

Figure 2.2 A decay scheme of Indium-111[17]. Numbers in red indicate the probability with which each of the two decays will occur.

Within the field of nuclear medicine Indium-111 is used as a radioactive tracer. Having a convenient half-life of 2.80 days and an appropriate energy for detection, Indium-111 has found a number of specialized diagnostic applications. With affinity for binding to both white blood cells and (their) antibodies, the immune system in particular has put Indium-111 to good use. In Indium leukocyte imaging for example, a patient's white blood cells, taken from the bloodstream, are tagged with Indium-111 as tracer. The tagged leukocytes can then be re-injected intravenously into the patient, and subsequentially be utilized for the localization newly infected sites[18]. Use of this technique is sometimes more commonly referred to as a "W.B.C." or Indium(-111) scan. Over the last 10 years Indium-111 has also been reported to be loaded in liposomes, allowing to assess their biodistribution in the body by means of whole body gamma camera imaging[19].

2.2.2 Passive targeting: Enhanced Permeability and Retention (EPR)

In radionuclide therapy targeting mechanisms for the localization and treatment of cancers at specific sites are essential. At large, targeting mechanisms can be classified as being either passive or active. Active targeted delivery, as discussed in the use of leukocyte imaging, utilizes the attachment of specific ligands to the surface of an entity in order to recognize and to bind the desired pathological cells[20].

In contrast, passive targeting relies on the inactive accumulation of nano-carriers at a certain site. Accumulation in this case occurs more due to the physical than chemical properties of the carrier. Furthermore in passive targeting, the physiological characteristics of the targeted area are of great importance.

This is particularly the case when dealing with tumour sites for example. Here passive targeting by means of the enhanced permeability and retention (EPR) effect occurs. Tumours characterized by vastly multiplying cancer cells stimulate rapid growth of neighbouring blood vessels in order to maintain blood supply. This rushed formation of angiogenic tumour vessels leads to increased spacing and misalignments between the endothelial cells of the blood vessels as seen in Figure 2.3

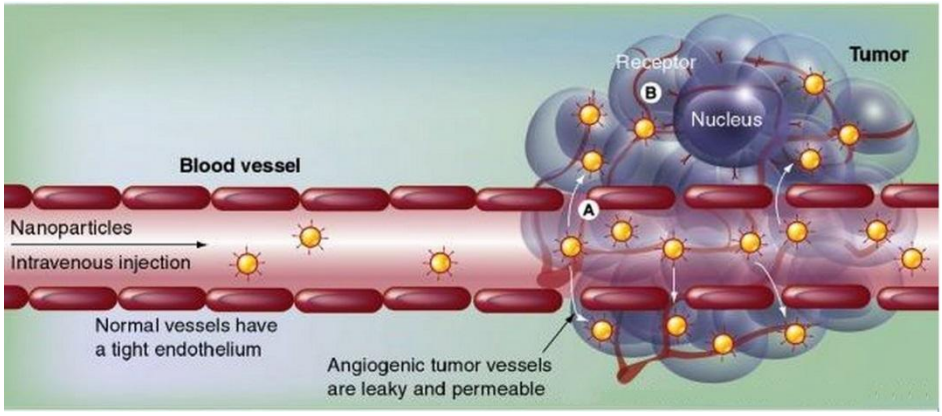

Figure 2.3 A graphical interpretation of the EPR targeting mechanism. Increased spacing between the cells of the endothelium at Ⓐ allows for nano-particles or nano-carries to enter the tumour around the blood vessel[21].

With increased spacing, nano-carriers of smaller dimensions can thus penetrate the widened physiological barrier of tumours passively. The rate at which accumulation occurs depends on both the on the size of the carrier and the spacing between the epithelial cells at the tumour site[22]. This is of great use as there are no tumour specific properties that the nano-carrier needs to be adapted to for efficient targeting. The EPR effect, although first confirmed through use of proteins, has been applied to a range of entities including drug–polymer conjugates, micelles and polymersomes[23].

For the EPR effect to work, the essential requirement is that the size of the penetrating body is less than that of the spacing at endothelial junctions. As an indication of gap size differences, tumours can have vessels spacing ranging between 380 and 780 nm depending on the tumour type[21] while tight endothelial junctions of normal vessels have spacing of typically 1 to 10 nm. For nano-carriers it is therefore is essential that a size below 380 nm is met and ideally a diameter lower than 200 nm for significant accumulation rates to be achieved[24,25]. These sizes cited in literature however are for

substances in general, and smaller limit sizes for the EPR effect to work with Indium-111 loaded polymersomes has be determined at 120 nm[6]. And furthermore for circulation in the blood with a biological half life of 24h, polymer vesicles sizes smaller 90 nm were required[6]. N.B. for a good indication of the relative sizes of entities encountered in this thesis, it is convenient to consider Figure 9.1 in Appendix A9.2.

An advantage of the EPR effect occurring passively is that nano-carriers, which are not detected by the body's immune system, can stay in the blood for longer periods of time further thus giving them a higher level of accumulation within the target[24]. A disadvantage of this passivity is however that the EPR cannot be chemical or biologically controlled; furthermore nano-carriers which are rapidly cleared would also have low accumulation rates. What is promising however is that targeting very high concentrations of polymeric drugs is possible with the tumour site, and accumulation can be 10 to 50 fold higher than in normal tissue in just a time span of 1–2 days delivery[21].

2.3 Polymersomes

A polymersome can be defined as an artificial vesicle made from amphiphilic block copolymers[5]. A diblock copolymer is a polymer composed of two (di-) different monomers which are arranged in homopolymer segments (-blocks). The two homopolymer blocks thus each compose one end of the diblock copolymer and are linked by a covalent bond. In being amphiphilic, the diblock copolymer implicitly has one hydrophobic homopolymer block and the other is hydrophilic. A representation of an amphiphilic diblock copolymer can be seen on the left side of Figure 2.4. Although polymersomes are frequently constructed with diblock copolymers, formation of polymer vesicles composed of triblock copolymers can also be realized[26].

When suspended in an aqueous solution, the hydrophilic part of the block copolymer will try to maximize its exposure to water while the hydrophobic part will want to minimize this. As a result of this behaviour block copolymer self-assembly is triggered and the amphiphiles can arrange in a number of possible morphologies. Likely structures upon hydration are spherical micelles, cylindrical micelles or polymer vesicles. Many conditions such as molecular mass, pH and temperature can influence the geometric shape that the amphiphiles will form[27]. Key parameters are however both the mass fraction (f) and interaction parameter (χ) of the hydrophobic block in water[28]. For block copolymers with a high interaction parameter, polymersome structures are favoured when the *hydrophilic* mass fraction ($f_2 = \frac{M_2}{M_1+M_2}$) lies between 25 and 45%. At a fraction between 45 and 55% cylindrical micelles are favoured and at even higher fractions spherical micelles show the greatest tendency[29,30].

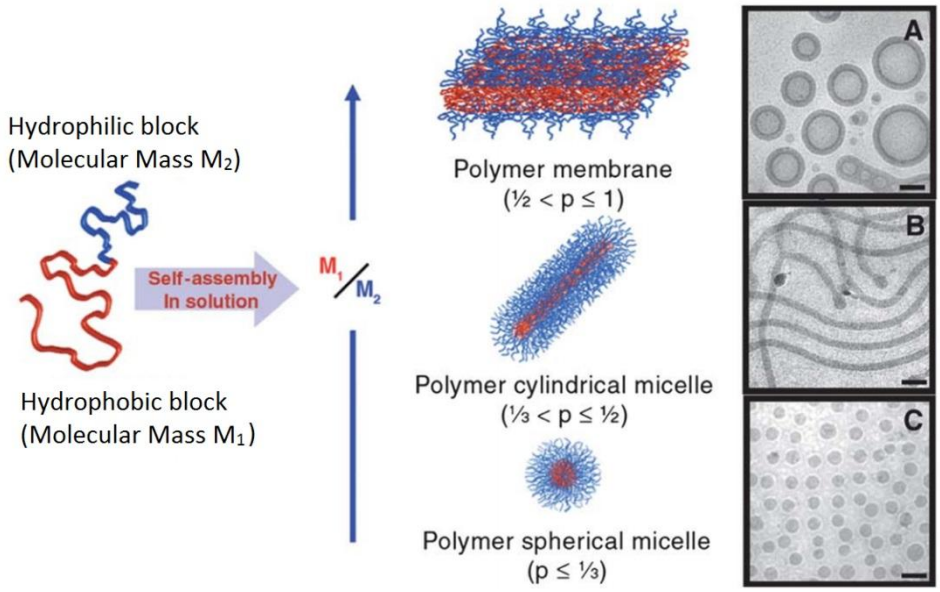

Figure 2.4 (Left) A Schematic illustrating the organisation of block copolymers in spherical and cylindrical micelles and vesicles with increasing hydrophobic M_w fraction. (Right) Letters A to C show Cryo-TEM micrographs of polymersomes aggregates. A shows polymersomes, B shows cylindrical micelles while C shows spherical micelles. Scale bars for A to C are 100 nm[31].

For determining the morphology upon self-assembly, a geometrical entity known as the packing parameter (p) can be used. The packing parameter can be derived from the mean curvature H and its associated Gaussian curvature is K, together they define the ratio between the copolymer chain length and the volume of the hydrophobic block.

Equation (2.4) explicitly defines this relation, with v being the volume of the hydrophobic part of the polymer, a the interfacial area per molecule and l the chain length of the hydrophobic block normalized to the interface[32]

$$p = 1 + Hl + \frac{Kl^2}{3} = \frac{v}{al} \tag{2.4}$$

The numerical value p thus determines the different possible morphologies of the body formed. For example: $p \leq \frac{1}{3}$ (spheres), $\frac{1}{3} \leq p \leq \frac{1}{2}$ (cylinders) and $\frac{1}{2} \leq p \leq 1$ (vesicles). A visual interpretation hereof can again be seen in Figure 2.4.

Provided small hydrophilic mass fractions, self-assembly of polymer vesicles is thus preferred. Structurally, polymersomes are synthetic supra-structures having an aqueous cavity in the core surrounded by a double layered membrane. This double or bilayered membrane is composed of two hydrated hydrophilic coronas both on the inside and outside of the membrane. A generated 3D cross section of a polymersome in Figure 2.5 clearly displays this multi-layer membrane construction.

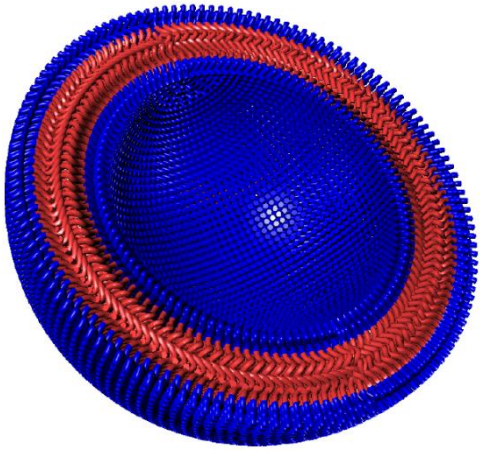

Figure 2.5 A three dimensional representation of a polymersome cross-section with the membrane a bilayer clearly visible. The two hydrated hydrophilic coronas (in blue) on the in and outside of the hydrophobic polymer core. The hydrophobic ring (in red), separates and protects the aqueous core from the surrounding environment[33].

Both hydrophilic coronas are composed of the hydrophilic blocks of amphiphilic copolymers which are aligned side by side along membrane (Figure 2.7 Right). The hydrophobic blocks of the amphiphile are thus found on the inside of the membrane, represented by the red ring in Figure 2.5. Furthermore the diblock copolymers themselves can also be distinguished in the figure, alternating between the small spaces in the membrane layers

The membrane thickness of polymersomes can largely be controlled by the molecular weight of the hydrophobic block of the copolymer[34]. A specific copolymer molecular weight thus determines polymersome properties such as elasticity, permeability and mechanical stability[29]. As can be observed that higher molecular weight greatly contributes to the improvement of these properties as can be seen in the Figure 2.6.

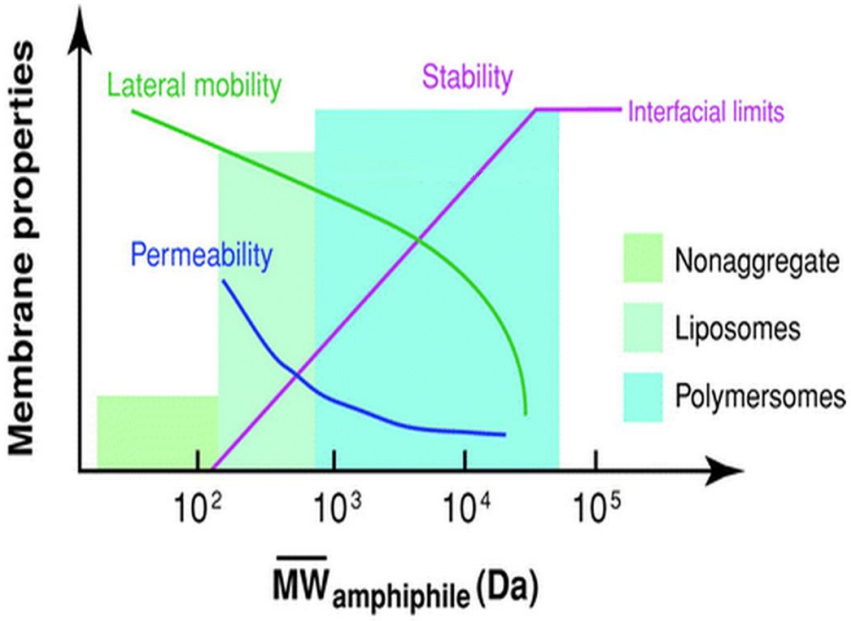

Figure 2.6 Schematic plot of vesicles stability, permeability and mobility versus molecular weight of the associated amphiphile[29].

Due to the higher molecular weight of polymers as compared to lipids, the membrane of polymer vesicles are generally thicker, stronger and tougher than that of liposomes. For example the maximal strain of poly(butadiene)-poly(ethylethylene)(PBd-PEE) polymersomes varies from 20 % to 40 % as compared to a typical <5 % for liposomes[34].

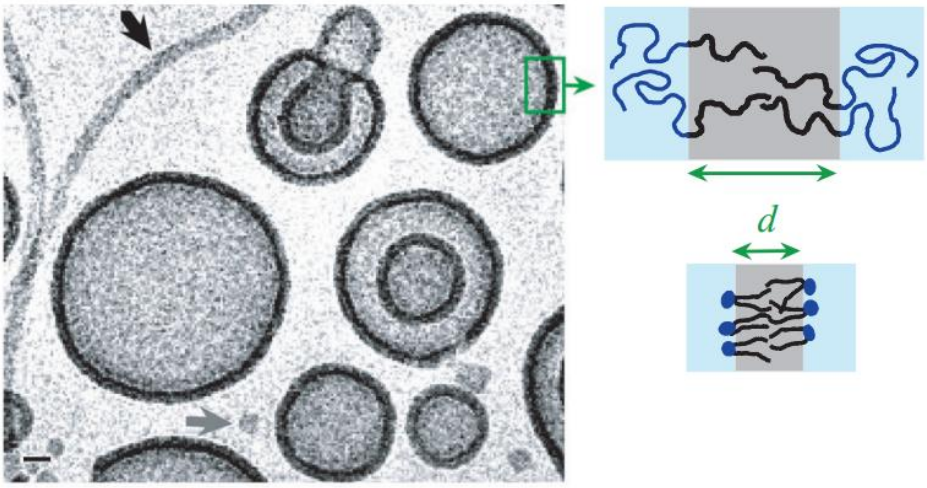

Figure 2.7 One of the first Cryo-TEM images of self-assembled copolymer structures of PEE-PEO[2]. The polymer vesicles are in dominant coexistence with wormlike (black arrow) and spherical (grey arrow) micelles. Lower left scale bar is 20 nm.

2.4 Biodegradability

Prior to discussing biodegradable polymersomes along with their properties it is of importance to consider the term biodegradability itself beforehand. There can sometimes be a sense of ambiguity to the word depending on whether a biological or chemical approach is taken.

Poly(lactic acid), a biodegradable block polymer used in this research for example has been found to be readily hydrolysed in the human body. Upon its hydrolysis the entire mass of the polymer disappears and all its constituents are turned into their respective monomers and oligomers[35]. Strictly speaking in this case the polymer losing weight over time in the body would best be described as being either absorbable, bioabsorbable or resorbable. Calling the polymers biodegradable here would by many be considered correct, but due to the word often being used for the enzymatic degradation of ecological polymers in nature, the definition could be interpreted as incorrect or confusing at the least.

Polymers and their assemblies with the purpose of being implanted in the human body would therefore be better off being described as resorbable or absorbable but very often this description is not used. Despite this confusion however, this thesis will use the term biodegradable in the biomedical sense. Use of the word biodegradable with respect to a polymer(some) thus describes its chemical breakdown after it has entered the body, regardless of whether an enzymatic or non-enzymatic degradation has taken place.

2.4.1 Biodegradable Polymersomes

Over the past decade the amazing drug delivery potential of polymersomes has been established, and, to large extent realized. Recent years have therefore also led to more attention being paid to improved biological properties polymersomes. Polymer vesicles assembled by a diblock copolymer such as poly(butadiene)-poly(ethylene oxide) (PBd-PEO) has been deemed unlikely to gain approval for application in humans due to their inability to be degraded or cleared out of the body.

The essential quality that gives polymersomes a biodegradable character is hydrolizability of one of the (di)block copolymers they are composed of. More specifically, the hydrolizability is attributed to either one of these copolymer blocks, which in all known published cases is found to be the (more) hydrophobic block. Polymersomes thus degrade through the hydrolysis of block copolymer chains on the inside of the membrane as displayed in Figure 2.8 and seen by Cryo-TEM imaging in Figure 2.9.

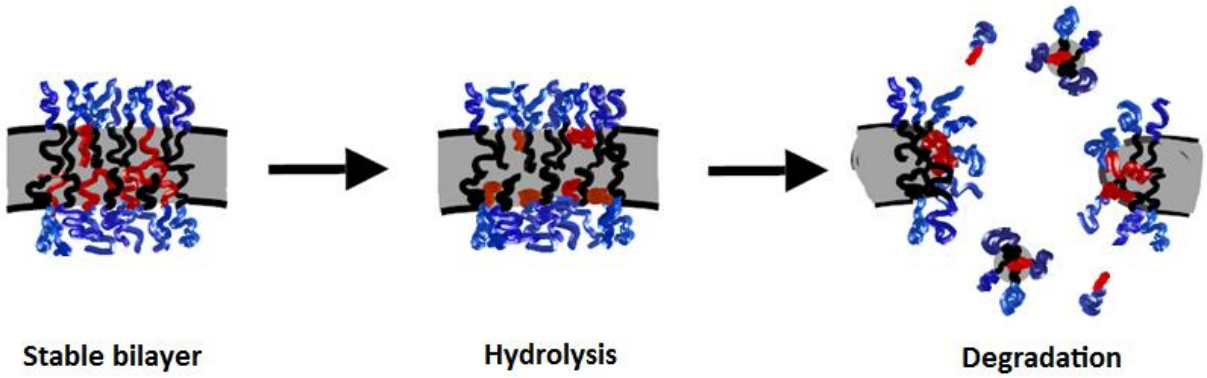

Figure 2.8 Hydrolysis of degradable hydrophobic polyester chains (in red) leads to shrinking of the bilayer, and eventual degradation. Chains (in black) are inert non-biodegradable block-polymers[30].

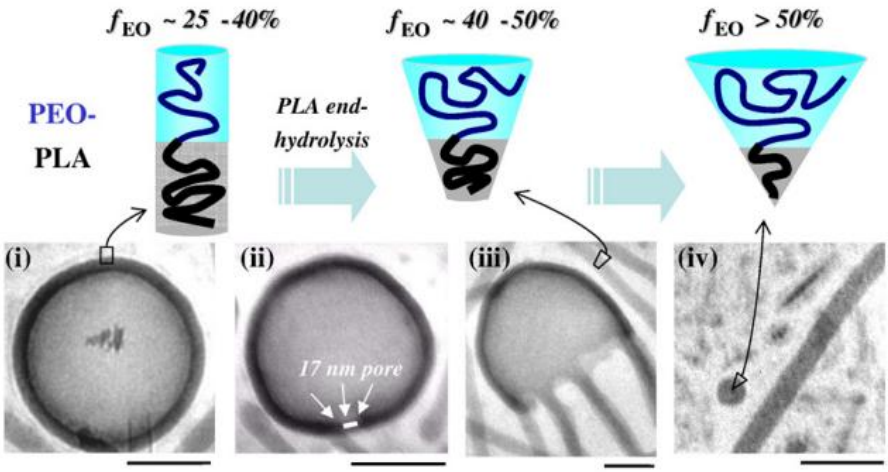

Figure 2.9 (A) Cryo-TEM images of empty PLA-PEO based self-assembled aggregates. Hydrolysis of the PLA block copolymer triggers the growth of pores, and over time shows the vesicles into turn into worm-like and spherical micelles. Scale bars are 100 nm[36].

Poly(caprolactone)(PCL) and poly(lactic acid)(PLA) covalently bonded to poly(ethylene oxide) (PEO) create the amphiphilic diblock copolymers PCL-PEO and PLA-PEO. These diblock copolymers self-assemble to create the biodegradable polymersomes which were specifically researched in this study. An understanding each individual block polymer of which the two amphiphiles are composed is thus of essential importance and will be briefly be discussed below.

Poly(caprolactone)

PCL is a biodegradable polyester with a wide range of applications and a number of interesting properties. PCL is polymerized by the ring opening of ε-caprolactone as observed in Figure 2.10. Despite its glass transition temperature of -60 °C, PCL is semicrystalline and has a melting point of approximately 60 °C. Applications of PCL are vast, ranging from scaffolds in tissue engineering to microelectronics to packaging. PCL has already been approved by the Food and Drug Administration (FDA) for use in the human body[37], providing possible future potential for clinical trials potential for PCL based polymersomes.

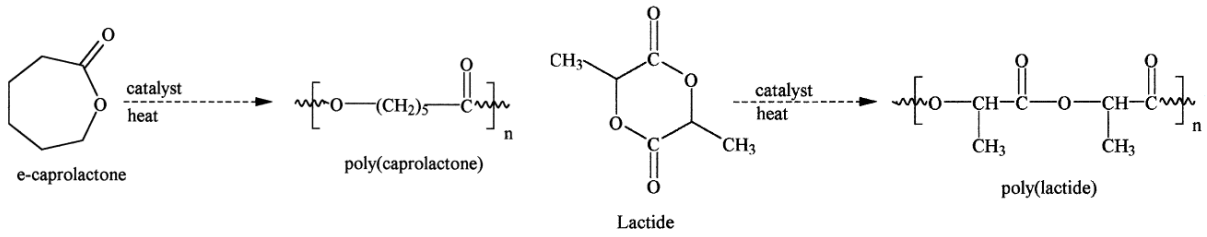

Figure 2.10 (Left) Ring opening polymerization of ε-caprolactone to make PCL. (Right) PLA being produced similarly by a ring opening polymerization of lactides[38].

Poly(lactic acid)

For PLA it is essential to note that its monomer exists as two optical isomers, D and L. The polymers of these two (LPLA and DLPLA) consequently have significantly different properties. LPLA is a semicrystalline polymer exhibiting high tensile strength, often used for load-bearing applications. In contrast, DLPLA is an amorphous polymer unable to arrange into a crystalline organized structure due to its random distribution of its isomers D and L. DPLA thus has a lower tensile strength than LPLA and a rapid degradation time, making it an attractive drug delivery agent[39]. LPLA is roughly 37 % crystalline having a melting point of 176 °C and a glass transition temperature of 62 °C. Synthesis of PLA can be observed on the right of Figure 2.10.

Poly(ethylene oxide)

Unlike PCL and PLA, PEO is non-biodegradable, it does however exhibit excellent hydrophilicity as well as solubility in water and organic solvents. Furthermore due to its flexible main chain PEO has the ability to minimize cell and protein interactions[40]. For this reason PEO is frequently used as the hydrophilic block in many block copolymers, and in this thesis research, this is equally the case.

2.5 Active Loading

Polymer vesicles were loaded with the radionuclide Indium-111 as diagnosis agent. Indium-111 transport through the polymer bilayer first requires bonding of a lipophilic ligand (Tropolone, Figure 2.13). The lipophilic ligand has great affinity for the hydrophobic part of the double layer of the polymersome and so the radionuclide-ligand complex moves to the double layer. Inside the core of the polymersome, a hydrophilic chelate, diethylene triamine pentaacetic acid (DTPA, Figure 2.13) is present. This chelate has been specifically chosen to exhibit preferential binding towards the radionuclide in comparison lipophilic ligand. With this being the case, radionuclides in the membrane express preferential binding to the hydrophilic chelate in the aqueous core. As result the radionuclides leave the membrane and enter the interior polymersome as seen in Figure 2.11.

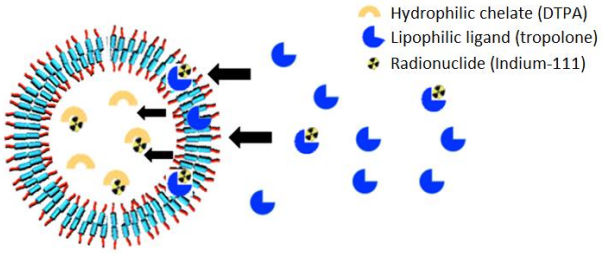

Figure 2.11 A schematic picture of the active loading process. Indium-111 is carried into the bilayer by the Tropolone and then into the aqueous cavity of the polymersome by the DTPA.

These steps taken together describe the active loading process, were through the use of preferential binding a substance is actively passed through a barrier. The mechanism by which the radionuclides are loaded in the interior remains speculative. Two hypothesized methods by which the Indium-111 propagates through the membrane are illustrated in Figure 2.12.

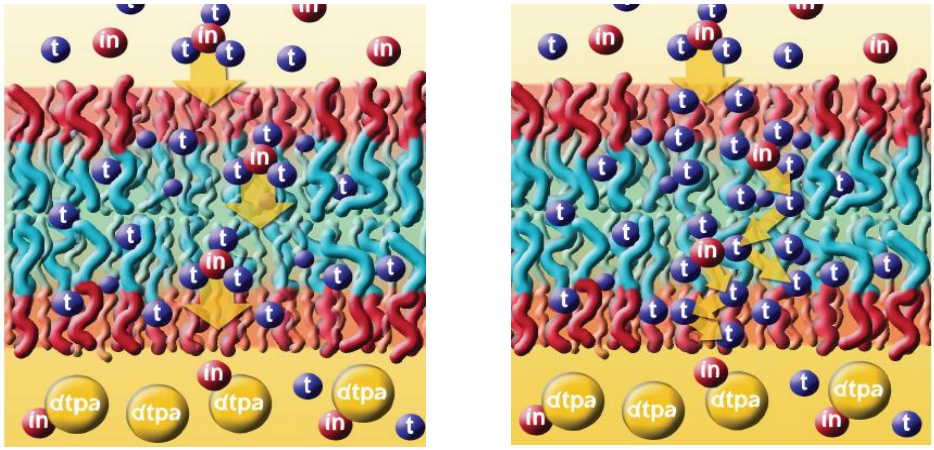

Figure 2.12 Schematic representation of the possible transport mechanism of Indium-111 through a polymersome bilayer (left) diffusion of In-Tropolone complexes as a whole and (right) In hopping from Tropolone molecule to Tropolone molecule, which form a channel of sorts through the membrane[41].

In active loading four requirements have to be met in order to achieve a successful drug transport, as listed below:

1. The ligand and chelator should be chosen such that they both express affinity towards binding with the substance that is to be loaded.
2. The ligand should be able to pass through the membrane, but the chelator should not because otherwise the substance-chelator complex could also diffuse out of the polymersome again.
3. The loaded substance is given the opportunity to bind to the ligand prior to the presence of the chelator, since otherwise almost everything will directly bind to the chelator.
4. The binding affinity of the substance with the chelator is stronger than that with the ligand, to maximize active transport through the internal membrane into the aqueous cavity.

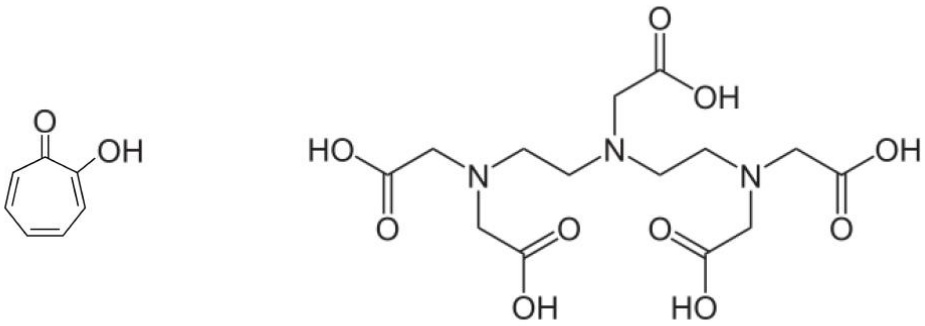

Figure 2.13 Chemical structures of lipophilic ligand Tropolone (left) and hydrophilic chelate DTPA (right)

3 Analytical Techniques

3.1 Dynamic Light Scattering

Dynamic Light Scattering (DLS), also sometimes referred to as Quasi-Elastic Light Scattering is a powerful tool in assessing both average particle diameter and polydispersity of certain particles. The technique is based on measuring the Brownian motion of particles in a solution. If monochromatic light from a laser interacts with moving particles, scattering of the light occurs. Due to the Brownian motion, small local changes in concentration lead to small intensity fluctuations of the scattered light. These time-dependent fluctuations can in turn be detected and interpreted as a signal. This signal can be digitalized by software which calculates an autocorrelation function associated with the incoming intensity of the scattered light[42,43]:

$$g^{(2)}(\tau) = \langle I(t) \cdot (t + \tau) \rangle / \langle I(t) \rangle^2 \qquad (3.1)$$

Where I is the intensity and τ is the delay time. This autocorrelation function in turn enables one to extract the diffusion coefficient (D) of the particles. This coefficient is conveniently related to the hydrodynamic radius (R_H) of the particles and can thus be calculated by means of the Stokes-Einstein equation:[44]:

$$D = \frac{k_B T}{6\pi\eta R_H} \qquad (3.2)$$

Where k_B is the Boltzmann constant, η the solvent viscosity and T the temperature.

Based on the fact that Brownian motion of particles is more rapid when the size of particles is smaller, faster diffusing particles will move in and out the laser beam more quickly and therefore generate a higher change in intensity signal. Based on these changes the DLS can differentiate different particles sizes and give average particle diameter of different sized particles in the solution.

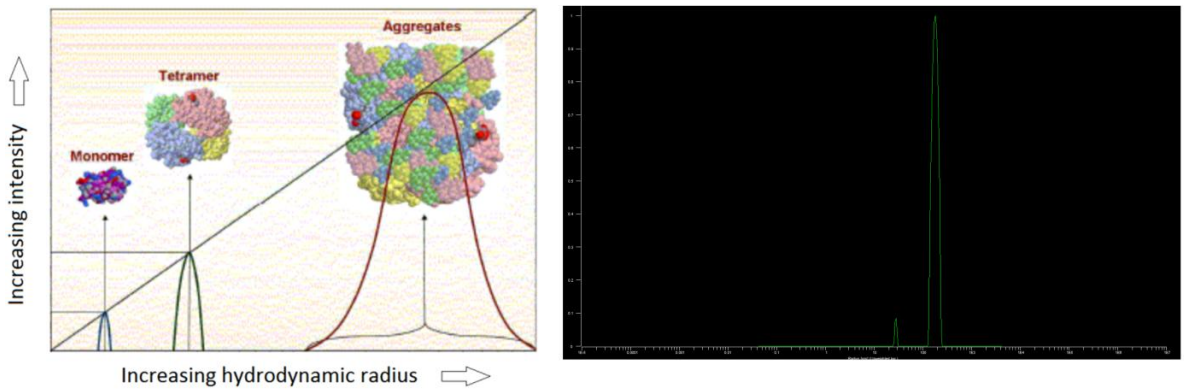

Figure 3.1 (Left) A schematic graph showing the relation between a laser intensity peak and the associated size of the scattered particle. (Right) A typical measurement of from a Dynamic light scattering setup.

It is important to note however that dynamic light scattering only works when particles are small enough compared to the incident light wavelength (Raleigh criterion gives ~250 nm). When this is not the case, the Raleigh specific scattering does not occur and fluctuations in light intensity will no longer be present. Radii as low as approximately 50 nm can thus be measured with the dynamic light scattering

3.2 Confocal Laser Scanning Microscopy

Confocal microscopy is a technique which utilizes optical sectioning in order to obtain in-focus images from selected depths. Optical sectioning allows for the acquisition of images from multiple sample depths providing an in-depth view of a sample. This is a huge advantage over conventional microscopy as superimposition of the selected depth images in this case occurs and leads to poor image quality. Furthermore in being able to make the optical sectioning layers very thin, confocal microscopes can ultimately generate 3D images by subsequently scanning across the consecutive planes. This technique has naturally also made confocal microscopy appealing for identifying cells and smaller sub-microscopic cellular components such as vesicles.

The confocal principle behind laser scanning microscopy can be observed in Figure 3.2. Coherent light emitted by the laser first passes through a collimator after which it is reflected by the dichromatic beamsplitter and scanned across the specimen in the defined focal plane.

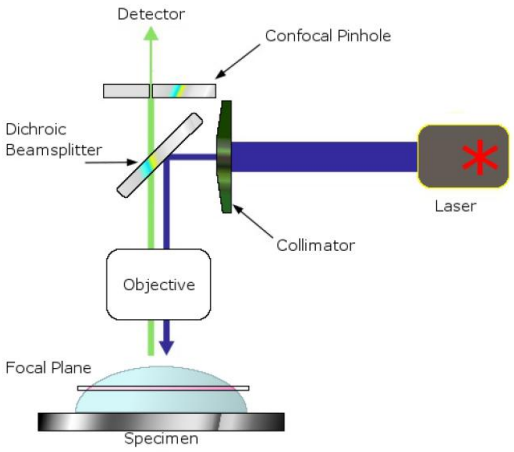

Figure 3.2 A schematic diagram of the different components of a confocal microscope setup[45]

Once the light has interacted with points the specimen, the secondary fluorescence emitted from these points passes back through the dichromatic beamsplitter and is focused as a confocal point on the detector's confocal pinhole. Furthermore when the light source used is a laser, this confocal technique is naturally specified and referred to as confocal laser scanning microscopy (CLSM).

4 Materials and Apparatus

This chapter will provide an overview of all the specific materials and apparatus used in conducting this research. First all materials will be listed and specified, followed by the specification of all apparatus used for formation, loading and the analysis of the polymersomes.

4.1 Materials

Both biodegradable diblock copolymers PCL-PEO and PLA-PEO were supplied by Polymer Source™ from Dorval, Quebec, Canada. Molecular weight ratios of copolymers used were PCL_{2800}–PEO_{2000}, PCL_{13000}-PEO_{5000}, PCL_{1100}-PEO_{550}, PLA_{1850}-PEO_{700} and PLA_{10500}-PEO_{5000}. Additional polymers of polybutadiene-polyethylene oxide PBd_{1800}-PEO_{900} as well as micelle forming PCL_{950}- PEO_{2000} were also purchased there.

Figure 4.1 An overview over the diblock-copolymers used in this research. With the three different molecular weights of PCL-PEO on the left, the high and low molecular weight PLA-PEO in the middle and PBd-PEO along with the micelle forming PCL-PEO to the right.

The radioactive isotope Indium-111 was delivered as an Indium-chloride solution, supplied by the Department of nuclear medicine of the Erasmus University, Rotterdam, the Netherlands.

Chelator *DTPA titriplex V* was purchased from Merck (Darmstadt, Germany) and the Tropolone from Merck-Schuchardt (Holvenbrunn, Germany).

Remaining chemicals were supplied by Sigma Aldrich (St. Louis, USA). This included the HEPES (H3375-500G) buffer solution, chloroform, hydrochloric acid, tetrahydrofuran and 2-propanol solutions. Furthermore the Sephadex G-25 Medium filtration medium and PD-10 desalting columns used were also supplied from Sigma Aldrich. The Sephadex G-25 SEC Econo-Column was purchased from Bio-Rad laboratories (Hercules, California, USA).

4.2 Apparatus

4.2.1 Dynamic Light Scattering

The setup of the dynamic light scattering system consisted of a JDS Uniphase 633 nm 35 mW laser and a Perkin Elmer photon counter (Waltham, USA). For data analysis, an ALV sp-125 s/w 93 goniometer and ALV-5000/epp correlator with associated A5ECORR software was used. The scattered light intensity was measured at a 90° angle and modelled with the $g^{(2)}(\tau)$ auto-correlation function as in equation (3.1). Data was and fitted using the CONTIN method with Stokes-Einstein equation (3.2) used to determine vesicle radii. Samples were immersed in a thermocoupled bath at 22 ± 1°C and toluene was used as the index-matching fluid.

4.2.2 Wallac Detector

Radioactivity was also measured with the use of a Wizard^2 Wallac 3'' 24800 Automatic Gamma Counter from Perkin Elmer (Waltham, USA).

Figure 4.2 (Left) The dynamic light scattering apparatus with which size distributions and polydispersity of the polymersomes was assessed. (Right) A Wizard^2 Wallac 3'' 24800 Automatic Gamma Counter used for measuring activity in radionuclide containing samples. The energy spectrum of Indium-111 can be observed on the screen.

4.2.3 Ge-detector

The activity of the samples was measured using a LG22 High Purity Germanium (HPGe) detector from Gamma Tech (Princeton, USA). The 245 keV gamma peak for Indium-111 was taken as measurement point for all activity measurements.

4.2.4 Rotavapor

Solvent evaporation was performed with an R-210 Rotavapor with associated V-850 Vacuum pump and controller from BUCHI (Essen, Germany). Samples were immersed in a BUCHI B-491 heat bath.

Figure 4.3 (Left) A LG22 High Purity Germanium (HPGe) detector from Gamma Tech used for measuring activity in radionuclide containing samples. (Right) A R-210 Rotavapor with a sample immersed in the corresponding B-491 heat bath.

4.2.5 Confocal Laser Scanning Microscope

For confocal laser scanning microscopy an inverted Axio Observer z1 microscope by Carl Zeiss was used. Images were acquired using a Fluar 40x 11.30 oil M27 objective. The setup was equipped with a HBO50 lamp.

4.2.6 Sonicators

Sonication at room temperature was performed with a Branson 200 Ultrasonic cleaner. For higher temperatures, a BANDELIN Sonorex Digital 10P heat bath, equipped internal sonicator was used.

4.2.7 Freeze-thawing

Freeze thawing was performed in a Julabo 6A heat bath connected to a Julabo U3 heater and water circulator.

4.2.8 Extruder

For the size exclusion by extrusion, a Lipex^{TM} Extruder from Northern Lipids^{inc} (Vancouver, Canada) was used. The extruder was equipped with a 25mm drain disk upon which 25 mm filters with pore sizes 800 nm, 400 nm and 200 nm purchased from GE Healthcare (Diechem, Belgium) were placed.

5 Methods

In this section, the various techniques and steps involved in preparing biodegradable polymersomes as suitable radionuclide nano-carriers will be discussed. Starting with formation, a general preparation scheme along with specific synthesis recipes will be given. Following formation, the methodology behind various instrumentation techniques required for vesicle observation will be described. Then the chapter will continue by reviewing methods used for both size reduction and the loading of polymersomes with radionuclides. Finishing off the chapter, Section 5.5 will explain a number of methods involved in assessing the biodegradability of the formed biodegradables.

5.1 Preparation of Polymersomes

In this research the biodegradable diblock copolymers poly(caprolactone) -poly(ethylene oxide) and poly(lactic acid)-poly(ethylene oxide) with a wide range of molecular weights were used. Furthermore various other diblock copolymers used in combination with the biodegradable copolymers were also utilized. An overview of all the diblock copolymers used along with their designated name, molecular weights and other features can be found in Table 1

Table 1 An overview of all the diblock copolymers used in this research[46,47,48].

Designated name	Diblock copolymer	Block formula	Molecular weight M_n (kg/mol)	Polydipersity Index M_w/M_n	f_{EO}	Comments
PCL28	PCL_{2800}-PEO_{2000}	25-b-45	4.8	1.15	0.42	
PCL130	PCL_{13000}-PEO_{5000}	114-b-114	18.0	1.70	0.28	
PCL11	PCL_{1100}-PEO_{550}	10-b-12	16.5	1.17	0.33	
PLA18	PLA_{1850}-PEO_{700}	16-b-26	2.55	1.40	0.27	
PLA105	PLA_{10500}-PEO_{5000}	114-b-147	15.5	1.09	0.32	
PCL9	PCL_{950}-PEO_{2000}	9-b-45	2.95	1.10	0.67	Micelle forming
PBd18	PBd_{1800}-PEO_{900}	31-b-21	2.7	1.09	0.33	Used for blending
PBd65	PBd_{6500}-PEO_{3900}	120-b-89	10.4	1.10	0.38	Used for blending

For future reference to researched polymersomes the designated names found in this table will be used. Furthermore the diblock copolymer column of the table specifies the number average molecular weights of both blocks. As an example PCL_{13000}-PEO_{5000} specifies the molecular weights of the PCL block being 13000 g/mol and that of PEO 5000 g/mol. The Polydispersity Index indicates the distribution of individual molecular masses within the batch of polymers and f_{EO} (with EO referring to the hydrophilic PEO block) describes the hydrophilic fraction of the polymersome as discussed in the Theory Chapter.

Polymersome preparation was conducted using various methods. Typically this first involved dissolving a diblock copolymer in an organic solvent. Once dissolved, the organic solvent was usually evaporated leaving a thin film behind on the containment vessel. Once dry the samples were typically rehydrated with a buffer such as HEPES. An overview of the specific methods used along with their designated names, which will be used throughout this research, can be found in Table 2.

Table 2 An overview of the various methods used for polymersome preparation in this research.

Source(s)	Method	Designated name
H.Marsden *et al.* Polymer Chemistry 2010[49]	- Dissolve 5mg of copolymer in 1 mL of chloroform. - Hydrate with 2 mL of HEPES buffer solution. - Stir for 30 min at 45°C - Sonicate for 30 min - Stir for 24 hours at 500 rpm	M1
J.Katz et al. Langmuir 2009[50] G.Liu *et al.* Soft Matter 2012[51]	- Dissolve 5mg of copolymer in 1 mL of chloroform - Evaporate chloroform with nitrogen gas. - Hydrate with 2 mL of HEPES buffer solution and stir for 1 hour - Sonicate for 30 minutes	M2
G.Wang et al. Soft Matter 2012[47]	- Dissolve 5 mg of copolymer in 2 mL of HEPES buffer. - Stir for 1 week at 500 rpm.	M3
F.Ahmed *et al.* Journal of Controlled Release 2003 [46]	- Dissolve 5 mg polymers in 1 mL chloroform. - Dry under a vacuum for 7 hours. - Add 2 mL of HEPES buffer solution and stir for 24 hours	M4
F.Meng *et al.* Macromolecules[52 53]	- Dissolve 10 mg copolymer in 1 mL of chloroform, - Hydrate with 5 mL of HEPES buffer solution and vortex for 1 min - Stir with op vial for 2 hours.	M5
U. Till *et al.* Paper in review 2014[54]	- Dissolve 20 mg copolymer in 1 mL of chloroform, - Evaporate chloroform on rotary evaportor. - Dry under a vacuum for 4 hours. - Rehydrate with 2 mL of HEPES buffer solution at 65°C for 30 minutes - Sonicate for 1 hour at 65°C	M6

For the synthesis of biodegradable polymersomes the first four methods M1-M4 were initially used and assessed. These methods were extensively used in the formation of polymersomes composed of diblock copolymers PCL28 and PCL130 and to some extent PCL11 and PCL9. Later on, more research was carried out with M5 particularly with the use of PLA105. The last method M6 was primarily performed with the use of PCL130.

Figure 5.1 Preparation of a PCL130 sample by use of the BUCHI Rotavapor (M6). Upon evaporation of the organic solvent, a thin homogenous film can be seen to form on the flask.

Throughout this research altercations to these methods such as polymer concentration or additional sonication were made. Any changes made in these methods are further specified and can be read as addition to the designated name. For example a synthesis of a Method 1 batch of PCL_{2800}-PEO_{2000} will have the connotation M1 PCL28. Furthermore larger amounts of polymer, organic solvent and buffer of the same proportions specified were also frequently used.

5.1.1 Confocal Laser Scanning Microscope Sample Preparation

For the observation of self-assembled copolymers morphologies real time Confocal Laser Scanning Microscope was used. Copolymers were first dissolved in chloroform with a concentration of 4 mg/mL. Once dissolved, 100 µL of the chloroform solution was gently added to a vial containing 4 ml of MilliQ. After immersion of the bubble, 1 µL of pink dye was carefully injected into the chloroform. The sample was then vortexed for 30 seconds and subsequently observed under the confocal microscope.

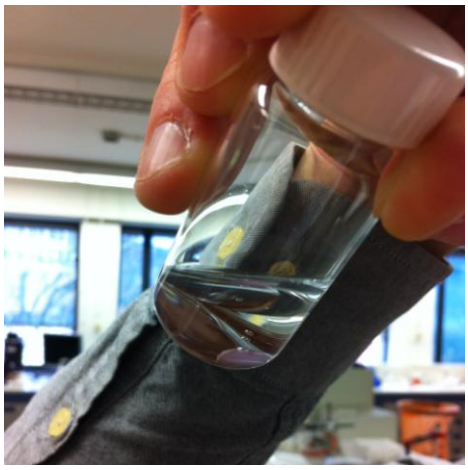

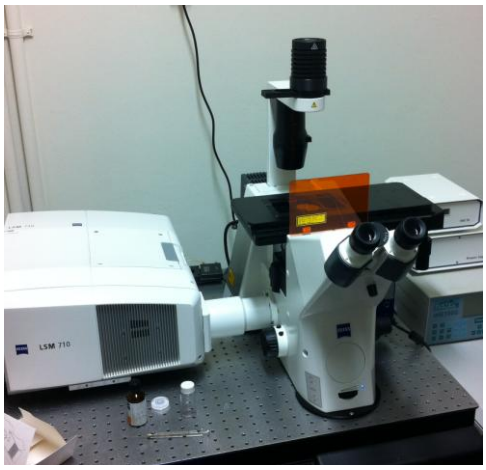

Figure 5.2 (left) Preparation of a PLA105 M5 sample for CLSM. The dyed chloroform bubble the polymersomes containing can be seen at the bottom of the vial. (right) CLSM Axio Observer z1 microscope

5.1.2 Cyro-TEM Sample Preparation

For cryo-TEM observation, 2 µL of the polymersome solution containing 0.5 mg/ml block copolymer were deposited on a perforated carbon film (quantifoil 3.5/1) supported on a TEM grid. In order to obtain a thin layer on the grid, filter paper was then used to blot the drop. The sample was vitrified by rapidly immersing it into liquid ethane (Vitrobot, FEI, Eindhoven, The Netherlands). The specimen was then inserted into a Cryo-transfer holder (Gatan model 626) and subsequently transferred to the electron-microscope (Philips CM12). Images were obtained at an acceleration voltage of 120 keV and under low-dose conditions on a slow scan CCD camera[41].

5.2 Size Exclusion

For reduction of both the size and polydispersity of polymersome samples three different size exclusion techniques were used. These were:

- Freeze-thawing
- Extrusion
- Sonication

5.2.1 Extrusion

For extrusion, polymersomes were forced through a double polycarbonate filter of several pore sizes. This was done under high pressure (c.14 Bar), starting with extrusion through two 800 nm pore sized filters. This was subsequently followed extrusion through two 400 nm filters and finally two 200 nm filters. The extrusion was performed twice for each pore size and DLS samples were taken after each extrusion step.

5.2.2 Sonication

Sonication was carried out either at room temperature or in a 65 °C heat bath where specified. Where referred to "a sonication" entails a 30 minute sonication period unless otherwise specified. For heat bath sonication, level 9 was chosen on the machines arbitrary scale.

5.2.3 Freeze-thawing

Freeze thawing was performed with two different setups for different temperature shifts. In the first case samples were alternated between a heat bath filled with water at 65 °C and a canister filled with liquid nitrogen[55]. Freeze thaw cycles were conducted in a total of 5 rounds also taking samples between each freeze thaw cycle step. Freeze thawing was also performed based on a smaller temperature shift[56]. These samples were cycled between a 2-propanol filled plaster beaker at -25 °C and air at room temperature.

5.3 Radiolabelling

Radiolabelling with Indium-111 was conducted after the synthesis of polymersomes. Radiolabelling was achieved by means of the active loading method as described in the theory chapter. Essential to note that polymersomes made with the intention of being loaded after formation were rehydrated with HEPES-DTPA instead of MilliQ for all methods as absence of chelator DTPA would render the used active loading mechanism useless. To specify concentrations, block copolymers with the intent of being loaded after polymersome formation were thus were (re)hydrated with a 1 mM DTPA[47] and a 10 mM HEPES solution.

Upon formation of polymersomes, DTPA is present both inside and outside of the polymersomes in solution. The unencapsulated DTPA was removed using a Sephadex G-25 medium mesh size exclusion column (SEC). 1 mL samples of the prepared HEPES-DTPA/polymersome solution were added to the column, catching the 1 mL faction as it came out. After the initial sample addition, 1mL of HEPES buffer solution was repetitively added again catching each fraction as it came out. Fractions containing the polymersomes typically ranged through from the 9^{th} to the 12^{th} fraction. Reason for this variance was due to differences in the column length.

After successful removal of surrounding DTPA, the loading of the radionuclide Indium-111 was initiated. For every sample of polymersome collected from the SEC column, a vial containing 200 µl of HEPES buffer solution, 10 µl of a 2 mM Tropolone and radionuclide Indium-111 dissolved in hydrochloric acid ($^{111}InCl_3$) was prepared. The required volume of the In-HCl solution varied, depending on the desired amount of activity desired for the experiment. This ranging typically between the orders of 10^2 to 10^6 Becquerels.

After the vials were prepared, 10 minutes time was given to allow for the binding of the Indium-111 to the ligand Tropolone. Then 800 µl of the collected fractions containing polymersomes were respectively added to the Indium-Tropolone prepared vials. After polymersome addition, 1 hour was allowed for the radionuclide to fully[57] actively load into the polymersomes.

5.4 Measuring the Loading Efficiency

As a measure for the loading efficiency, measurements for the relative amounts of activity in the polymersome were taken. This was done either with the Wallac of Germanium detector.

First the total activity in each of the polymersome containing vials was measured. Then using the PD-10 desalting (Sephadex G-25) columns the encapsulated radionuclides were separated. 1 mL samples of the radionuclide loaded polymersome solution were added to the column again catching the 1 mL faction as its came out. After the initial sample addition, 1 mL of HEPES buffer solution was repetitively added again catching each fraction as it came out. Fractions containing the polymersomes were collected in the 3th, 4th and 5th fraction. Fractions 6-8, containing DTPA, were also collected.

After the PD-10 SEC samples were collected, the same detector was again used to measure the activity in each fraction. This was compared then compared to the original activity, and the loading efficiency could be calculated by:

$$\varepsilon = \frac{A_{polymersome\ fractions}}{A_{original} - A_{empty\ vial}} \tag{5.1}$$

Size exclusion chromatography conducted for assessing the loading efficiency of polymersomes will occasionally be referred to as “PD-10 size exclusion”. This, solely due to the fact that size exclusion here was done through the use of the PD-10 desalting columns.

5.4.1 Leakage

Leakage of polymersomes was tested by measuring the relative amount of activity with held within the polymersome over time. Polymersomes were initially loaded as explained in the radiolabelling section with a high amount of radionuclide activity (>100 kBq). Over the course of 4 days, 250 µL of the fourth collected PD-10 fraction was removed and diluted to 1 mL with HEPES-DTPA. The initial activity of these daily samples was measured after which PD-10 column separation was again performed.

5.5 Biodegradability

Polymersome samples were made using the M5 method with different HEPES buffer solutions of pH 7.4, 6.7, 6 and 5.5. Samples of each pH were then subsequently placed in three environments of different temperatures. These were in a fridge at 5°C, in the laboratory space at room temperature and in the HELA incubator at 37°C. DLS samples were taken weekly over the course of 5 weeks.

Figure 5.3 Image of the four different pH PLA105 samples inside the HELA cell incubator.

Loading efficiencies of biodegradable polymersomes were also assessed with varying pH. PLA105 polymersome samples were made using the M5 method with HEPES-DTPA buffer solutions of pH 7.4, 6.7, 6.0 and 5.5. Once made, samples were subsequently radio-labelled and loading efficiency was measured as described in the preceding sections.

6 Results and Discussion

In the first part of this research the formation, size reduction techniques and loading efficiencies for PCL-PEO based polymersomes were assessed. Particularly PCL28 was investigated, both pure and as a blend with PBd18. Following research into PCL-PEO, PLA-PEO polymersomes were also assessed. Research was predominantly conducted with the higher molecular weight copolymer PLA105. Results on PLA-PEO formation, size exclusion and loading have however been spread through the chapter for convenience of argumentation. Results on the formation of polymersomes will first be discussed in Section 6.1 followed by the size reduction results and their corresponding discussion. Radionuclide loading efficiency and retention of PCL-PEO based polymersomes will then be discussed in Section 6.3. Flowing this section a review of PCL-PEO and its preparation will be discussed. Finishing off the chapter results for polymersome biodegradability with respect to time, loading and pH will be evaluated and discussed.

6.1 Polymersome Formation

6.1.1 DLS

In an initial way to assess formation of polymersomes, DLS size distribution measurements were made. PCL28 samples were first synthesized by methods M1 through M4 as specified in Table 2 of in the Methods Chapter. For DLS measurements, samples of each polymersome solution were diluted to concentrations 0.05, 0.1 and 0.2 mg/ml (This being the mass of diblock copolymer in the buffer solution) Size distributions were then measured for each of these concentrations for all four methods. The size distribution spectra were then individually viewed and assed for having radii profiles likely to that of polymersomes. Figure 6.1 shows one of these size distribution spectra in which polymersomes presence was best indicated. This measurement was for a Method 3 synthesized sample, measured at a concentration of 0.05 mg/ml

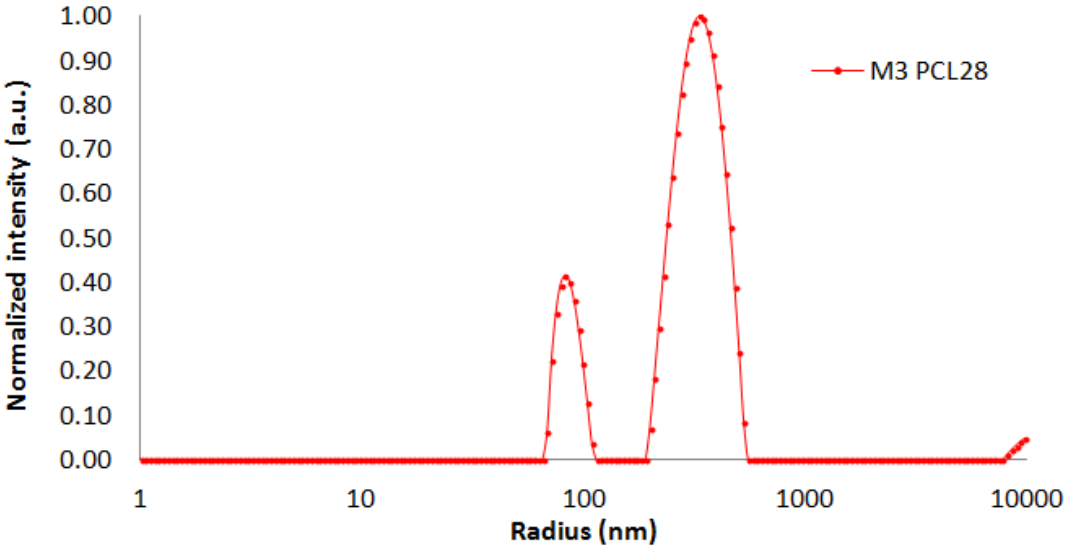

Figure 6.1 Initial DLS size distribution measurement from of a non-extruded M3 PCL28 sample. DLS sample concentration is 0.05 mg/mL with a mean count rate of 1173 kHz.

From the spectra seen above the left peak indicated the presence of a population of particles having radii ranging between approximately 70 nm and 110 nm. Specifically, DLS measurements gave a peak value of 82.4 nm at a relative intensity of 0.415. With PCL-PEO polymersomes forming in this range, a good indicator that polymersomes were made through Method 3 were found. Furthermore size distributions for PCL28 samples of concentrations 0.1 and 0.2 mg/ml also made by Method 3 also shows good indications. Samples formed by M2 also showed good DLS measurements. Bearing these results in mind, synthesis of polymersomes was particularly carried out by method M3 and also to some extent M2 for further PCL-PEO research.

In another initial way to assess the (possible) formation of polymersomes, DLS mean count rate intensities were also taken into account. Mean count rate intensities taken at constant concentration of 0.05 mg/ml for each sample can be seen below in Figure 6.2.

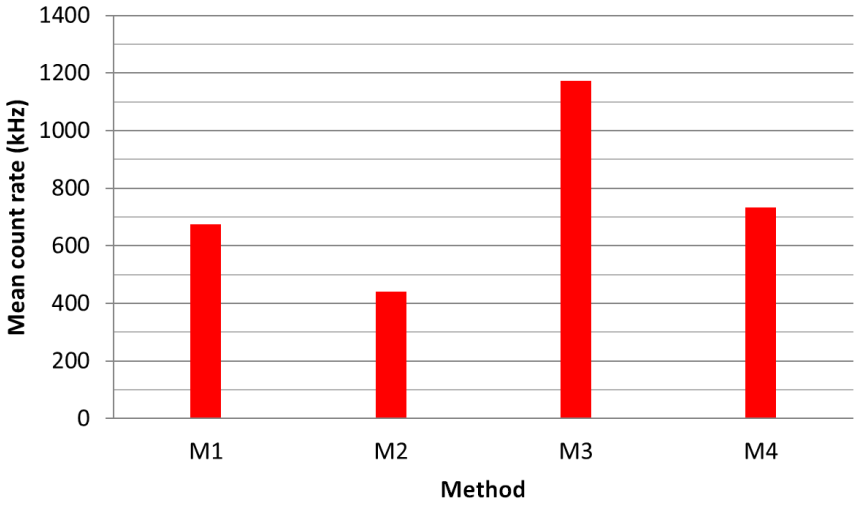

Figure 6.2 Best mean count rate intensities measured by the DLS system for non-extruded PCL28 for methods M1-M4 as described in the Methods Section. Measurements were conduction using a DLS sample concentration of 0.05 mg/ML.

It was found that methods M3 and M4 showed the highest count rates. In this being a quick and convenient method to early assess in which ways future polymersome samples should be made, M3 again was chosen in particular. Similar to M2, further synthesis by M4 was also conducted for some experiments, however M3 was primarily chosen in the majority of the research which followed.

It should clearly be noted however that mean count rate here was merely a preliminary and highly speculative indicator of a “best” or “most” formation of polymersomes. Direct correlation of mean count rate intensity to polymersome formation could be considered highly debatable. Firstly no distinction in size or polydispersity is made. Large aggregations of numerous possible self-assemblies can easily account for the lion’s share of a high mean intensity. The idea that the mean count rate is solely due to presence of polymersomes is much too big of an assumption when a sample has not been assessed by any other measurements techniques. With just these points, proportionality between the two is a big assumption but nevertheless, and as stated, this was an initial assessment and is mentioned here to underline the motivation in use of each method. For the confirmation of the presence of polymersomes in the samples, Cryo-TEM images were taken.

6.1.2 Cryo-TEM

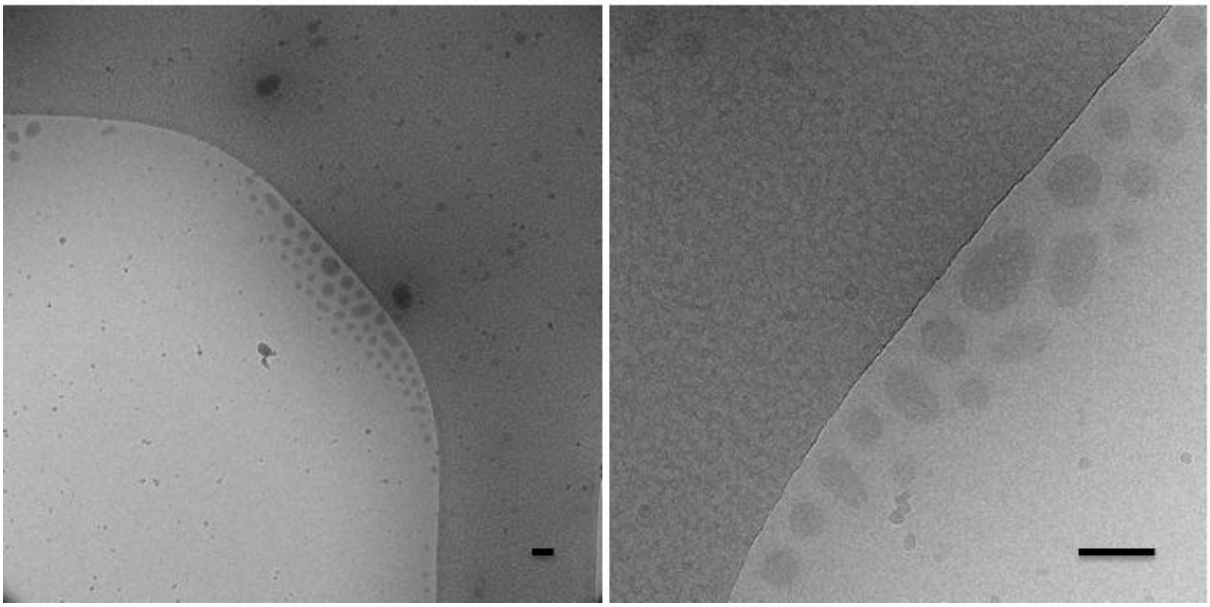

Figure 6.3 Cryo-TEM images of PLA18 sample prepared by through M5 method. Presence of polydisperse polymersomes is clearly confirmed. Polymersome diameters range from 50 to 100 nm. Scale bars are 100 nm[53].

Cyro-TEM imaging confirmed the successful formation of PLA18 polymersomes by use of the M5 method. In Figure 6.3 the spherically shaped polymersomes located at the hole of the TEM grid can be observed. Unfortunately estimation of membrane thickness proves to be a difficult task in this case. Poor contrast and resolution for both but particularly the right-hand image makes it difficult to determine a clear boundary between the membrane layer and the aqueous cavity.

6.1.3 Confocal Laser Scanning Microscopy

In order to assess possible block copolymer self-assemblies in real time, the confocal microscope was used as described in Section 5.1.1. The observation of the co-polymer dissolved chloroform droplets under the CSLM lead to promising animations. The self-assembly of macromolecule sized entities were seen to form of time. After approximately three minutes of suspension in the vortexed solution, collective disintegration the chloroform droplets could be observed. A time lapse of three key frames capturing this process can be observed in Figure 6.4

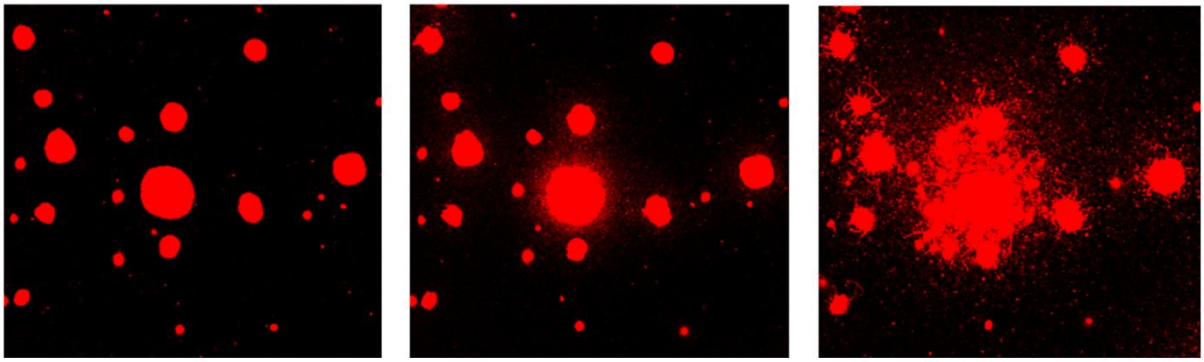

Figure 6.4 Time lapse images of possible polymersome formation obtained from confocal laser scanning microscopy. The chloroform droplets seen above in red burst collectively upon which the PLA105 diblock co-polymers assemble to form smaller aggregates, seen as smaller spots in the rightmost picture. Images were taken at 30 second intervals.

Looking at the first picture, stable chloroform bubbles can be seen suspended in solution. Over the course of 30 seconds, the bubbles are first seen to deform followed by collective bursting of the entire population. This can be seen in the middle picture, where small specs, particularly around the larger bubbles can be seen. In the last frame the situation slightly after collective bursting can be seen. Multiple polymersomes and other entities can been seen to emerge from each of the chloroform bubbles, this all happening within a very short time-span of approximately 30 seconds.

The hypothesis on which polymersome self-assembly is based in this case can be envisioned with the help of Figure 6.5. In being amphiphilic, the diblock copolymers dissolved in the chloroform will naturally seek the droplet interface with the buffer solution (as seen in the intermediate step below).

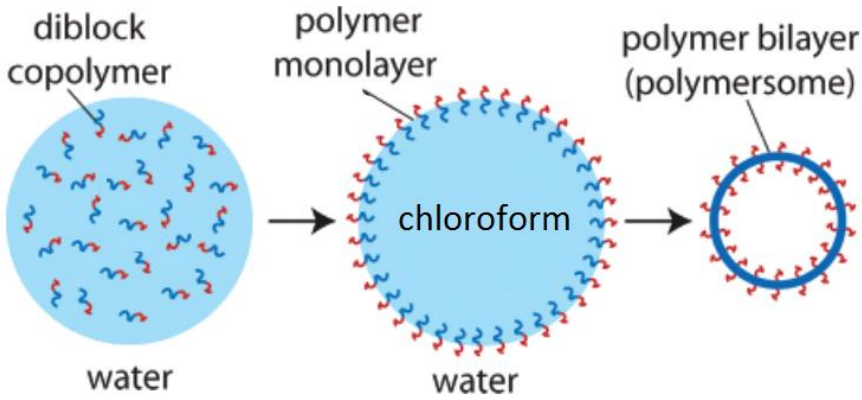

Figure 6.5 Schematic for the formation of polymersomes from a chloroform drop in water based buffer. Amphiphilic diblock copolymers dissolved in the chloroform assemble into a monolayer at the water-chloroform interface. Instability of the droplets in water eventually leads to the formation of polymer bilayers and thus polymersomes.

With the hydrophilic PEO block suspended in the buffer solution and PLA still in the bubble a polymer monolayer is formed. Over time, natural accumulation of all copolymers on the interface boundary precedes, leading to overall instability of the entire bubble. Once the overly instable the droplet collapses, the copolymers are left to re-assemble into in the buffer solution. As discussed in Section 2.3 of the theory, characteristics such as packing parameter p and the molecular weights of the two block polymers will largely determine the both self-assembly mechanism as well as the morphology. Considering PLA105 with a f_{EO} of 0.42 self-assembly into (primarily) polymersomes would be probable. Unfortunately optical confirmation of these macromolecules/self-assemblies indeed being self-assembled polymersomes is not possible with the magnifying power of the CSLM. But although not giving a confirmation, CLSM is still very useful in giving a decent idea of how the PLA-PEO polymersome formation method works.

6.2 Polymersome Size Reduction

For the eventual application of biodegradable polymersomes as tumour targeting agents, it is seen as essential that they become of size small enough to be able to utilize the EPR effect. Size reduction techniques for PCL-PEO and PLA-PEO polymersomes were thus conducted and assessed. As reported earlier accumulation by means of the EPR effect requires nano-carriers to have an upper diameter cut-off limit of around 200 nm. Beyond this size, they would be too large for promising accumulation be means of the EPR effect. Results in this section thus worked towards attaining polymer vesicles below this cut of limit, bearing in mind that actually even lower diameters should be taken into consideration (Section 2.2.2).

6.2.1 Extrusion

Size exclusion by extrusion was conducted for all three PCL molecular weight samples as well as the heavier PLA105 as described in Section 5.2.1. For PCL28, PCL130 and PLA105 polymersome samples, extrusion ultimately led to the extraction of colourless samples, demonstrating low mean intensities measured by the DLS. Particularly in extruding through the 200 nm filter, PCL28 was observed to lose a very large portion of its contents. PCL130 showed substantial loss of contents after only having passed through the initial 800 nm filter. PLA105 showed a more gradual decrease in intensity per step, but ultimately filtrated significant amounts of block copolymer (structures). Mean count rates of the various PCL and the PLA105 samples along with their reductions per filter can be observed in Figure 6.6 along with Table 6 found in Appendix 9.1.

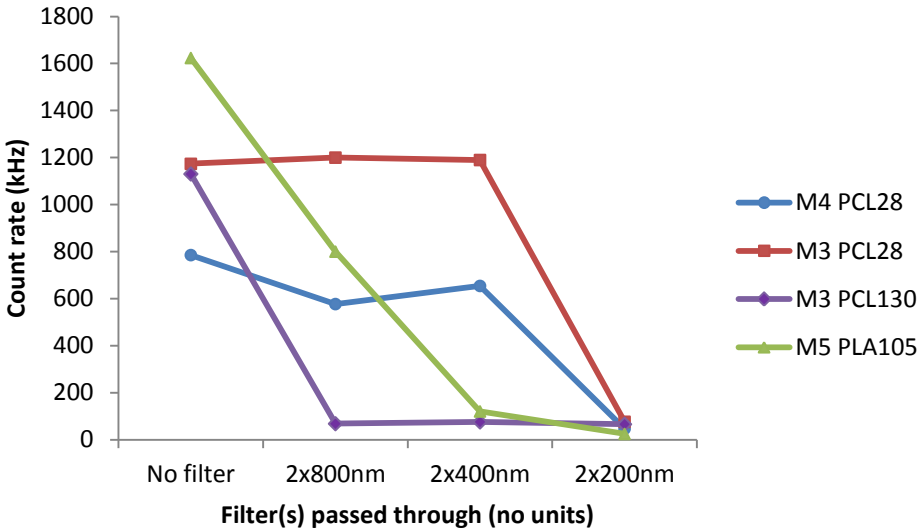

Figure 6.6 Mean intensities of various polymersome samples after sequential two-fold extrusion through 800 nm, 400 nm and 200 nm filters. Concentrations of DLS samples were 0.05 mg/mL for PCL28 and PCL130 samples and 0.2 mg/mL for PLA105.

For M3 and M4 of PCL28 we observe a steep declination in the mean intensity after extrusion through the 200 nm filter. Whereas polymersome solutions are usually whitish of colour, the extruded solutions were colourless, indicating that polymersomes (or polymer aggregates) remained in the filter and only few or no polymersomes could successfully pass through the filter.

Furthermore for the extrusion of PCL130 samples very low count rates were observed after only passing through the 800 nm filter. This could be attributed to the fact that the higher molecular weight PCL-PEO block copolymers prefer formation of rigid low curvature (f_{EO}=0.28) polymer vesicles[58]. High pressured extrusion through filters of these large rigid polymersomes could then lead to the significant rupturing of the membrane, especially when forced onto the filter pore holes. With the membrane disintegrated into significantly smaller membrane fragments, it seems plausible that after the first extrusion near zero count rates on the DLS are measured. This is furthermore was found to be the case in recent research[59] where at 25 °C rigid PCL-PEO vesicles placed under increasing pressure initially showed no deformation after which abrupt rupturing was observed.

Deformation upon filter extrusion in this case is found to be opposite to the desired fluid-like deformation found in earlier work with amorphous PBd-PEO polymersomes. In an attempt for improving size exclusion prospect for PCL-PEO, preparation of blended PCL-PEO PBd-PEO polymersome samples for size exclusion were later performed and accordingly discussed over the page.

Noteworthy was however that the mean intensities of the PCL11 sample remained relatively high after each extrusion filter step and, more importantly, extrusion through the 200 nm filter still allowed for a mean intensity above 400 kHz indicating possible polymersome presence. Furthermore the size distributions from these DLS measurements after every filtration step consistently showed promising, comprehensive results.

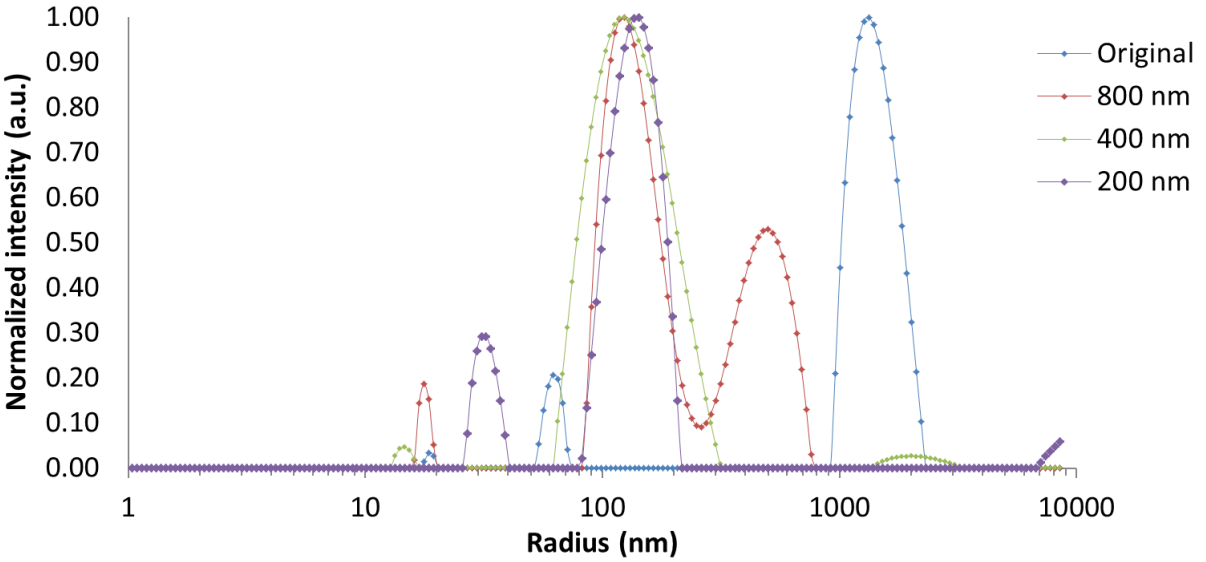

Figure 6.7 An overlay of DLS size distributions for an M2 PCL11 sample. Extrusions are subsequent, with two-fold extrusion through each filter. Sample mean intensities are 1614 kHz, 1545 kHz, 1150 kHz and 228 kHz respectively. DLS vial concentrations were 0.2 mg/mL for the original, 800 nm and 400 nm filters and 0.125 mg/mL for the 200 nm filter.

As seen in Figure 6.7 it can be deduced that extrusion through the initial 800 nm filter led to the complete removal of aggregates of radii larger then about 900 nm. Subsequent extrusion through the 400 nm filters also led to the filtration of larger polymersomes and aggregates with radii of about 350 nm and larger. Size distribution for the 200 nm also confirms the absence of aggregates and particles larger than about 200 nm.

Along with its size distribution, the relative decrease per filter in mean intensity for PCL11 samples show that it has good extrusion prospects. This could indicate that either less rigid polymersomes are formed, allowing them to pass through filters more easily, or that the polymersomes which are formed are smaller to begin with and therefore disaggregate more easily than heavier variants.

Along with the extrusion of PCL11, a blend of PCL28-PBd18 made by method M3 was also found to successfully undergo size reduction. For preparation of the blended polymersomes sample, PBd_{1800}-PEO_{900} block copolymers were dissolved in equal mass ratio with the PCL_{2800}-PEO_{2000} block copolymers. The remaining steps in the M3 method were then identically conducted, to obtain a blended polymersome formation.

Extrusion through the 800, 400, and 200 nm filters for PCL28-PBd18 blended polymersomes as said, led to promising DLS size distribution measurements as seen in Figure 6.8

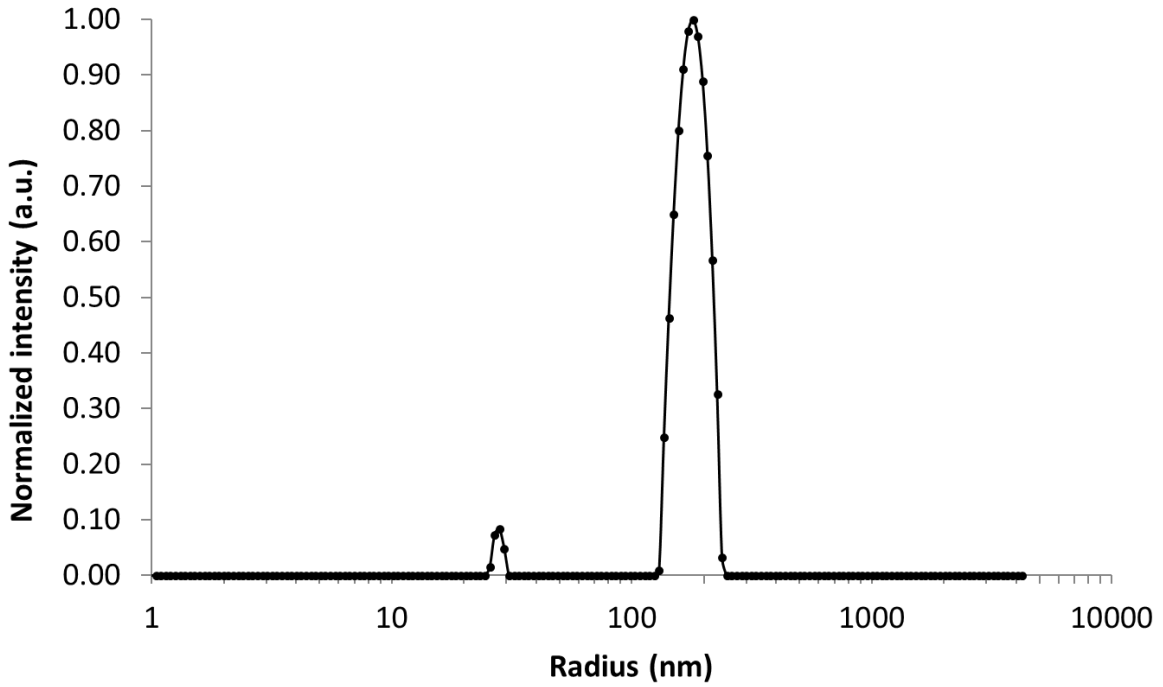

Figure 6.8 Size distribution an extruded M3 PCL28-PB18 blend sample, measured by a Dynamic Light Scattering setup. Sample mean intensity is 501 kHz.

Extrusion produced a monodisperse solution of particles having an average radius of 188.5 ± 8.5 nm. As a remark, the small peak in the 20-30 nm range gives the notion that the solution is not entirely monodisperse, this probably owing to the presence of PCL28 self-assembled micelles. Formation of some PCL28 copolymer micelles would be likely due to the relatively high hydrophilic fraction (0.42) of PCL28.

Furthermore noteworthy is that extrusion in the presence of PBd-PEO composed polymersomes did not show any significant decrease in DLS mean intensity. This in contrast to numerous other extrusion attempts containing solely PCL-PEO based polymersomes. PCL28 and PCL130 formed polymersomes that particularly proved to have great difficulty in passing the polycarbonate filters. Underling reasons for this finding can be largely attributed to the difference in polymer packing properties of the two hydrophobic blocks. As seen in Figure 6.9, the two hydrophobic blocks PCL and PBd possess distinctly different space filling models.

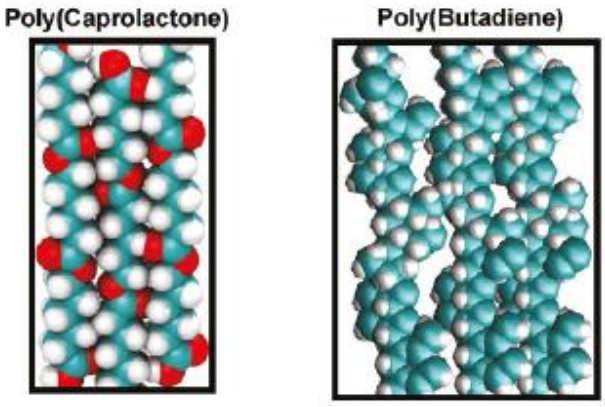

Figure 6.9 Chemical structure space filling models of polycaprolactone (left) and polybutadiene (right) blocks[59]. Here semicrystalline packing of PCL is observed in comparison to the lose amorphous configuration of the PBd polymer block.

Here PBd is observed to have much more spacing between polymer chains, leading to an amorphous configuration. This in contrast to PCL, where semicrystalline packing allows for no manoeuvrability between polymers making the membranes it composes rigid. Extrusion therefore would largely favour solely the passing of PBd containing polymersomes. Measurements here could therefore be pure PB18 samples.

Whether synthesis of PCL28 and PBd18 did indeed lead to the formation of blended polymersomes remains hard to determine using DLS instrumentation. Radii measured by DLS of 200 nm filter extruded PBd18 samples in other works were reported to be 118 nm[47]. This value lying below the established radius range of 188.5 ± 8.5 nm makes it unlikely that the polymersomes are entirely PBd-PEO based. It however remains difficult to establish the composition of the polymersomes and a secondary means to assess the polymersomes size and membrane thickness would be of great value. Cryo-TEM imaging of this sample and comparison to earlier Cryo-TEM images of pure PBd18 polymersomes prepared by the non-organic (M3) solvent method could confirm blended formations or the absence thereof.

6.2.2 Freeze-thawing

Due to the poor intensities of the PCL-PEO samples, particularly after the 200 nm filter, freeze-thawing methods were also assessed in an attempt to reduce polymersome size. Freeze-thawing methods for PCL28 were carried out for two different temperature ranges as specified in the Methods Chapter, Section 5.2.3. PCL28 was freeze-thawed both as a pure and as a PBd18 blended sample. After freeze-thawing, both samples retained their milky character, indicating macromolecular structures still remained with the samples. In assessing these structures, DLS sample measurements were once again taken. For each freeze-thaw cycle a measurement of the size distribution was assessed, and the mean intensities for each cycle were accordingly observed. Mean intensity changes after each cycle for both samples are shown in Figure 6.10

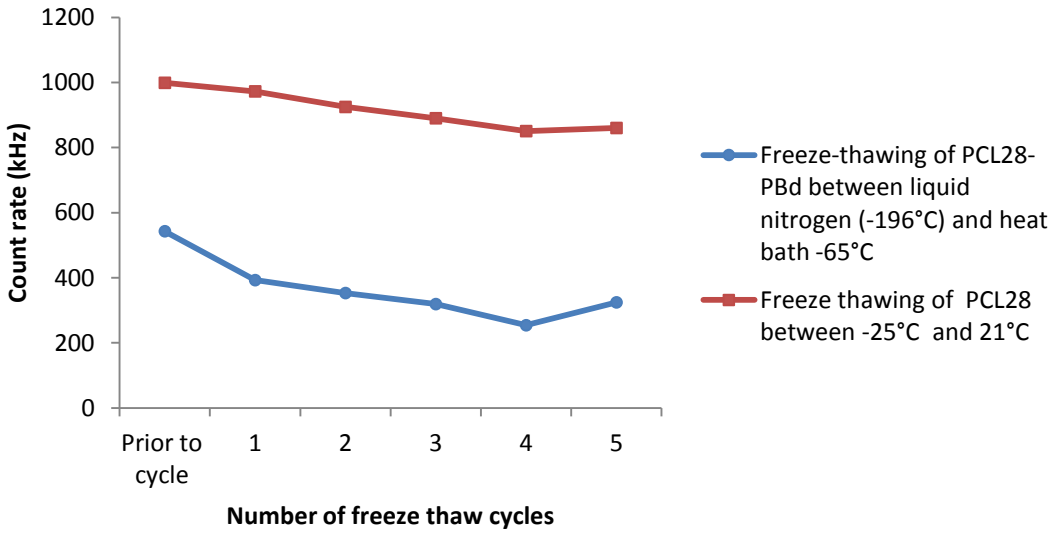

Figure 6.10 Mean intensities of an M3 PCL28 and an M2 PCL28-PBd18 sample after accumulative freeze-thaw cycles. DLS sample concentrations were 0.05 mg/mL.

For both samples significantly less loss of mean intensity as compared to extrusion was observed. Size exclusion prospects in both cases are however disappointing. After five complete freeze thaw cycles in each case, the largest size peaks were still found in the ≥700 nm radii range, indicating that the breaking up of larger aggregates did rarely occur. The freeze-thawing of PCL28 did not prove to be an effective way of achieving a smaller monodisperse population of polymersomes.

In contrast to the PCL based samples, PLA105 size exclusion methods did show better prospects. Size distributions for an original, sonicated and freeze-thawed samples of M5 PLA105 polymersomes can observed in Figure 6.11.

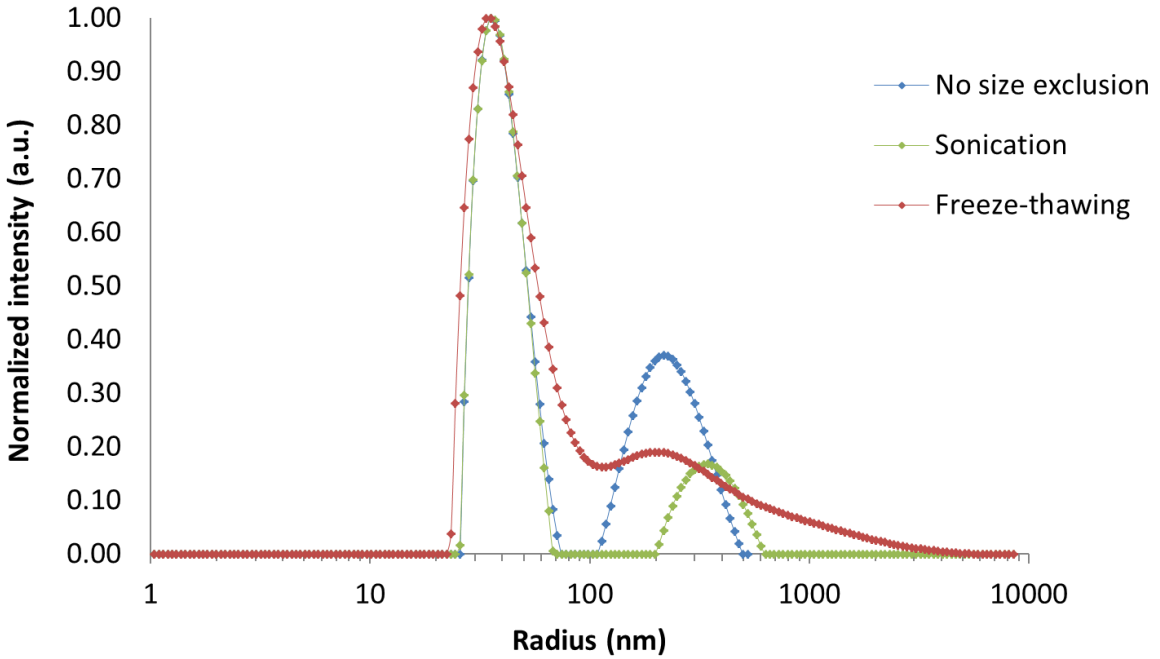

Figure 6.11 Size distributions of non-size excluded (blue), sonicated (green) and (red) freeze-thawed M5 PLA105 samples, measured by a Dynamic Light Scattering setup. Sample mean intensities are 564 kHz, 600 kHz and 583 kHz respectively. The large peak of the non-size exclusioned sample is overlayed by the other two peaks. Freeze-thawing was conducted for 5 cycles and between -196 and 65 °C as with PCL28.

The original non-size excluded sample (in blue) shows a wide aggregate peak off to the right at 210 nm. Upon sonication an approximate 2 fold decrease in intensity of the aggregate peak occurred, indicating a significant aggregate population decrease. Aggregates which did remain however were of larger sizes, as seen by the peak shifting to the right. Similarly for Freeze-thawing, reduction of the aggregate peak was observed and size distribution overall moved to smaller radii populations. Sonication and freeze-thawing were thus successful with the use of PLA105 polymersome samples.

Size exclusion methods for PLA based polymersomes proved to be more successful with PCL block copolymers. Earlier research[53] conducted by N. Stigter showed also that for lighter weight PLA based polymersomes, samples could easily be extruded through the 800, 400 and 200 nm filters. Reason for PLA outperforming PCL in size reduction prospects could largely be attributed to high crystallinity of the PCL polymer block, as observed with PCL130. In the following section, more results will also show to be affected by PCL's block crystallinity, these will be addressed accordingly.

6.3 Loading of Indium-111

As established in the Theory Chapter encapsulation of radionuclides into polymersomes vesicles is of key essence for their application in nuclear medicine. In this subsection, the extent to which biodegradable polymersomes PCL28, PCL130 could encapsulate Indium-111 was assessed. This was done by determining the loading efficiencies of the polymersomes after active loading of the radionuclide had taken place (Section 5.4).

6.3.1 Loading Efficiencies

Loading efficiencies for PCL28 based polymersomes were determined for preparation methods M2 and M3. Table 3 provides an overview of the highest loading efficiencies obtained for various samples. Measurements were taken from multiple SEC fractions and loading efficiencies were averaged from fractions containing the highest amount of relative activity. Furthermore loading efficiencies for the heavier PCL130 were also assessed and can be observed over the page in Table 4.

.

Table 3 An overview of the highest loading efficiencies of PCL28 through use of the different methods measured using the Wallac detector. Original activity was not kept constant based on the fact that the amount of activity loaded is independent of the loading efficiency for small activities[60].

Method	Diblock copolymer	Loading efficiency	Stn. Dev.	Original activity (Bq)
M2	PCL28	29%	2%	11249
M3	PCL28	36%	7%	27127
M3	PCL28-PBD18 blend	50%	5%	22235
M3S	PCL28 (Cryo-TEM sample)	76%	6%	40035
M2	PCL28	60%	14%	33463
M6	PCL28	80%	13%	34928

Table 4 An overview of the highest loading efficiencies of PCL130 through use of the methods M2 and M6 measured using the Wallac detector.

Method	Diblock copolymer	Loading efficiency	Stn. Dev.	Original activity (Bq)
M2	PCL130	64%	8%	19463
M6	PCL130	82%	7%	36003

As reflected in the two tables, method M6 showed to have significantly higher loading efficiencies both for PCL28 and PCL130. For PCL28 loading efficiencies of up to 80 ± 13 % were found. Furthermore for PCL130 based samples, loading efficiencies of 82 ± 7 % were established from three individual loading trials of separately prepared samples. This entails that M6 not only had the highest degree of loading efficiency but also by far the highest amount of repreduciblity for the loading PCL-PEO based polymersome samples. This in contrast to numerous loading attempts by preparation methods M2-M4 for the PCL-PEO based polymersomes and M5 preparation of PLA105, which lead to poor loading efficiencies.

More promising prospects for the high loading efficiencies by method M6 could be found in the activity distribution of their PD-10 size exclusion fractions. Relative activities collected per fraction for both PCL28 and PCL130 by Method 6 are shown below in Figure 6.12

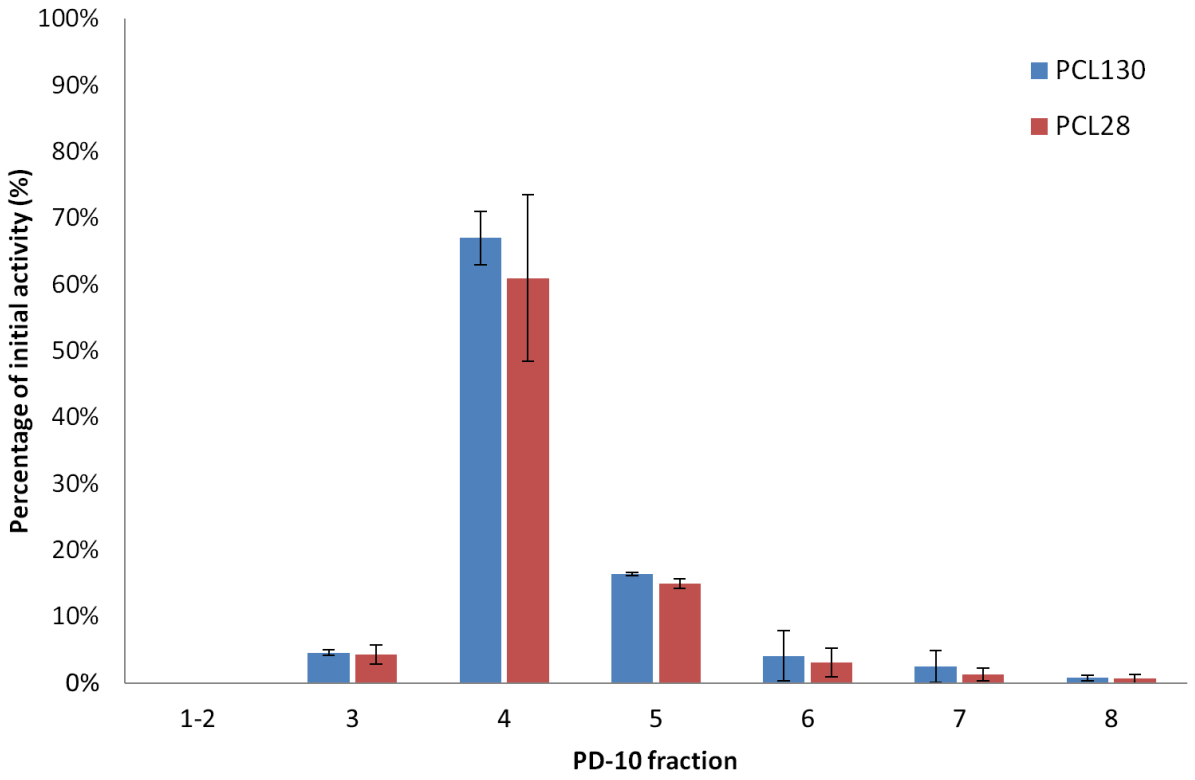

Figure 6.12 Relative amounts of radionuclide activity collected in SEC fractions for a loading trial of both PCL28 and PCL130 samples made through method M6. As explained in the Methods Sections, fractions 3 to 5 represent the fractions in which the polymersomes were collected. Samples were measured with the Wallac and an initial activity of 35 ± 2 kBq was administered in both runs.

As seen above and noted from individual loading trials, all M6 samples by far showed the largest amount of activity to be found in the fourth fraction. From previous work[57] it is known that the majority of polymersomes deposit in the fourth fraction after PD-10 column size exclusion has been conducted. A high amount of relative activity in this fraction is therefore a good indicator of loaded polymersomes, which is the case here.

PCL based polymersomes, synthesized by method M6 thus indicated to have a significant capability in encapsulating Indium-111 radionuclides. Bearing their improved encapsulating ability in mind, there thus is a strong notion that PCL-PEO polymersome formation here is particularly successful.

To determine how much of the activity was actually loaded into the aqueous core of the PCL130 polymersomes, the loading efficiency in the absence of the chelator DTPA was determined. Results for two separate non-DTPA loading trials can be observed in Table 5.

Table 5 Loading efficiencies of M6 PCL130 formed and loaded in absence of chelator DTPA.

Method	Diblock copolymer sample	Loading efficiency	Stn. Dev.	Original activity (Bq)
M6	PCL130 made with chelator DTPA	59%	15%	7772
M6	PCL130 made with chelator DTPA	55%	10%	12305
M6	PCL130 with Indium precipitate removed (from former loaded sample above)	65%	1%	4610

Loading of radionuclides in PCL130 polymersomes in the absence of DTPA led to loading efficiencies of 59 ± 15 % and 55 ± 10 % for Method M6. This indicates that well over half of the Indium-Tropolone complexes could have accumulated in the hydrophobic membrane. Compared to loading efficiencies found for PBd-PEO polymersomes containing no DTPA, these loading efficiencies could be regarded relatively high[60].

However considering the long hydrophobic block length and a closely linked low f_{EO} fraction of 0.28 of PCL130, it is thus quite likely that the lipophilic Indium-Tropolone complexes are encapsulated in the relatively large hydrophobic membrane of the polymersomes. In verification of this amount of activity actually being loaded into the polymersome membrane, a separate experiment was conducted to ensure that the presence of Indium-111 (in the form of a precipitate) is not accounting for activity assumed to be loaded in the polymersome.

Explaining this experiment in slightly in more detail; activity collected in fractions 3-5 from PD-10 could, beside the presence of loaded polymersomes, also be attributed to free Indium precipitate floating around inside the prepared solution. Addition of hydrochloric acid to decrease the pH in the buffer solution surrounding the loaded polymersome containing fractions allows for the free Indium ions (In^{3+}) to form. Since the Indium ions do not collect in the polymersomes associated fractions 3-5, an improved assessment of the amount of loaded activity can be made.

Loading after removal of Indium precipitate can also be seen as the in last row of Table 5. It should be noted that for the precipitate check, loading efficiency with respect to activity in the fourth collected fraction is taken and not of the initial (total) administered activity. Loading efficiencies with Indium precipitate removed still showed to be 65 ± 1 %, indicating that the high loading efficiencies found earlier can mostly be accounted to polymersome loading.

6.3.2 Leakage

To further assess the leakiness of PCL polymer vesicles, the retention of the Indium-111 radionuclide by the loaded polymersomes determined. This was conducted by means of the process described in Section 5.4.1 of the Methods Chapter. M6 PCL130 block copolymer based samples were loaded and over the course of 3 days the relative amount of activity which remained in the polymersomes was determined. Figure 6.13 shows the amount of activity with held by the M6 PCL130 polymersomes over 24 hour intervals.

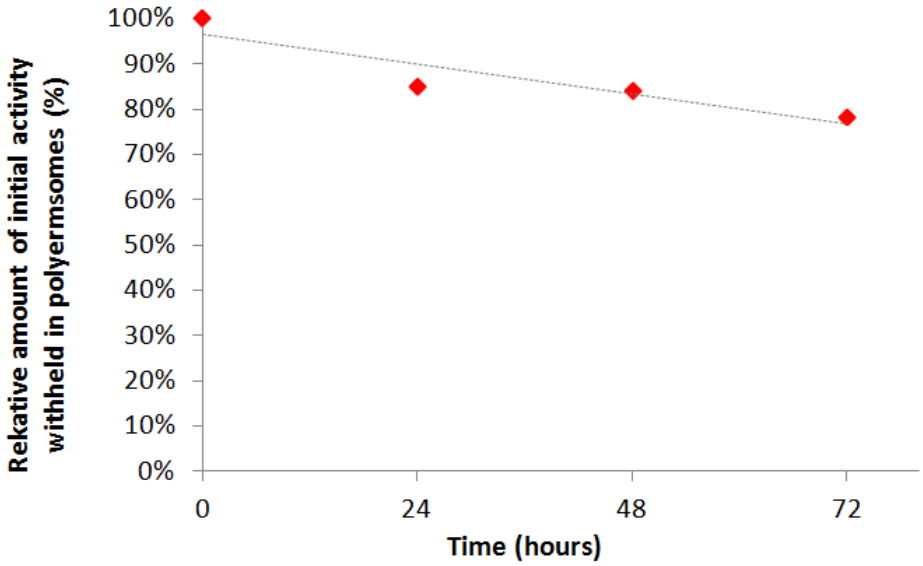

Figure 6.13 Retention of the relative amount of radionuclide activity from Indium-111 of M6 PCL130 polymersome samples over time.

Retention here showed a gradual decrease over 72 hours, PCL130 polymersomes were samples were still able to retain 78% of the initial administered activity. This has however only been determined on the basis of one data set and so remains unreliable, but it is however a good indicator the polymersome membranes largely remained intact with this time.

6.4 PCL-PEO Preparation and Formation

With the preparation method M6 having achieved much better results both loading efficiencies and retention rates, it remains yet to be discussed why for PCL-PEO, M6 worked so much better in comparison to earlier methods. In looking at as to what makes this method different from the other it can be noted that there were two key important changes which could have led to these improved results.

These two changes were namely:

- How the samples were stirred upon block copolymer film rehydration
- The temperature at which film rehydration (and thus self-assembly) occurred.

Both of these will be discussed below.

To begin with stirring, samples synthesized using M6 were mixed by the Rotavapor. Upon rehydration, stirring occurred exclusively due to the slow turning of the conical flask. The stirring here was thus smooth and gentle and upon rehydration, M6 solution samples were found to be “milky” in character, greatly resembling that of samples containing PBd-PEO based block copolymers.

This stirring method and corresponding results are in great opposition to what was found in methods M1-M4 for PCL-PEO. Stirring after rehydration here was performed by use of a stir bar spinning the self-assembling copolymers dissolved in the organic solvent rapidly around the small scintillation vials in which they were contained. Although stirring through use of the rotating magnet does not have to be considered rapid, necessity for a more delicate stirring could possibly help. This is furthermore mentioned in research conducted by Discher *et al.* concerning the formation of PCL-PEO polymer vesicles[59]. Here PCL-PEO samples are prepared by a number of different methods. In each approach however "gentle stirring to avoid fragmentation of growing assemblies" was conducted. With Discher et al.'s preparation methods leading to successful PCL-PEO polymersomes formation here, stirring might play a role in successful PCL-PEO polymersome synthesis. Considerations above could allow us to argue that stirring plays at least a small part in improving their formation.

The temperature at which self-assembly of PCL based vesicles occurs could also play an important role in their successful formation. From earlier research, clear evidence can be found that during film rehydration, increased temperatures led to less leaky and more polymersomes. This is clearly demonstrated in a paper by K.Rajagopal and co-workers, where PCL-PEO block copolymer based polymersomes are observed after rehydration occurred at temperatures of 60, 43, and 25 °C, as seen in Figure 6.14.

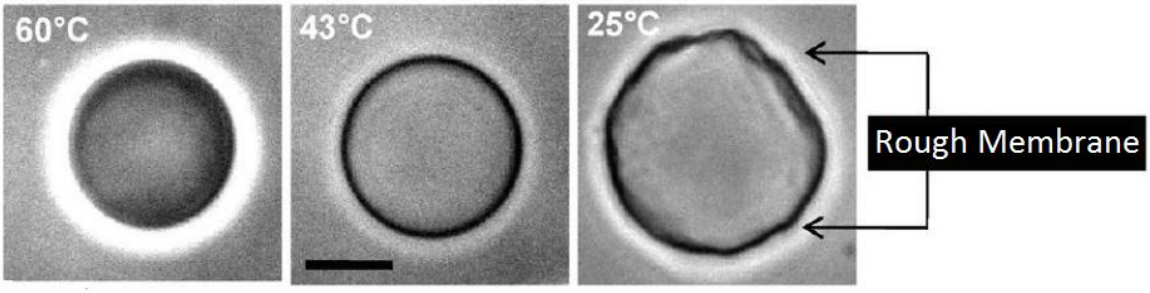

Figure 6.14 Representative phase contrast images demonstrating the rigidity of PCL-PEO membranes. PCL_{13000}-PEO_{2000} vesicles imaged after equilibrating at 60, 43, and 25 °C. The vesicles were prepared by film rehydration at 60 °C in. The retention of sucrose within vesicle at 60 °C is evident from the phase dark image shown in left panel while the image of a crystalline membrane roughened by a dislocation defects can be seen on the right[59,61].

Phase contrast images of PCL based vesicles appear smooth and rounded at 60 °C. At the intermediate temperature of 40 °C the PCL-PEO vesicles appear smooth but most have lost their phase contrast. It can be seen that film rehydration at 60 °C yields larger vesicles and that they appear to be smoother and rounded at 60 °C.

In considering vesicle leakiness here, polymersomes were made in a solution of 300 mOsmolar sucrose, which gave a dark colour on the phase contrast image. The 60 °C polymersomes can be seen to appear dark due to the refractive difference between outer solution and the retained inner solution. While with 25 °C, the vesicles not only appeared rough and irregular as said earlier, but also lost the phase dark contrast from its former sucrose contents. Though this research was conducted with sucrose as encapsulant, it is however very coherent to what was observed to be the case with radionuclide loading of PCL-PEO polymersomes (Section 6.3.1) prepared by methods at room temperature (M1-M5). Thus from literature and our experiments discussed above it can be verified that at lower temperatures membranes composed the PCL-PEO blocks exhibit increased leakiness.

At lower temperatures, self-assembly of PCL-PEO polymersomes have thus been observed to lead to cracks and/or holes in the membrane. Furthermore in other research[59], cases of poor and even no initial formation of PCL-PEO based vesicles has been observed for these temperatures (See Figure 9.2 of A9.2). It was found that At 25 °C PCL-PEO polymers did not assemble under similar conditions to that of method M3, even after 2 weeks, whereas PBd-PEO samples generated worm micelles overnight. Findings here prove to be consistent our own findings from Cryo-TEM imaging. Pictures taken PCL28 based samples prepared under similar conditions can be seen in Figure 6.15. These Cyro-TEM pictures demonstrate the absence of self-assembled polymersomes, correspondence to the paper discussed. Furthermore from the images, one can infer from the formation of lamellar disks, possible indicators of rigid PCL-PEO morphology formation. Further discussion on the scientific interpretation of the Cryo-TEM images of Figure 6.15 follows.

Although the combination of sharp defined peaks from DLS measurements along with a high loading efficiency can provide an excellent indication of polymersome presence (and size), for the actual verification of their existence, Cryo-TEM images are necessary. Figure 6.15 for example shows a Cryo-TEM image taken of what was assumed to be a PCL28 polymersome sample.

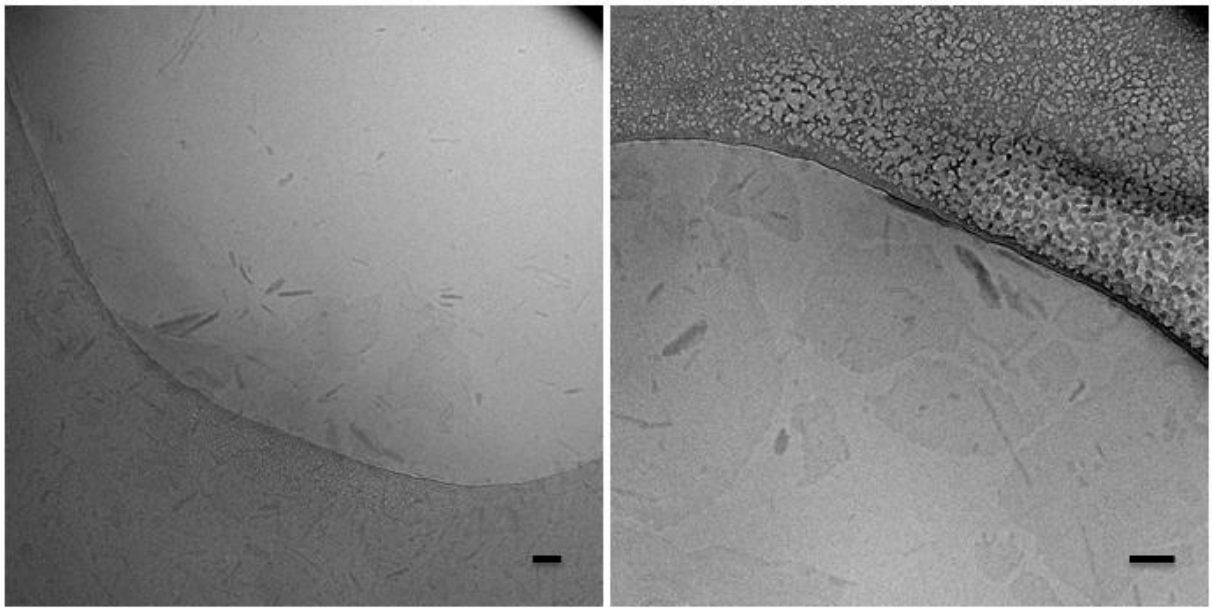

Figure 6.15 Cryo-TEM images of a M3 PCL28 (conc. 2.5 mg/ml) which was daily sonicated for 30 minutes over a period 5 days. As clearly can be seen the sample contains flaky shaped disks in what mostly likely seems to be a (multi-)lamellar phase in absence of nano-particles. Polymersomes cannot be observed. Scale bars are 100 nm.

The Cryo-TEM images here however show no supporting evidence for biodegradable polymersome self-assembly. What can be seen is solely the formation large (possibly multi-)lamellar disks, lying both flat and perpendicularly towards the camera lens.

Despite these images, size distribution spectra of this sample from DLS measurements seemed to be slightly more promising. As seen from one of these distributions in Figure 6.16, sample solutions were indicated to have a collection of particles with radii of ± 100 nm (as indicated by the left peak). Even though this peak can still be considered somewhat wide, there could still be presence of particles smaller than that of the lamellar phases observed in Figure 6.15. Poor correspondence between the Cryo-TEM and the DLS system could thus be noted here.

On the other hand, the wideness of the peaks allows for a size range which could correspond to the small and large lamellar disks. This remains a limitation for DLS measurements as it can never tell you whether you have polymersomes or not but just a smaller species. The Cryo-TEM sample was however not only chosen because of its size but also because of its loading efficiencies, discussed below.

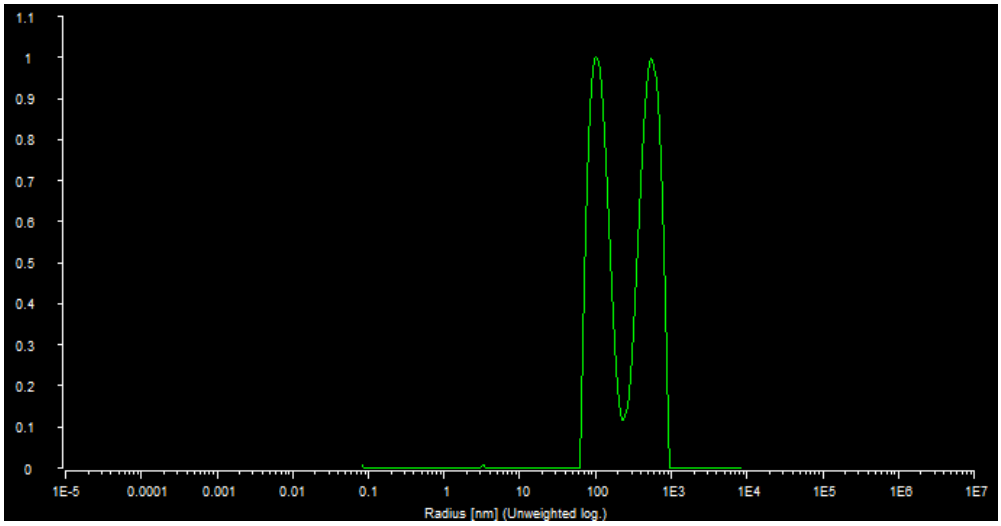

Figure 6.16 DLS measurement of the non extruded M3 size distribution of the PCL28 Cryo-TEM sample measured at a concentration of 0.1 mg/ml and a net count rate of 507 kHz.

The radionuclide loading efficiency of this sample was found be up to 76 ± 6 % as seen earlier in Table 3. In noting this, one could suggest the idea that high loading efficiencies need not imply that there be polymersomes present at all, a rather unfavourable claim considering the context of this research. Luckily, there are a number of arguments which can alleviate this inconsistency.

One could make the assumption that there is some sort of entity or mechanism causing radionuclides to be deposited in the polymersome containing fractions (3-5) during PD-10 size exclusion. Whether this is to do with the possible carrying of radionuclides by unusual block copolymers structures (i.e. possible entrapment of radionuclides in between lamellar layers) or perhaps the deposition of Indium precipitate remains speculative, but these mechanisms could provide an explanation as to why this inconsistency occurred.

A second explanation accounting for this inconsistency would be to consider the quality with which the actual taking of the Cryo-TEM images took place. It was thought that these externally taken Cryo-TEM images were made by an individual having little experience in providing quality Cryo-TEM images. Furthermore only two images were delivered for the sample sent. The Cyro-TEM images therefore need not to represent what the complete the contents of the supplied sample would be. Ideas as to how to increase and improve Cryo-TEM sampling can be found later on in the Recommendations Chapter.

6.5 Biodegradability

After the formation polymersomes it was also of interest to assess their biodegradability. In order to assess a profile of how well these polymersomes break down over time as well as when the undergo acidity and temperature changes found in the body.

6.5.1 Mean Intensity

In assessing the biodegradability of the polymersomes, experiments were thus conducted as described in Section 5.5. The figures below show the mean count rates measured every week by the DLS, the top graph being in the fridge (4 °C), the second being in the laboratory (22 °C), and the third inside the HELA incubator (37 °C).

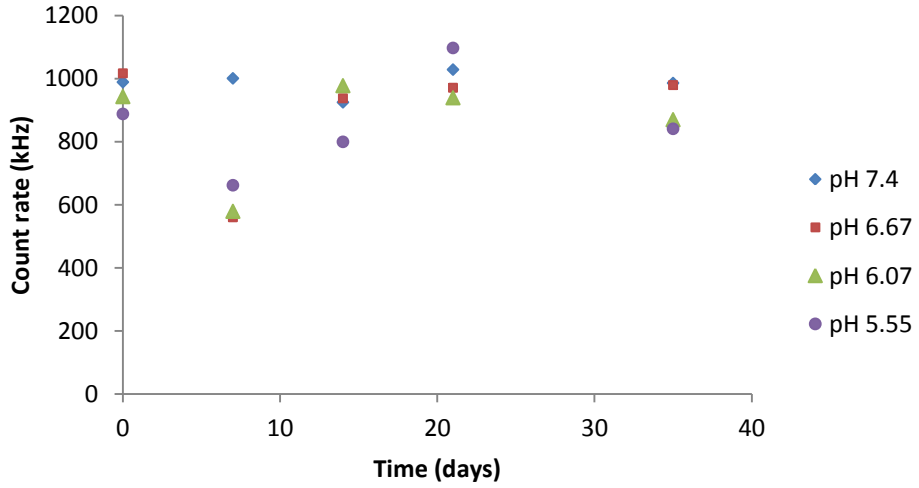

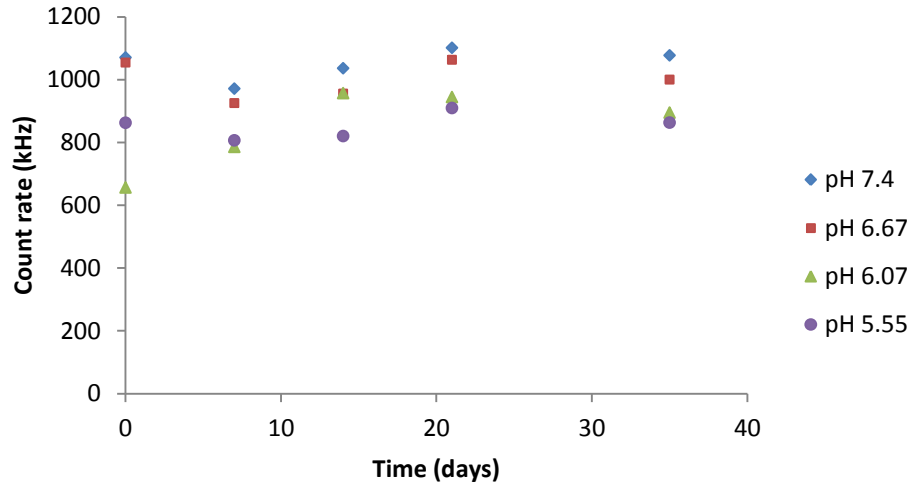

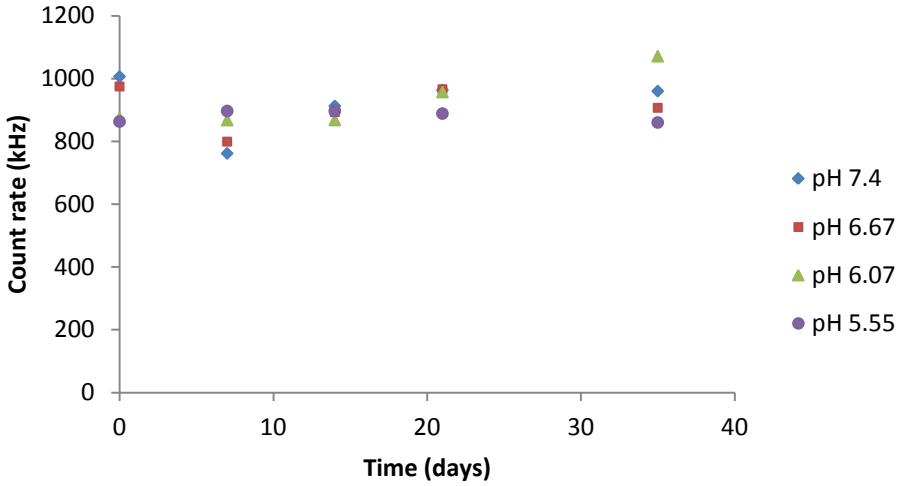

Figure 6.17 Intensity over time for different pH's of M5 PLA105 in three different temperature environments. (Top) samples refrigerated at 4 °C (middle) samples stored at a 22 °C ambient temperature. (Bottom) HELA incubator samples stored at 37 °C. DLS sample all had concentrations of 0.1 mg/mL

As it can clearly be seen after four measurements, no real decrease or other trends could be determined for any pH or environment. A final measurement was performed another two weeks after this establishment as a last check (last data point), but unfortunately no real trends in any of the environments could be found.

In all three conditions, samples of different pHs seem to increase together from weeks 2 to 4 and decrease together from the first to the second week. Little can be deduced from the weekly measurements; it even seems as though the conditions of the day of measurements in and around the DLS machine are of greater influence. These could for example be fluctuations in temperature between DLS measurements.

Monitoring of the mean intensities of PLA based samples over time however showed no significant trends, regardless of temperature or pH. This seems rather peculiar as it has already been determined that pH and temperature both play a key role in polymersome stability[32]. Furthermore, a great deal of research into biodegradable vesicles leads to arguments which strongly speak in favour of there being increased (bio)degradation with both increased acidity[46,48] and temperature[62,63].

6.5.2 Dependency on pH

To begin with pH, a look may be taken into two papers put forward by Discher and co-workers. Both studies asses the hydrolysis of PBd-PEO blended PLA-PEO vesicles, loaded with either chemotherapeutic DOX[48] or labelled with a rhodamine-5 fluorescent tag[46]. The first takes fixed pH values, determining release times of set doses of DOX and TAX out of the blended polymersomes. Results of one of these releases can be seen in Figure 6.18.

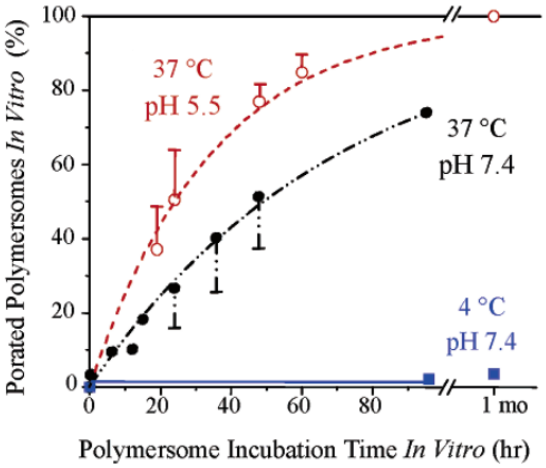

Figure 6.18 Graph of the percentage of polymersomes having hydrolysed pores in membranes over time. (Black) and (blue) curve samples used PBS as buffer and (red) HEPES[48] . Degradable polymer vesicles here were composed of a PLA_{8000}-PEO_{2000} and PBd_{6500}-PEO_{3900} copolymer blend of a 25:75 molar ratio[48].

From the black curve it can be seen that at pH 7.4 poration of 70 % of the polymersomes occurred within 100 hours. Even faster rates at pH 5.5 were observed, drawn in red. According to the authors, giant vesicles could be seen to porate and release encapsulants. Especially in increasing the pH this seems to be the case. The release time in a buffer solution of pH 5.5 was found to be twice as fast as that of pH, already being an indication that partial degradation occurs with more acidity.

From a quantitative point of view these finding can also be supported. Decreasing pH, increases the total number of H^+ ions present. A pH decrease from 7.4 to 5.5 in our case would amount to an increase of ~$1.89 \cdot 10$ H^+ ions[18] for a litre of sample (A9.4). This increase in hydrogen ions would thus lead hydrolysis resulting in cleavage of the PLA ester bonds (A9.3). Shorter and smaller PLA polymer blocks would then be the result, and with further cleavage the degradation of the vesicles could be observed. Furthermore this degradation need not only be applicable to the assemblies of polymersomes but also to those of micelles and aggregates copolymer assemblies.

With regard to the pH, the experimental DLS made measurements of mean intensity which were seen above (Figure 6.17) could perhaps have some logical conclusions drawn from them. If more degradation occurs at a lower pH, the particles (along with the aggregates they could be part of) could decrease in size, leading to a lower mean intensity (Reduced Brownian motion of larger particles). As can be seen in the three plots of Figure 6.17, the low pH samples (i.e. purple circle and green triangle) almost consistently have the lowest intensity for all time intervals, particularly at 22 °C and inside HELA incubator at 37 °C. Furthermore at 22 °C all four pH's seem to be perfectly ordered regardless of time.

6.5.3 Dependency on Loading Efficiency

To further assess acidity induce on biodegradability, loading efficiencies of the M5 PLA105 samples were assessed under varying pH. PLA105 samples were prepared as specified by Method 5 with the pH of the buffer solution adjusted accordingly as described in the Section 5.5 of the Methods Chapter. Figure 6.19 shows the polymersome loading efficiencies plotted for each of the corresponding buffer pH.

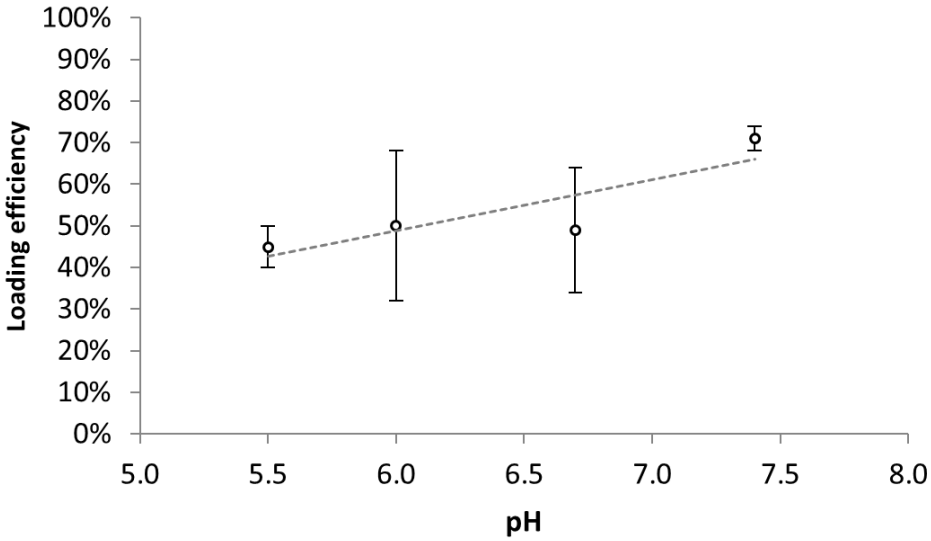

Figure 6.19 Average relative amount of activity collected by M5 PLA105 polymersomes, prepared and loaded with varying pH. Standard deviations come from two or more separate loading trials.

What can immediately be observed is a decreasing loading efficiency with decreasing pH, especially when comparing loading efficiencies in pH of 5.5 and 7.4. Loading efficiencies of polymersomes in pH 6.0 and 6.7 were also found to be consistently lower than those prepared in a pH of 7.4.

The decreasing trend in loading efficiency with decreasing pH could be an indicator of increased hydrolysis of the PLA block polymer. As discussed earlier, a higher pH would theoretically lead to increased poration and degradation of polymer vesicles. With more vesicles porated and degraded as a result of this hydrolysis, loading of polymersomes with an encapsulant would then logically be reduced. Assuming this to be the case, use of radionuclide as encapsulant would then show a decrease in loading efficiency, which was observed. That being hypothesized however, it could also possible that the decrease in loading efficiency is due to a decrease in binding between the Tropolone and Indium-111. This being due to the fact that Tropolone does not bind that well at low pH. Due to this therefore argument therefore, one unfortunately has to remain inconclusive on this topic.

Moving on to another supporting argument, Discher *et al.*'s second specified paper[46] furthermore underlines the pH/degradability correlation as can be found in their assessment of PLA_{3900}-PEO_{2000} based polymersome populations over time. Figure 6.20 shows the populations of empty and loaded biodegradable vesicles suspended in a water-based buffer (PBS) of pH 7.0.

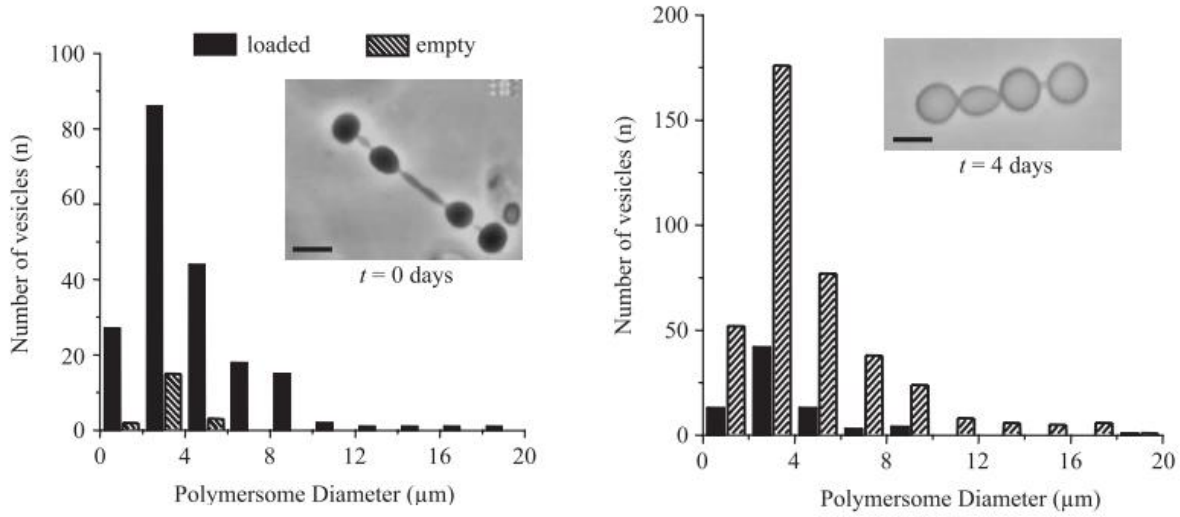

Figure 6.20 Historgrams of loaded and empty PLA_{3900}-PEO_{2000} PBd_{6500}-PEO_{3900} blended vesicles over the course of 4 days. Initially, 90% of the polymersomes are observed to be loaded, after four days in the pH 7 evironment 80% of the vesicles had their encapsulant released[46].

What can be observed is a large change in number of loaded to empty polymersomes over time regardless of polymersome diameter. The blended PLA-PEO polymersomes here were thought to have lost their contents by means of a "surface erosion mechanism" suggested by the diameters remaining constant. Findings above were in contrast to findings with the pure PBd-PEO, which was also control-tested. PBd was found to show essentially no loss of encapsulant over the course of the 4 days. The hydrolysability of hydrophobic PLA block can thus only be the reason for this change in encapsulant retention.

6.5.4 Temperature

As for the temperature, a number of arguments speak in favour of increased degradation due to increased temperature. Firstly, the previous paper discussed by Discher *et al.* which found the hydrolysis of PLA is to be accelerated with mild acidity, also insinuated that "temperature shifts can possibly even have a greater effect". Looking back at Figure 6.18 in the preceding section, the (in blue plotted) porated population at 4 °C shows to be and remain non-existent over the course of the experiment. Furthermore drug release here does not occur, this in sheer contrast to the measurements found for 37 °C samples.

Furthermore research investigating the properties of PCL[64] and PLA[65] polymer blocks have established that increased cleavage of ester bonds occur with increased temperature. While PCL prefers end chain scission and PLA random chain scission when ester bonds are broken, both naturally lead to shorter polymer chains as seen for PCL in Figure 6.21 below for example.

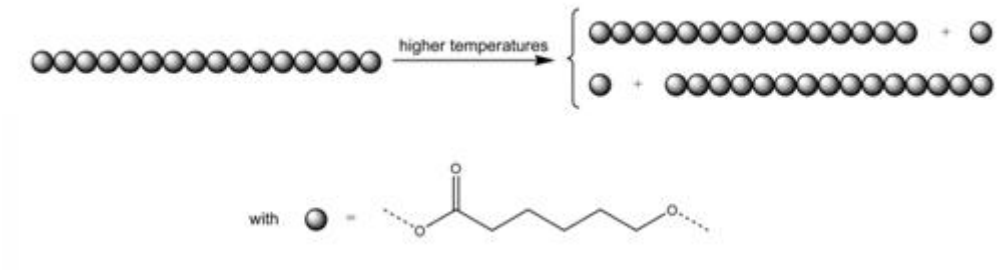

Figure 6.21 Degradation of PCL, showing the end chain cleavage of polymeric chains[66].

With respect to vesicles, shorter PLA and PCL chains would result in the loss of the hydrophobic polymer layer in the membrane, both in mass and volume. The vesicle membranes thus reduce in thickness also losing out in mass and stability, ultimately leading to their degradation. With increased temperature thus, increased degradation of polymersomes and their aggregates would be the case. As a result, these aggregates would reduce in size leading to smaller particle sized populations. With smaller species and aggregates becoming the case, DLS measurements would thus be predicted to have lower mean intensities for higher temperatures. Noting again our DLS readings over time from Figure 6.17, (this time paying attention to the differences between the 3 plots for, i.e. changes for degradation temperatures) none of such trends could be established however. Even when taking the averages of mean intensities (for all pH measurements) at fixed environment temperature into account results unfortunately remain inconclusive (see Figure 9.3 A9.5).

6.5.5 Size Distribution over Time

Despite the mean count rates from the DLS not proving to be a useful parameter in assessing biodegradability over time, the viewing of their size distribution profiles over time did however lead to some useful insights. Figure 6.22, Figure 6.23 and Figure 6.24 show DLS measurements of the same non-extruded sample taken 50 and 80 days apart.

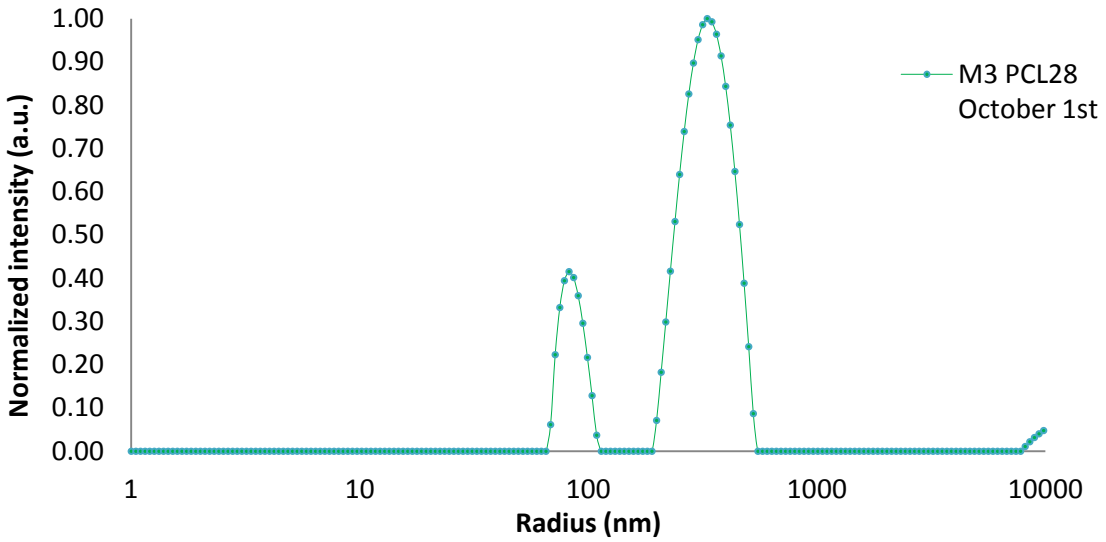

Figure 6.22 Size distribution of a M3 PCL28 sample. Sample was synthesized and measured on October 1st. DLS sample concentration is 0.05 mg/mL with a mean count rate of 1173 kHz.

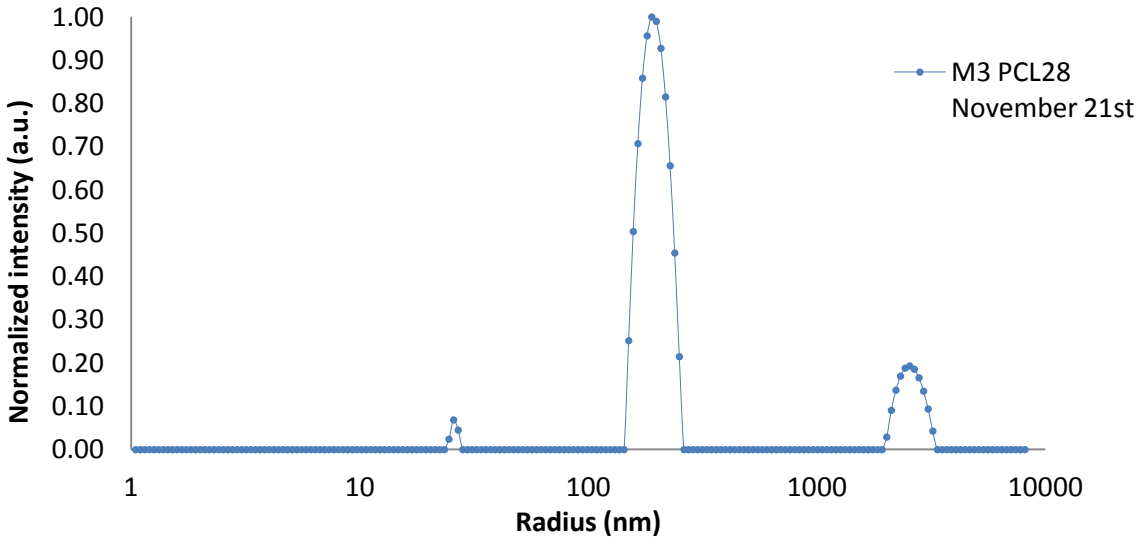

Figure 6.23 Size distribution of the M3 PCL28 sample synthesized on October 1st, measured on November 21st (50 days later). DLS sample concentration is 0.05 mg/mL. Sample mean count rate is 615 kHz.

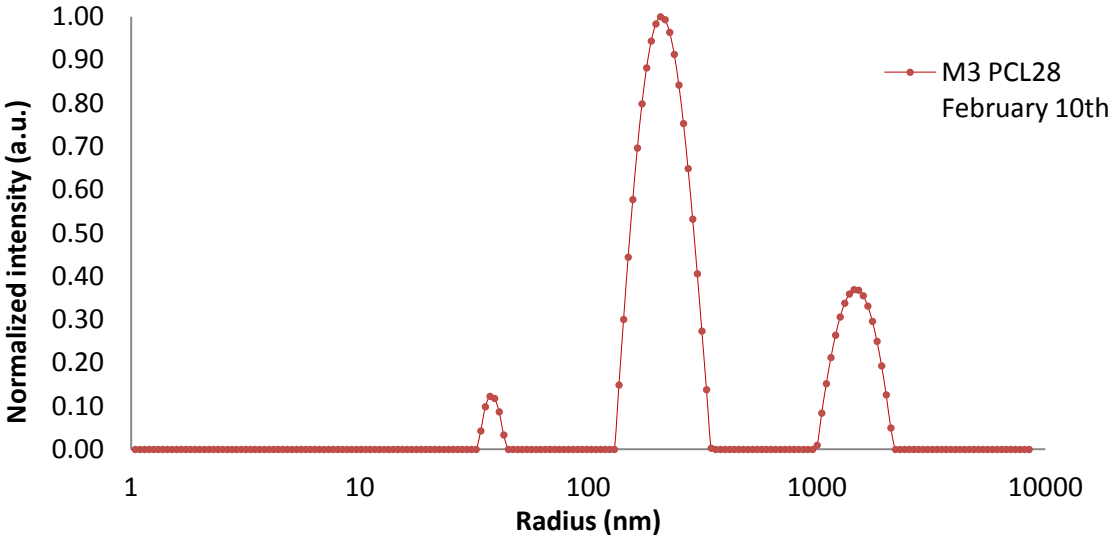

Figure 6.24 Size distribution of the M3 PCL28 sample synthesized on October 1st, measured on February 10th (130 days later). DLS sample concentration is 0.05 mg/mL. Sample mean count rate is 1003 kHz.

The DLS size distribution taken on the day of polymersome formation shows the presence of a two populations of nano-carriers being of approximately 164 and 664 nm in average diameter. In the next distribution it can be noticed that the original left peak no longer remains, in its place the presence of a new peak off to the right if noted, indicating possible aggregation of the two former particle populations. That being considered, it could also be accredited to dust suspended in the samples. This aggregation peak is furthermore observed to increase of the course of another 80 days of as seen in Figure 6.24. It can be noted that over time, formation of what could be micelles seem to occur. This possibly be attributed to the fact that hydrolysis of the PCL chain over time would lead to the rerelease of an amount PCL-PEO copolymers with slightly shortened (hydrolysed) PCL polymer block. These having shorter PCL chains would thus have give a higher f_{EO} fraction and thus naturally tend more to form micelles. Increase of this intensity/population in the micelle radius range can be observed from Figure 6.23 to Figure 6.24. In this being concluded however it should be taken into consideration that these were DLS measurements two-fold taken for this sample and from the point of view that DLS is a statistical method, it can seldom be known with certainty whether polymersomes or smaller species of some sort are present.

6.6 Closing Remark

As a final remark of the Results and Discussion Chapter, a reference to a table found in the supplementary information found in a paper by Discher and co-workers should be made[59]. This table can be found in the Supplementary Table of Appendix 9.1. What it shows the characterization of various PCL-PEO copolymer based polymersomes which self-assemble in to their respective morphologies. As indicated with arrows next to the table, PCL-PEO polymersomes here having a weight PCL_{2900}-PEO_{2000} were found to have a hydrophilic fraction (f_{EO}) of 0.57 although this previously determined at 0.42. This value was found due a novel approach in calculating this hydrophilic fraction. This could lead to the conclusion that PCL_{2900}-PEO_{2000} copolymer based polymersomes, exhibit a tendency towards micelle forming self-assemblies and not polymersomes, which for PCL_{2800}-PEO_{2000} was presumed to be the case. In assuming that the predominant self-assembly for PCL_{2800}-PEO_{2000} would be similar to that of PCL_{2900}-PEO_{2000} namely micelle forming interpretations of results could be altered.

These however came to be the case when experimental research was terminated and theoretical hypotheses had been drawn. It is however convenient to be aware of this at this stage, particularly for future research involving biodegradable PCL-PEO based polymersomes.

7 Conclusions

Initial aims in this research were to investigate and optimize various methods for the formation and size reduction of PCL-PEO and PLA-PEO. This accompanied by assessing their fictionalization as radionuclide carriers by actively loading them with radionuclide Indium-111. Finally the biodegradable character of the polymersomes was also assessed. In view of these aims and alongside the results and discussion established, a comprehensive list of conclusions can be drawn:

- Semicrystalline PCL-PEO block copolymers forming polymersomes are invaluable in their unique properties, such as their biodegradability and amphiphilicity, but it is apparent that the crystallinity of PCL has a significant negative effect on the formation, size reduction and as a consequence, drug encapsulation ability of PCL-PEO polymersomes.

- Crystallinity of PCL blocks at temperatures below those conducted in M6 (60 °C) can complicate the membrane integrity and the ability to make the nano-sized polymersomes. Rehydration in the preparation of PCL-PEO block copolymers at higher temperatures greatly improved PCL-PEO vesicle self assembly.

  This is reflected by the loading of M6 PCL130 and PCL28 samples giving efficiencies of 82 ± 7 % and 80 ± 13 % respectively. With three-fold indidividual loading trials for PCL130 and verification of the absence inidium of precpitate, the loading eff. of PCL130 gives most reliable estimates for loading efficiency with a high degree repreduciblity.

- The successful formation of PLA-PEO based polymersomes was confirmed by Cryo-TEM imaging and reliable loading efficiencies of 71 ± 3 % were found for PLA105 samples. Furthermore confocal laser scanning microscopy gave a clear representation of the self-assembly mechanism in the formation PLA105 based morphologies.

- DLS mean intensities experimentally found not to be a good means for assessing biodegradability over time. This most likely due to fluctuations in temperature during separate DLS measurements. The mean intensities were however useful in observing that lower acidities consistently gave lower mean intensities, regardless of time. Changes in mean intensity for different environmental temperatures of PLA105 polymersomes samples unfortunately did not give conclusive results with or without respect to time. Observation of DLS size distributions over time did however lead to indications of degradation.

- Loading radionuclides while varying acidity for PLA105 led to reduced loading efficiencies with reduced pH. This fits in nicely with theory on biodegradability but however due to poor binding behaviour of Tropolone at low pH, results here have to remain inconclusive.

8 Recommendations

Research in the effective formation and radionuclide carrying fictionalization of biodegradable polymersomes in this report provides a foundation from which several interesting directions for further studies emerge.

- As discussed in Section 6.4 actual confirmation of polymersomes remains speculative with solely the use of the DLS system and activity detectors. Due to this, more frequent use of Cryo-TEM imaging would be strongly advised. Cryo-TEM images will not only confirm the actual presence of polymersomes but also give an indication of possible morphologies, (membrane) sizes, (multi)-lamilarities and so forth. Furthermore other observation techniques for polymersome observation could be advised. These could be phase contrast imaging or fluorescence microscopy with a high degree (60x) of magnification.

- For size exclusion of PCL-PEO polymersomes, extrusion through filters performed at a higher temperature is highly advised. Just as with formation, increased temperature will great reduce the rigidity the crystalline polymersomes posses. Increasing temperatures towards PCL's melting temperature (60 °C), will give PCL-PEO based membranes an essential difference in fluidity require for penetration through the polycarbonate filters.

  Increasing the temperature in (particularly our) extruder could prove to be somewhat of a "risky" endeavour but nevertheless remains essential for getting polymersome diameters below the essential quoted 200 nm, not to mention the 90 nm limited for the more ideal situation.

- For *in vivo* studies, investigating the degradation of biodegradable polymersomes under more similar conditions found in the blood stream and within the tumour sites remains an aspect to be further assessed. Besides pH and temperature factors such salinity, viscosity and flow rates of the blood could be assessed for affecting polymersome biostability.

  Furthermore biodegradability could be assessed as function enzyme abundance. Enzyme degradation of polymersomes when injected intravenously is however is quoted to be limited[67] but could nevertheless it could still assessed (i.e. with enzymes found in the liver).

- Encapsulation of a large (UV) fluorescent (tagged) macromolecular substances could be used to asses biodegradability in terms of the percentage of porated polymersomes. The macromolecules being large could not escape the polymersome by bypassing the membrane but only if poration would have occurred. In essence this is already being done with Indium-DTPA complexes, but with UV fluorescent a second assessment could be made. Furthermore it could be interesting to combine encapsulation of chemotherapeutics with that of radionuclides and asses the drug loading (and delivery) prospects.

- As extensively discussed, PCL-PEO based polymer vesicles are limited by the crystallinity of their membranes. As a suggestion, possible copolymerizing the caprolactone with a monomer could be an option. In this way an approach to synthesizing a hydrolysable polymersomes with reduced membrane crystallinity could be made.

  Research investigating copolymerization with specific monomers is already being conducted, trioxaspiro-undecanone (or TOSUO) is current being assessed by Katz and co-workers[58] while Discher and co-works are assessing the use of racemic biocompatible lactide in order to disrupt crystallization[59] see Figure 9.4 in Appendix 9.5 for more details.

- Another minor remark to which more attention should be paid, especially for students and co-workers in the future, is the reliability of the Wallac detector. Prior to its use in this research, activity measurements by the Wallac were quoted with as being trustworthy when measuring samples with activities lower than 100 kBq. However later on, co-workers debated the Wallac's accuracy below this limit, and over time, lower activity boundaries such as 60, 50 and even 40 kBq were cited. Particularly between the 60-100 kBq range measurements can come across as deceiving, being able to deviate small but credible amounts. Thus reflecting back on Wallac measured loading efficiencies of 96.9 ± 2.9 %[53] and 97.7 ± 2.1 % (both upper of limits 99.8 %) within this activity range it has to be concluded that these high values simply have to be discredited. Care should thus be taken in >40 kBq sample measurements at the Wallac.

- Optimal loading used parameters in the loading of PCL-PEO and PLA-PEO polymersomes were determined largely based on findings based on PBd-PEO polymersome loading[41,47,60]. Similar experiments performed with the biodegradables and one could be conducted to assess whether these are also indeed optimal for the biodegradable polymersomes.

- More research to fully assess the biodegradability of polymersomes made with M6 would be useful. The synthesis by M6 with buffers of pH 5.5, 6.0 6.7 and 7.4 could be conducted and their loading efficiencies assessed.

- Finally if it would be interesting to assess whether the reduced loading efficiencies of PLA105 with decreased pH is due to poor Tropolone binding or increased leakiness of the polymersome membranes. Perhaps a different ligand (binding at lower pH) could be used and loading efficiency accordingly assessed.

9 Appendices

9.1 Supplementary Tables

Table 6 Overview of mean intensities of before and during extrusion of PCL111, PCL28, PCL130 and PLA105

Sample	Filter	Mean intensity (kHz)	Reduction in mean intensity by filtration step (kHz)
M2 PCL11	None	1614	-
M2 PCL11	2x 800 nm	1545	69
M2 PCL11	2x 400 nm	1150	395
M2 PCL11	2x 200 nm	456	694
M4 PCL28	None	786	-
M4 PCL28	2x 800 nm	577	209
M4 PCL28	2x 400 nm	655	-78
M4 PCL28	2x 200 nm	56	599
M3 PCL28	None	1174	-
M3 PCL28	2x 800 nm	1200	-26
M3 PCL28	2x 400 nm	1190	10
M3 PCL28	2x 200 nm	77	1113
M3 PCL130	None	1131	-
M3 PCL130	2x 800 nm	272	859
M3 PCL130	2x 400 nm	304	10
M3 PCL130	2x 200 nm	132	0
M5 PLA105	None	1624	-
M5 PLA105	2x 800 nm	800	824
M5 PLA105	2x 400 nm	120	680
M5 PLA105	2x 200 nm	24	96

Table 7 Loading efficiencies of PLA105 polymersomes formed with HEPES buffer solutions of varying pH. DTPA containing samples are plotted above. PLA105 loaded in absence of DTPA showed loading of up to 30% of the activity into the vesicle membrane.

Method	Diblock copolymer	pH	Loading efficiency	Stn. Dev.
M5	PLA105	7.4	71%	3%
M5	PLA105	6.7	49%	15%
M5	PLA105	6.0	50%	18%
M5	PLA105	5.5	45%	5%
M5 (no DTPA)	PLA105	7.4	30%	9%

Table 8 Characterization of 35 different PCL-PEO block copolymers used in research conducted by Discher *et. al* concerning rigidity and crytsalinity[59]. Block copolymers indicated with red shows PCL-PEO samples of those used in this research, for PCL_{2900}-PEO_{2000} micelle forming self-assemblies are observed.

Polymer OCL (X,Y)	MW of PEO (g/mole)	MW of PCL (g/mole)	MW of OCL (g/mole)	M_{CH_2} (g/mole)	f_{EO}	PDI by GPC	Morphology
OCL (1, 0.5)	1000	540	1540	388	0.75		monomers
OCL (1, 1)	1000	966	1966	695	0.65		loose aggregates
OCL (1, 3)	1000	3067	4067	2206	0.46		vesicles
OCL (1, 4)	1000	4100	5100	2949	0.42		vesicles
OCL (1, 6)	1000	6315	7315	4543	0.38		vesicles
OCL (1, 12)	1000	12444	13444	8951	0.33	1.48	precipitates
OCL (2, 3)	2000	2900	4900	2086	0.57	1.23	spheres
OCL (2, 6)	2000	5900	7900	4244	0.46	1.6	vesicles, worms
OCL (2, 7)	2000	7080	9080	5092	0.44	1.45	worms, vesicles
OCL (2, 8)	2000	8020	10020	5769	0.42	1.51	worms, vesicles
OCL (2, 9)	2000	9000	11000	6474	0.41	1.42	worms, vesicles
OCL (2, 10)	2000	10100	12100	7265	0.40	1.52	worms, vesicles
OCL (2, 11)	2000	11200	13200	8056	0.39	1.65	worms, vesicles
OCL (2, 12)	2000	11900	13900	8560	0.38	1.6	worms, vesicles
OCL (2, 13.5)	2000	13000	15500	9800	0.37	1.46	worms, vesicles
OCL (2, 15)	2000	15500	17500	11149	0.36	1.57	precipitates
OCL (2, 18)	2000	18613	20613	13388	0.35		precipitates
OCL (3.5, 4)	3500	3954	7454	2844	0.62		wpheres
OCL (3.5, 9)	3500	9155	12655	6585	0.48	1.55	wpheres
OCL (3.5, 12)	3500	12628	16128	9083	0.44		vesicles, spheres
OCL (3.5, 16)	3500	16395	19895	11793	0.41		vesicles, spheres
OCL (5, 3)	5000	2952	7952	2123	0.73		spheres
OCL (5, 6)	5000	5900	10900	4244	0.61	1.4	spheres
OCL (5, 9)	5000	8755	13755	6297	0.54		spheres, vesicles
OCL (5, 10)	5000	10511	15511	7561	0.51	1.6	vesicles, spheres
OCL (5, 11)	5000	11093	16093	7979	0.50		vesicles
OCL (5, 12)	5000	11700	16700	8416	0.49		vesicles
OCL (5, 18)	5000	17900	22900	12875	0.44		vesicles
OCL (5, 24)	5000	24284	29284	17467	0.40		vesicles
OCL (5, 30)	5000	29600	34600	24888	0.28		vesicles

9.2 Supplementary Figures

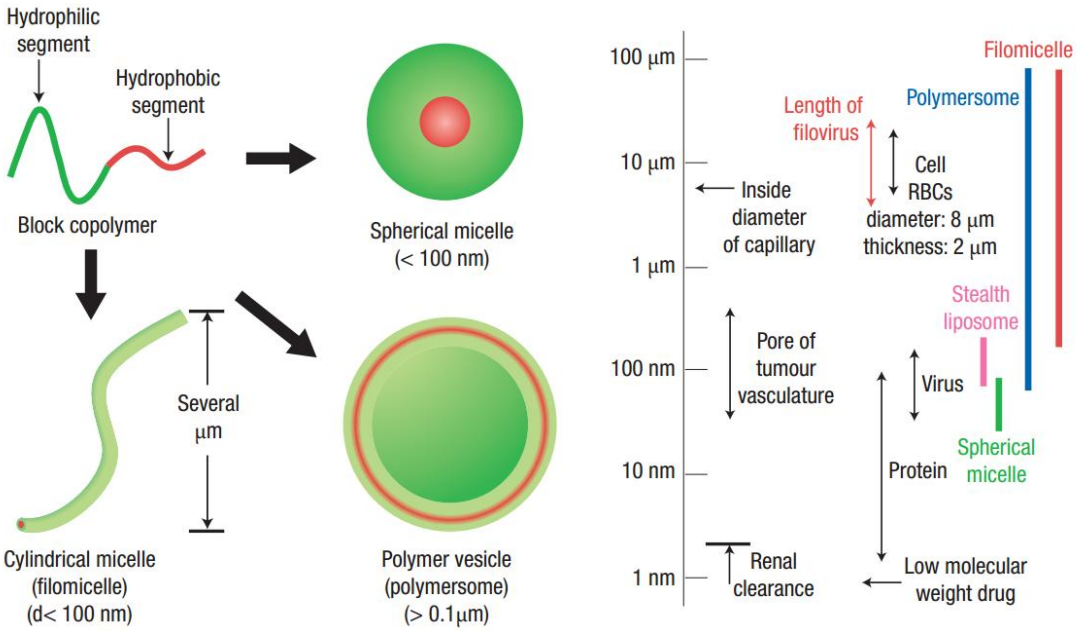

Figure 9.1 (Left) Block copolymers bearing a hydrophilic (green) and hydrophobic (red) segment can form different shapes and sizes. Depending on rigidity, length and ratio of the polymer segments, these synthetic copolymers can self-assemble into spherical micelles, polymer vesicles (polymersomes) or cylindrical micelles. (Right) Length scales showing how the various copolymer assemblies compare with structures in the body[4].

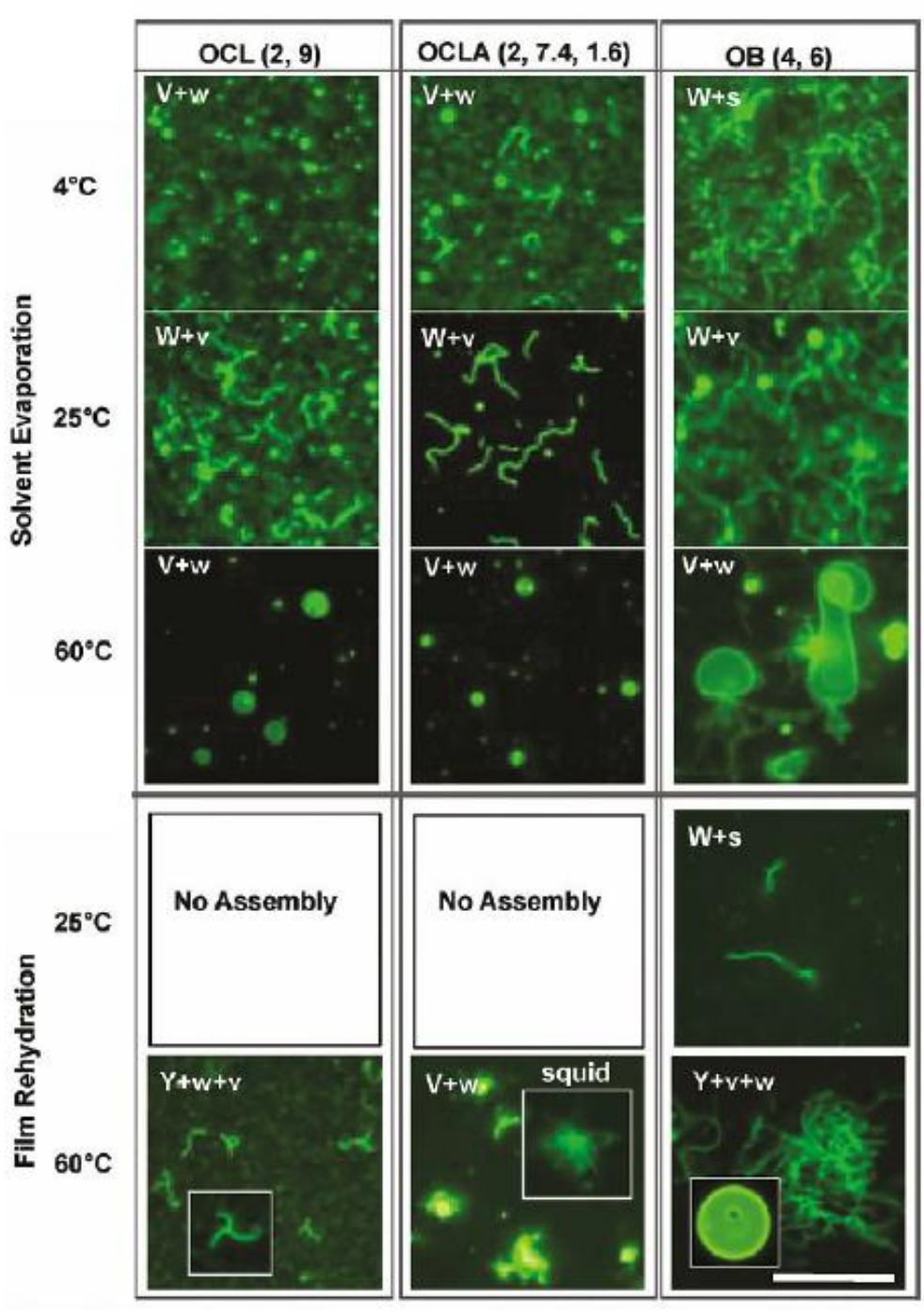

Figure 9.2 Temperature and process dependence of morphologies. Morphologies of PCL_{9000}-PEO_{2000} (2, 9), $PCLA_{7400}$-PEO_{2000}, $PCLA_{1600}$-PEO_{2000} and PBd_{6000}-PEO_{4000} polymers formed by solvent evaporation and film rehydration methods at different temperatures is shown. At 4 °C no significant self-assembly was observed by film rehydration method for PCL-PEO and PCLA-PEO polymers after 2 weeks. The morphologies obtained are indicated by letter codes on the top left of each panel: S for spherical micelles, W for wormlike micelles, V for vesicles. Scale bar is 10 μm[59].

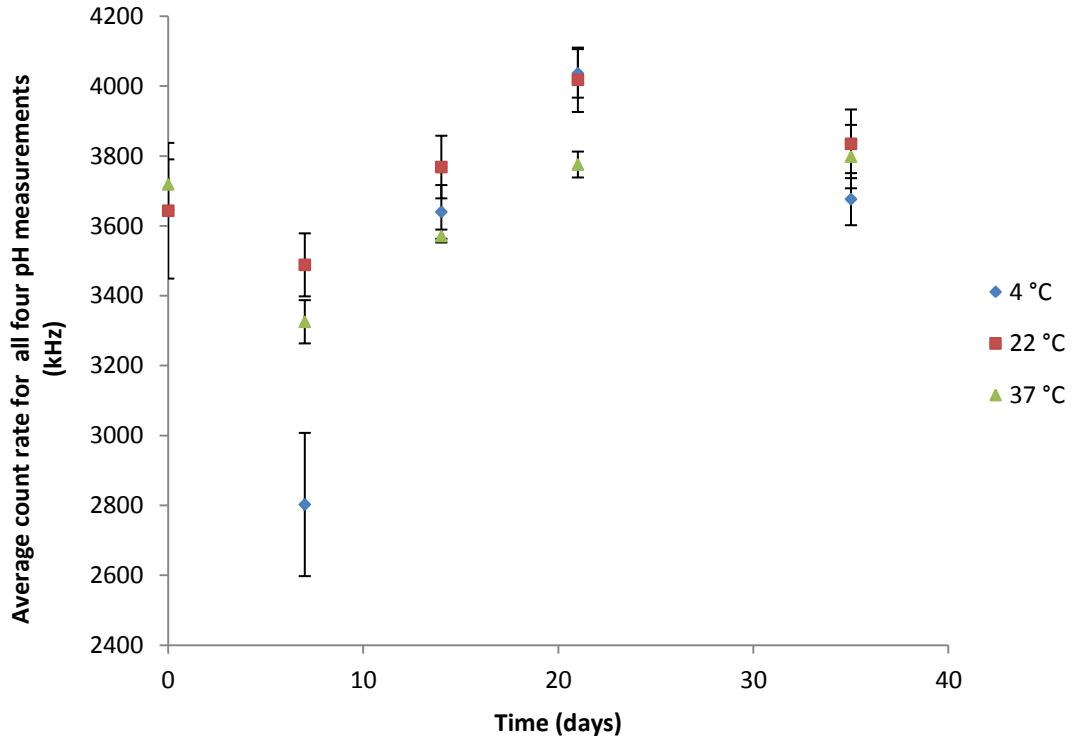

Figure 9.3 Average of mean intensities from pH 5.5, 6.0, 6.7 and 7.4 measured samples for the three different environmental temperatures. As can be seen no increasing trends occur, furthermore no specific environmental temperature seems to consistently highest or lowest (even when taking error bars into consideration).

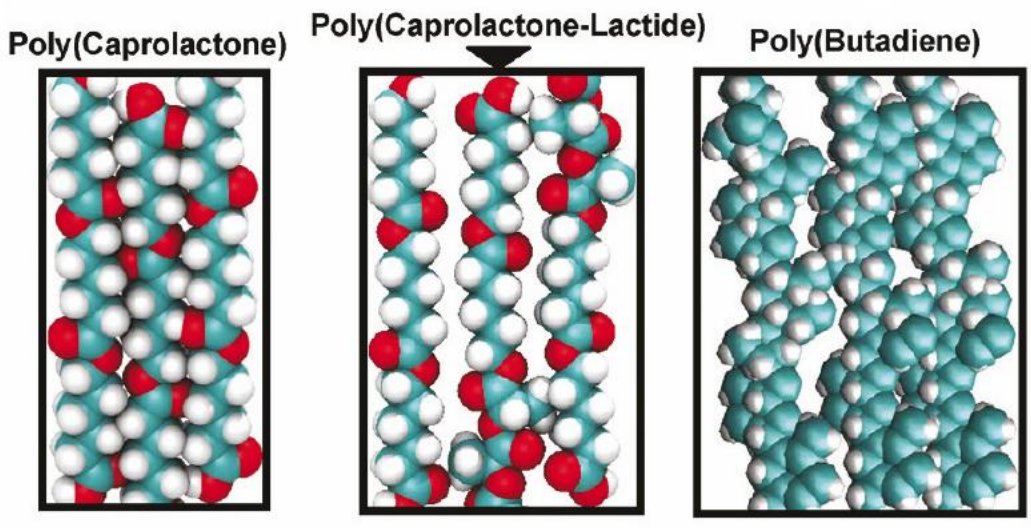

Figure 9.4 Panels from left toright showthe space fillingmodels of polycaprolactone, poly(caprolactoner- D,L-lactide), and 1,4 polybutadiene blocks. The presence of DL-lactide affects molecular level packing and possibly limits the extent of crystallization[59].

9.3 Mechanisms

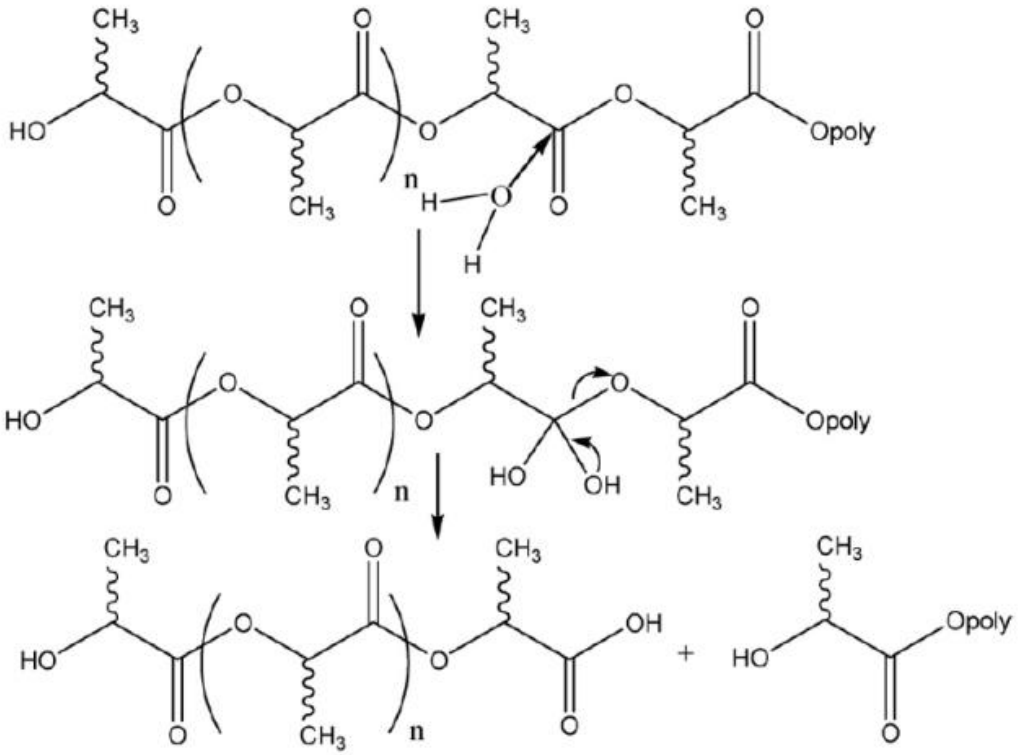

Figure 9.5 Hydrolysis mechanism of poly(lactic acid)[68].

9.4 Calculations

Calculation of increase in number of hydrogen ions

pH is defined by the negative log rhythm of the hydrogen ion concentration as:

$$pH = -log[H^+] \tag{9.1}$$

So for a pH of 7.5 and 5.5 the corresponding hydrogen ion concentration can be calculated by:

$$7.5 = -log[H^+] \rightarrow [H^+] = 10^{-7.5}\ mol \cdot L^{-1} \tag{9.2}$$

$$5.5 = -log[H^+] \rightarrow [H^+] = 10^{-5.5}\ mol \cdot L^{-1} \tag{9.3}$$

This gives a difference in hydrogen ion concentration of:

$$\Delta[H^+] = 10^{-5.5} - 10^{-7.5} = 3.13 \cdot 10^{-6}\ mol \cdot L^{-1} \tag{9.4}$$

Which multiplied by Avogadro's constant

$$\Delta[H^+] \cdot N_A = 3.13 \cdot 10^{-6}\ mol \cdot L^{-1} \cdot 6.022 \cdot 10^{23}\ mol^{-1} \tag{9.5}$$

gives the number of hydrogen ions added as:

$$\Delta[H^+] \cdot N_A = 1.89 \cdot 10^{\ 18}\ H^+\ ions \cdot L^{-1} \tag{9.6}$$

9.5 List of Figures

Figure 2.1 A radionuclide chart with the shaded regions roughly indicating unstable nuclei along with their respective modes of decay. 11

Figure 2.2 A decay scheme of Indium-111[17]. Numbers in red indicate the probability with which each of the two decays will occur. 13

Figure 2.3 A graphical interpretation of the EPR targeting mechanism. 14

Figure 2.4 A Schematic illustrating the organisation of block copolymers in spherical and cylindrical micelles and vesicles with increasing hydrophobic M_w fraction. 16

Figure 2.5 A three dimensional representation of a polymersome cross-section with the membrane a bilayer clearly visible. 17

Figure 2.6 Schematic plot of vesicles stability, permeability and mobility versus molecular weight of the associated amphiphile..... 17

Figure 2.7 One of the first Cryo-TEM images of self-assembled copolymer structures of PEE-PEO 18

Figure 2.8 Hydrolysis of degradable hydrophobic polyester chains (in red) leads to shrinking of the bilayer, and eventual degradation. Chains (in black) are inert non-biodegradable block-polymers 19

Figure 2.9 Cryo-TEM images of empty PLA-PEO based self-assembled aggregates. 19

Figure 2.10 Ring opening polymerization of ε-caprolactone to make PCL. 20

Figure 2.11 A schematic picture of the active loading process. Indium-111 is carried into the bilayer by the Tropolone and then into the aqueous cavity of the polymersome by the DTPA. 21

Figure 2.12 Schematic representation of the possible transport mechanism of Indium-111 through a polymersome bilayer diffusion of In-Tropolone complexes as a whole and 21

Figure 2.13 Chemical structures of lipophilic ligand Tropolone (left) and hydrophilic chelate DTPA (right) 22

Figure 3.1 A schematic graph showing the relation between a laser intensity peak and the associated size of the scattered particle. 23

Figure 3.2 A schematic diagram of the different components of a confocal microscope setup 24

Figure 4.1 An overview over the diblock-copolymers used in this research. 25

Figure 4.2 The dynamic light scattering apparatus with which size distributions and polydispersity of the polymersomes was assessed..... 26

Figure 4.3 A LG22 High Purity Germanium (HPGe) detector from Gamma Tech used for measuring activity in radionuclide containing samples. 27

Table 1 An overview of all the diblock copolymers used in this research. 28

Table 2 An overview of the various methods used for polymersome preparation in this research. 29

Figure 5.1 Preparation of a PCL130 sample by use of the BUCHI Rotavapor (M6). 30

Figure 5.2 (left) Preparation of a PLA105 M5 sample for CLSM. 31

Figure 5.3 Image of the four different pH PLA105 samples inside the HELA cell incubator. 34

Figure 6.1 Initial DLS size distribution measurement from of a M3 PCL28 sample. 35

Figure 6.2 Best mean count rate intensities measured by the DLS system for PCL28 for methods M1-M4 as described in the Methods Section. 36

Figure 6.3 Cryo-TEM images of PLA18 sample prepared by through M5 method. 37

Figure 6.4 Time lapse images of possible polymersome formation obtained from confocal laser scanning microscopy. 38

Figure 6.5 Schematic for the formation of polymersomes from a chloroform drop in water based buffer. 38

Figure 6.6 Mean intensities of various polymersome samples after sequential two-fold extrusion through 800 nm, 400 nm and 200 nm filters. 40

Figure 6.7 An overlay of DLS size distributions for an M2 PCL11 sample. 41

Figure 6.8 Size distribution an extruded M3 PCL28-PB18 blend sample, measured by a Dynamic Light Scattering setup. 42

Figure 6.9 Chemical structure space filling models of polycaprolactone (left) and polybutadiene (right) blocks 42

Figure 6.10 Mean intensities of an M3 PCL28 and an M2 PCL28-PBd18 sample after accumulative freeze-thaw cycles. 43

Figure 6.11 Size distributions of non-size excluded (blue), sonicated (green) and (red) freeze-thawed M5 PLA105 samples, measured by a Dynamic Light Scattering setup. 44

Table 3 An overview of the highest loading efficiencies of PCL28 through use of the different methods measured using the Wallac detector. Original activity was not kept constant based on the fact that the amount of activity loaded is independent of the loading efficiency for small activities. 46

Table 4 An overview of the highest loading efficiencies of PCL130 through use of the methods M2 and M6 measured using the Wallac detector. 46

Figure 6.12 Relative amounts of radionuclide activity collected in SEC fractions for a loading trial of both PCL28 and PCL130 samples made through method M6. 47

Table 5 Loading efficiencies of M6 PCL130 formed and loaded in absence of chelator DTPA. 47

Figure 6.13 Retention of the relative amount of radionuclide activity from Indium-111 of M6 PCL130 polymersome samples over time..... 49

Figure 6.14 Representative phase contrast images demonstrating the rigidity of PCL-PEO membranes. PCL_{13000}-PEO_{2000} vesicles imaged after equilibrating at 60, 43, and 25 °C. 50

Figure 6.15 Cryo-TEM images of a M3 PCL28 (conc. 2.5mg/ml) which was daily sonicated for 30 minutes over a period 5 days. 51

Figure 6.16 DLS measurement of the M3 size distribution of the PCL28 "Cryo-TEMed" sample measured at a concentration of 0.1 mg/ml and a net count rate of 507 kHz. 52

Figure 6.17 Intensity over time for different pH's of M5 PLA105 in three different temperature environments. 54

Figure 6.18 Graph of the percentage of polymersomes having hydrolysed pores in membranes over time. 55

Figure 6.19 Average relative amount of activity collected by M5 PLA105 polymersomes, prepared and loaded with varying pH. 56

Figure 6.20 Historgrams of loaded and empty PLA_{3900}-PEO_{2000} PBd_{6500}-PEO_{3900} blended vesicles over the course of 4 days. 57

Figure 6.21 Degradation of PCL, showing the end chain cleavage of polymeric chains. 58

Figure 6.22 Size distribution of a M3 PCL28 sample. Sample was synthesized and measured on October 1st. 59

Figure 6.23 Size distribution of the M3 PCL28 sample synthesized on October 1st, measured on November 21st (50 days later). 59

Figure 6.24 Size distribution of the M3 PCL28 sample synthesized on October 1st, measured on February 10th (130 days later). 60

Table 6 Overview of mean intensities of before and during extrusion of PCL111, PCL28, PCL130 and PLA105 65

Table 7 Loading efficiencies of PLA105 polymersomes formed with HEPES buffer solutions of varying pH. 65

Table 8 Characterization of 35 different PCL-PEO block copolymers used in research conducted by Discher *et. al* concerning rigidity and crytsalinity 66

Figure 9.1 (Left) Block copolymers bearing a hydrophilic (green) and hydrophobic (red) segment can form different shapes and sizes. 67

Figure 9.2 Temperature and process dependence of morphologies. Morphologies of PCL_{9000}-PEO_{2000} (2, 9), $PCLA_{7400}$-PEO_{2000}, $PCLA_{1600}$-PEO_{2000} and PBd_{6000}-PEO_{4000} polymers formed by solvent evaporation and film rehydration methods at different temperatures is shown. 68

Figure 9.3 Average of mean intensities from pH 5.5, 6.0, 6.7 and 7.4 measured samples for the three different environmental temperatures. 69

Figure 9.4 Panels from left toright showthe space fillingmodels of polycaprolactone, poly(caprolactoner- D,L-lactide), and 1,4 polybutadiene blocks. 69

Figure 9.5 Hydrolysis of Polylactic Acid. 70

9.6 Poster

Active Loading of Biodegradable PLA-PEO and PCL-PEO Polymersome Vesicles

T.J. Sanders[1], R.M. de Kruijff[1], N. Stigter[1], E. Mendes[2], H.T. Wolterbeek[1], A.G. Denkova[1]

[1] Radiation, Science and Technology, Delft University of Technology, Mekelweg 15, 2629 JB Delft, The Netherlands
[2] Department of Chemical Engineering, Delft University of Technology, Julianalaan 136, 2628 BL Delft, The Netherlands.

Introduction

The WHO estimates a total of 14.1 million new cancer cases were diagnosed in 2012. This compared to the 12.7 million in 2008 continually reminds us of the mounting presence and severity of this disease. One of the main treatment methods, external irradiation of the tumour site, has been used in cancer treatment for decades. This has proven to be very useful for local tumour control, but it is not very effective against the major cause of high mortality rates: metastases. These are difficult to detect and difficult to treat. A very promising solution can be found in the encapsulation of radionuclides in polymersomes[1]: nano-carriers that travel to the tumour site, where the encapsulated radionuclides irradiate and kill the tumour cells.

Polymersome formation

- PLA-PEO and PCL-PEO diblock co-polymers are first dissolved in an organic solvent (i.e. chloroform)
- A buffer solution containing a hydrophilic chelate (hepes-DTPA) is added to the sample having 5:1 volumetric ratio with the solvent.
- The mixture is vortexed for 2 minutes and subsequently openly stirred for evaporation of the organic solvent.

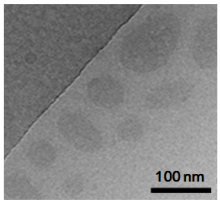

Figure 1: A Cryo-TEM image of PLA_{1850}-PEO_{700} polymersomes.

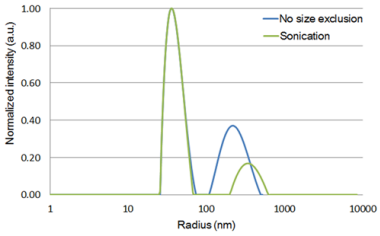

Figure 2: Normalized intensities of non size excluded and sonicated PLA_{10500}-PEO_{5000} polymersomes measured by a Dynamic Light Scattering setup. Sample mean intensities are 564 kHz and 600 kHz respectively.

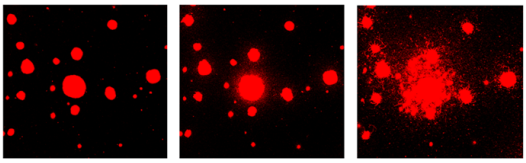

Figure 3: Time lapse images of polymersome formation obtained from confocal laser scanning microscopy. The chloroform droplets seen above burst collectively upon which the di-block co-polymers assemble to form the polymersomes (smaller spots in the rightmost picture). Images were taken at 30 second intervals.

Biodegradable Polymersomes

With the ever increasing research into drug delivery agents, polymersomes possessing biodegradable properties have become of great interest. The advantages lie mainly in the fact that they are degraded in physiological conditions (as in the human body) and can thus ideally be manufactured to e.g. controlled-release the radionuclides and chemotherapeutics that are encapsulated.

In recent research biodegradable polymersomes composed of hydrophobic polyester blocks, such as polylactic acid (PLA) or poly ε-caprolactone (PCL) together with polyethylene oxide (PEO) have been shown to have promising biodegradable characteristics. Whilst PEO is non-biodegradable with excellent hydrophilicity, solubility in water and organic solvents and its ability to minimize cell and protein interactions[2], PLA and PCL are block co-polymers that slowly degrade by hydrolysis of their ester linkages in physiological conditions[3]

Polymersome loading

- Polymersomes were loaded with the radionuclide ^{111}In as cancer diagnosis agent.
- ^{111}In transport through polymer bi-layer requires bonding of a lipophilic ligand (Tropolone) followed by hydrophilic chelate (DTPA).

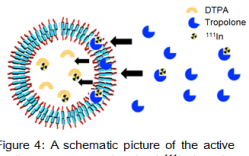

Figure 4: A schematic picture of the active loading process used to load ^{111}In into the polymersome.

- The lipophilic ligand has great affinity for the hydrophobic part of the double layer of the polymersome and so the radionuclide-ligand complex moves to the double layer.
- As the binding strength of the hydrophilic chelate in the polymersome core to the radionuclide is stronger than that of the lipophilic chelate, the radionuclide will eventually bind to the hydrophilic chelate in the aqueous core. The radionuclide is therefore loaded into the polymersome core.

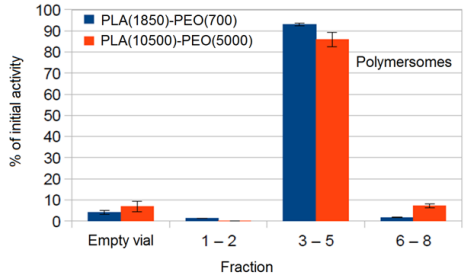

Figure 5: Relative amounts of activity from the ^{111}In radionuclide found in fractions collected from a size exclusion Sephadex G-25 column. Fractions 3 to 5 represent the fractions in which the polymersomes are collected.

Conclusions

- Cryo-TEM images together with DLS size distribution profiles confirm the presence of polydisperse PLA-PEO polymersome vesicles.
- Biodegradable polymersomes composed of PCL and PLA as hydrophobic block co-polymers have been able to load up to 64% and 92% of initial administered activity.

References

[1] R. Brinkhuis, P. Laverman, J. Eilander, I. Zuhorn, F. Rutjes, J.van Hest *Size Dependent Biodistribution and SPECT Imaging of ^{111}In-Labeled Polymersomes*, 2012.
[2] M. Meier, S. Aerts, B. Staal, M. Rasa, U. Schubert, *PEO-b-PCL Block Copolymers: Synthesis, Detailed Characterization, and Selected Micellar Drug Encapsulation Behavior*, 2005
[3] S. Petrova, I. Kolev, S. Miloshev, R. Mateva, *Amphiphilic diblock copolymers sythesis and characterization*, 2012

TU Delft Delft University of Technology

REACTOR INSTITUTE DELFT

Challenge the future

10 References

Reference List

1. N.Gaudin; W.Thielemans *Latest world cancer statistics.*; The International Agency for Research on Cancer (IARC) is part of the World Health Organization.: Dec 1, 13.

2. B.Discher; Y.Won; D.Discher Polymersomes: Tough Vesicles Made from Diblock Copolymers. *Science,* **May 14, 1999,** pp 1143-1145.

3. D.Discher; A.Eisenberg Polymer Vesicles. *Science,* **Aug 9, 202,** pp 967-973.

4. N.Nishiyama Nano-carriers shape up for long life. *Nanomedicine,* **Apr 1, 2007,** pp 203-204.

5. M.Massignani; H.Lomas; G.Battaglia Polymersomes: A Synthetic Biological Approach to Encapsulation and Delivery. *Advanced Polymer Science,* **Feb, 2010,** pp 115-154.

6. R.Brinkhuis; P.Laverman; J.Eilander; I.Zuhorn; J.van Hest Size Dependent Biodistribution and SPECT Imaging of ^{111}In-Labeled Polymersomes. *Bioconjugate Chemistry,* **2012,** pp 958-965.

7. K.Engin; L.Tupchong; J.D.Mcfarlane Extracellular Ph Distribution in Human Tumors. *International Journal of Hypothermia,* **1995,** pp 211-216.

8. S.Petrova; I.Kolev; S.Miloshev; R.Mateva Amphiphilic PCL-b-PEO diblock copolymers sythesis and characterization. *Journal of the University of Chemical Technology and Metallurgy,* **Apr, 2012,** pp 136-146.

9. F.L'Annunziata; M.ElBaradei; W.Burkart Nuclear Radiation, its interaction with matter and radioiotope decay. In *Handbook of Radioactivity Analysis*, second edition ed.; 2003.

10. D.Shams The Nucleus of the Atom and Radioactivity. 2014.

11. A.Martin; S.Harbison; K.Beach; P.Cole 2. Radioactivity and radiation. In *An Introduction to Radiation Protection*, Taylor & Francis Group: 2012.

12. J.Williams Donner Laboratory: The Birthplace of Nuclear Medicine. *The Journal of Nuclear Medicine,* **1999,** pp 16N-20N.

13. Barbara E.Hertz; Kristin E.Schuller Saul Hertz, MD (1905-1950):
A Pioneer in the use of Radioactive Iodine. *ENDOCRINE PRACTICE,* **Jun 4, 2010,** pp 713-715.

14. No authors listed Distinguished Nuclear Pioneer--1970 John Hundale Lawrence, M. D. *The Journal of Nuclear Medicine,* **1970,** pp 292-293.

15. P.Richards; W.Tuckers; S.Srivastava Technetium-99m" An Historical Perspective. *The International Journal of Applied Radiation and Isotopes,* **1982,** p 799.

16. R.Jaszczak The early years of single photon emission computed tomography (SPECT): an anthology of selected reminiscences. *Physics in Medicine and Biology,* **2006,** p R99-R115.

17. M.Bé; V.Chisté; C.Dulieu; E.Browne; V.Chechev; C.Baglin; N.Kuzmenco; R.Helmer; F.Kondev; D.MacMahon; K.B.Lee Table of Radionuclides. *Monographie BIPM-5,* **2006,** pp 3-244.

18. D.van Nostrand; H.Abreu; J.Callaghan; C.Savory In-111-labeled white blood cell uptake in noninfected closed fracture in humans: prospective study. *Radiology,* **1988,** pp 495-498.

19. K.Harrington; S.Paul; S.Stewart Effective Targeting of Solid Tumors in Patients With Locally Advanced Cancers by Radiolabeled Pegylated Liposomes. *Clinical Cancer Research,* **2001,** pp 243-254.

20. V.Torchilin Passive and Active Drug Targeting: Drug Delivery to Tumors as an Example. In *Handbook of Experimental Pharmacology*, 197 ed.; 2010.

21. X.Dong; R.Mumper Nanomedicinal Strategies to Treat Multidrug-resistant Tumors: Current Progress. *Nanomedicine,* **Jun, 2010,** pp 597-615.

22. J.Daruwalla; G.Y.Bharate; H.Maeda Polymeric drugs for effecient tumor-targeted drug delivery based on the EPR-effect. *European J. of Pharmaceutics and Biopharmaceutics,* **2008,** pp 409-419.

23. J.Fang; H.Maeda; T.Sawa Factors and mechanism of "EPR" effect and the enhanced antitumor effects of macromolecular drugs including SMANCS ., 519 (2003), pp. 29-49. *Advances in Expertimental Medicine and Biology,* **2003,** pp 29-49.

24. H.Maeda Macromolecular therapeutics in cancer treatment: the EPR effect and beyond. 164 ed.; 2012; pp 138-144.

25. S.Hong; M.Karp; R.Langer Nano-carriers as an emerging platform for cancer therapy. *Nature Nanotechnology,* **2017,** p 1748.

26. T.Bailey; T.Epps; F.Bates A noncubic triply periodic network morphology in poly(isoprene-b-styrene-b-ethylene oxide) copolymers. *Macromolecules,* **2002,** pp 7007-7017.

27. C.Houga; J.Giermanska; J.Meins Micelles and polymersomes obtained by self-assembly of dextran and polystyrene based block copolymers. *Biomacromolecules,* **2009,** pp 32-40.

28. Y.Won; H.Davis; F.Bates Giant wormlike rubber micelles. *Science,* **1999,** pp 960-962.

29. D.Discher; F.Ahmed Polymersomes. *Annual Review of Biomedical Engineering,* **Jan 8, 2006,** pp 323-341.

30. F.Ahmer; D.Discher Self-porating polymersomes of PEG-PLA and PEG-PCL: hydrolysis-triggered controlled release vesicles. *Journal of Controlled release,* **Dec 31, 2003,** pp 37-53.

31. S.Holder; Nico A.J.M.Sommerdijk New micellar morphologies from amphiphilic block copolymers: disks, toroids and bicontinuous micelles. *Polymer Chemistry,* **Feb, 2011,** pp 1018-1028.

32. M.Antonietti; S.Forster Vesicles and liposomes: A self-assembly principle beyond lipids. *Adv. Mater.,* **2013,** pp 1323-1333.

33. J.Lee; J.Feijen Polymersomes for drug delivery: Design, formation and characterization. *Journal of Controlled release,* **2012,** pp 473-483.

34. H.Bermudez; A.Brannan; D.Hammer; F.Bates; D.Discher Molecular weight dependence of polymersome structure, elasticity and stability. *Macromolecules,* **2002,** p 8203.

35. D.Williams; D.Gilding *Biocompatibility of Clinical Omplant Materials;* 1981.

36. F.Ahmed; R.Pakunlu; D.Discher Biodegradable polymersomes loaded with both paclitaxel and doxorubicin permeate and shrink tumors, inducing apoptosis in proportion to accumulated drug. *Journal of Controlled release,* **2006,** pp 150-158.

37. J.Kohn; R.Langer Bioresorbable and bioerodible materials. *Biomaterial Science,* **1996,** p 72.

38. J.Middleton; A.Tipton Synthetic biodegradable polymers as orthopedic devices. *Biomaterials,* **2000,** pp 2335-2436.

39. M.Vert; G.Schwarch; J.Coudane Present and Future of PLA Polymers. *Journal of Macromolecular Science,* **1995,** pp 787-796.

40. M.Meier; S.Aerts; B.Staa; a; M.Ras; U.Schuber PEO-b-PCL Block Copolymers: Synthesis, Detailed Characterization, and Selected Micellar Drug Encapsulation Behavior. *Macromolecular Rapid Communications,* **Aug, 5 A.D.,** pp 1918-19-24.

41. G.Wang Polymersomes as a potential tool in nuclear medicine. 2014.

42. A.Denkova; E.Mendes; M.Coppens Effects of Salts and Ethanol on the Population and Morphology of Triblock Copolymer Micelles in Solution. *Journal of Physical Chemistry,* **Oct 10, 207,** p 801.

43. S.Provencher Inverse Problems in Polymer Characterization: Direct Analysis of Polydispersity with Photon Correlation Spectroscopy. *Macromolecular Chemistry,* **1979,** pp 201-209.

44. R.Pecora; B.Berne Model Systems of Spherical Molecules. In *Dynamic Light Scattering: With Applications in Chemistry, Biology and Physics.*, 2010.

45. L.Jennings *Study of the morphology and persistence length of PS-PEO wormlike micelles using atomic force and confocal microscopy*; Oct 1, 11.

46. F.Ahmed; D.Discher Self-porating polymersomes of PEG-PLA and PEG-PCL: hydrolysis-triggered controlled release vesicles. *Journal of Controlled release,* **Dec 31, 2003,** pp 37-53.

47. G.Wang; R.de Kruijff; M.Stuart; E.Mendes; H.Wolterbeek; A.Denkova Polymersomes as radionuclide carriers loaded via active ion transport through the hydrophobic bilayer. *Soft Matter,* **Oct 29, 2012**.

48. F.Ahmed; R.Pakunlu; D.Discher Shrinkage of a Rapidly Growing Tumor by Drug-Loaded Polymersomes: pH-Triggered Release through Copolymer Degradation. *Molecular Pharmaceutics,* **2005,** pp 340-350.

49. H.Marsden; L.Gabrielli; A.Kros Rapid preparation of polymersomes by a water addition/solvent evaporation method. *Polymer Chemistry,* **Jul 8, 2010,** pp 1512-1518.

50. J.Katz; D.Levine; K.Davis; J.Burdick Membrane stabilization of biodegradable polymersomes. *Langmuir,* **Apr 21, 2009,** pp 4429-4434.

51. G.Liu; C.Chen; J.Jian Biocompatible and biodegradablepolymersomes as delivery vehicles in biomedical applications. *Soft Matter,* **2012,** pp 8811-8821.

52. F.Meng; Hiemstra; G.Engbers; J.Feijen Biodegradable Polymersomes. *Macromolecules,* **Oct 13, 2003,** pp 3004-3006.

53. N.Stigter The Preparation and Radiolabeling of polymersomes composed of PEO-PLA block copolymers. Dec 2013.

54. U.Till Asymmetrical Flow Field-Flow Fractionation with Multi-Angle Light Scattering and Quasi Elastic Light Scattering for characterization of polymersomes:comparison with classical techniques. *Unpublished paper (in revision),* **2014**.

55. J.Katz; D.Levine; K.Davis; F.Bates; D.Hammer; J.Burdick Membrane Stabilization of Biodegradeble Polymersomes. *Langmuir,* **2009,** pp 4429-4434.

56. F.Li; S.Prevost; E.Sudholter Small monodisperse unilamelaar vesicles from binary copolymer mixtures. *Soft Matter,* **2009,** pp 4169-4172.

57. R.de Kruyff The loading characteristics of polymersomes as radionuclide carriers. 2013.

58. J.Katz; M.Therien; D.Hammer Soft biodegradable polymersomes from caprolactone-derived polymers. *Soft Matter,* **2012,** p 10853.

59. K.Rajagopal; A.Mahmud; D.Christian; J.Pajerowski; D.Discher Curvature-Coupled Hydration of Semicrystalline Polymer Amphiphiles Yields flexible Worm Micelles but Favors Rigid Vesicles: Polycaprolactone-Based Block Copolymers. *Macromolecules,* **2010**.

60. R.de Kruyff The loading characteristics of polymersomes as radionuclide carriers. 2013.

61. H.Seung; D.Nelson Defects in flexible membranes with crystalline order. *Physics Review A,* **1988,** pp 1005-1018.

62. Y.Li; B.Lokitz; C.McCormick Thermally responsive vesicles and their structural "locking" through polyelectrolyte complex formation. Edition. ;(35):5792-5795. *Angewandte Chemie-International,* **2006,** pp 5792-5795.

63. A.Grayson; M.Cima; R.Labnger Size and temperature effects on poly(lactic-co-glycolic acid) degradation and microreservoir device performance. *Biomaterials,* **2005,** p 2145.

64. J.Pena; M.Vallet-Regy Long term degradation of poly(caprolactone) films in biologically related fluids. *Polymer Degradation and Stability,* **2006,** pp 1424-1432.

65. R.Al-Itry; A.Maazouz Improvement of thermal stability, rheological and mechanical properties of PLA, PBAT and their blends by reactive extrusion with functionalized epoxy. *Polymer Degradation and Stability,* **2012,** pp 1898-1914.

66. P.Joshi; G.Madras Degradation of polycaprolactone in supercritical fluids. *Polymer Degradation and Stability,* **2008,** pp 1901-1908.

67. Y.Ikada; H.Tsuji Biodegradable polyestersfor medical and ecological applications. *Macromolecular Rapid Communications,* **2000,** pp 117-132.

68. T.Maharana; B.Mohanty; S.Negi Melt-solid polycondensation of lactic acid and its biodegradability. *Progress in Polymer Science,* **2009,** p 199.